Aalto-yliopisto
Insinööritieteiden
korkeakoulu

Mats Böök

# Dimensioning of air flow rate and potential for energy savings in the ventilation of a large scale parking space

Master's thesis, submitted as a partial fulfillment of the requirements for the degree of Master of Science in Technology

Espoo 16.08.2018
Supervisor: Professor Risto Kosonen, Aalto-yliopisto
Ohjaaja: M.Sc. Niklas Söderholm, Ramboll Finland

Aalto-yliopisto
Insinööritieteiden korkeakoulu

Aalto-yliopisto, PL 11000, 00076 AALTO
www.aalto.fi

**Diplomityön tiivistelmä**

**Tekijä** Mats Emil Böök

**Työn nimi** Ilmamäärän mitoitus ja energiansäästön potentiaali suurikokoisen parrkitilan ilmanvaihdossa

**Koulutusohjelma** Masters Programme in Energy Technology

**Pää-/sivuaine** Energy Technology **Koodi** ENG21

**Työn valvoja** Prof. Risto Kosonen

**Työn ohjaaja(t)** Niklas Söderholm, DI, Ramboll Finland Oy

**Päivämäärä** 16.08.2018 **Sivumäärä** 83 **Kieli** englanti

Viimeaikaiset muutokset Suomen Rakennusmääräyskokoelmassa toimivat motivaationa insinööritoimisto Ramboll Finland Oy:n tilaamalle diplomityölle. Työn tavoitteena on selvittää, ylimitoitetaanko parkkihallien ilmanvaihtoja ja kuinka optimaaliset ilmamäärät on paras laskea suurikokoisten parkkitilojen ilmanvaihtoon. Tampereen Kansi, rakennusprojekti jonka teknistä suunnittelua Ramboll parhaillaan toteuttaa, toimii koekohteena. Hypoteesi työhön lähdettäessä on, että perinteisten mitoituskaavojen käyttö johtaa ylimitoitukseen ja että pohjaamalla mitoitus tunnettuun modernin autokannan tuottamaan hiilimonoksidikuormaan voidaan saavuttaa säästöjä. Työn rahoittaa Ramboll ja se toteutetaan sisäisenä tutkimus- ja kehitysprojektina.

Aluksi nykyaikaisten henkilöautojen päästöprofiili tutkitaan. Parkkihallin ilmatilavuuden ja ilmanvaihdon muodostaman virtauskentän mallintamiseksi luodaan MS Excel pohjainen Visual Basic -ohjelma. Ohjelman toteuttaman laskennan ydin on implementaatio painekorjausmenetelmästä. Parkkihallia käyttävät ajoneuvot mallinnetaan liikkuvina pistemäisinä päästölähteinä. Kun virtauskenttä ja ajoneuvot on mallinnettu, ajasta riippuva hiilimonoksidipitoisuus parkkihallissa ratkaistaan, jonka jälkeen ilmanvaihdon määrän riittävyyttä voidaan arvioida. Excel –mallin tuottamia tuloksia verrataan Ansys Fluent CFD-simulaatioiden tuottamiin tuloksiin ja Excel –mallia kalibroidaan virtausvastuskertoimilla, jotka lasketaan Fluent -simulaatioista.

Pääasiallisena tuloksena Tampereen Kannen parkkihallin ilmanvaihdon mitoituksen todetaan olevan 64 % suurempi toteutettuna tunnetun CO-kuorman simuloinnin pohjalta lämpötilassa – 29 °C, kuin toteutettuna perinteisellä, tähänasti laajasti käytetyllä mitoituskaavalla. Tulos on täysin ristiriidassa hypoteesin kanssa. Suurin selittävä tekijä saadulle tulokselle on, että johtuen autojen kylmäajon lisäpäästöistä ja katalysaattoreiden alentuneesta toimintakyvystä kylmissä olosuhteissa, päästöt kylmäajosta ovat yhä korkeat vaikka autokannan raportoidut päästöt ovat pudonneet huomattavasti. Optimaaliset ilmamäärät on kuvattu lämpötilan funktiona ja sen perusteella säästöjä voidaan odottaa jos ilmamäärien mitoitustilanteen lämpötilaksi valitaan korkeampi lämpötila kuin -20 °C.

Toissijaisena tuloksena Ansys Fluent simulaatioiden pohjalta tehtävän mitoituksen todetaan olevan suurempi, kuin ajasta riippuvan Excel laskennan pohjalta tehtävä mitoitus, mikä selittyy suurelta osin mallien resoluution suurella erolla sekä Fluent simulaation kykenemättömyydellä mallintaa CO-pitoisuuden ajoittainen tasoittuminen liikennepulssien välissä.

**Avainsanat** parkkitilat, ilmanvaihto, mitoitus, kontaminanttipitoisuus, painekorjausmenetelmä, laskennallinen virtausmekaniikka, energiatehokkuus

**Author** Mats Emil Böök

**Title of thesis** Dimensioning of air flow rate and potential for energy savings in the ventilation of a large scale parking space

**Degree programme** Masters Programme in Energy Technology

**Major/minor** Energy Technology **Code** ENG21

**Thesis supervisor** Prof. Risto Kosonen

**Thesis advisor(s)** Niklas Söderholm, M.Sc., Ramboll Finland Oy

**Date** 16.08.2018 **Number of pages** 83 **Language** English

Recent changes in the Finnish National Building Code have motivated the ordering of a master's thesis by engineering and technical design bureau Ramboll Finland Ltd. The goal of the thesis is to research whether parking space ventilation is being over-dimensioned at present and how to best calculate optimal air flow rates for large scale parking space ventilation. Tampereen Kansi, a civil engineering project currently undergoing technical design at Ramboll, is used as a test case. The hypothesis started with is that using conventional dimensioning formulae leads to over-dimensioning and that savings can be made by basing the sizing of the ventilation system on known carbon monoxide load from a modern vehicle fleet. The master's thesis is funded by Ramboll and carried out as an internal R&D project.

Emission profiles of modern passenger vehicles are first researched. A MS Excel based Visual Basic Macro is created for modelling the flow field of air produced by the parking space air volume and ventilation components. The core of the calculation done in the macro is an implementation of the pressure correction method. Vehicles using the parking space are modelled as moving transient contaminant point sources. Once the flow field and vehicles are modelled, transient carbon monoxide concentration is solved for in the parking space, after which the adequacy of air flow rate can be assessed. Results produced by the Excel model are compared to results produced by Ansys Fluent CFD simulation and the Excel model is calibrated with pressure loss coefficients computed from Fluent simulations.

As the main result, dimensioning of air flow rates for the ventilation system of Tampereen Kansi parking space, when based on simulated transient carbon monoxide load in -29 °C, is found to produce a total air flow rate 64 % times larger than a dimensioning computed by a conventional, up until now widely applied dimensioning formula. The result is in stark contrast with the hypothesis. The main explaining factor is that due to cold start extra emissions and the cold temperature hindering the performance of catalyzers, emissions from cold-driven vehicles are high, even though reported vehicle emission rates have declined significantly. Optimal air flow rates are graphed as a function of temperature and on that basis savings can be expected if the dimensioning scenario temperature is chosen to be higher than -20 °C.

As a secondary result, Ansys Fluent simulation is found to suggest larger sizing for the ventilation system than transient Excel simulation, largely due to the difference in resolution of the two models and the inability of the Fluent calculation to model the intermittent leveling of CO concentration between impulses of traffic.

**Keywords** parking spaces, ventilation, dimensioning, contaminant concentration, pressure correction method, computational fluid dynamics, energy efficiency

# Foreword

Initiated by Ramboll Finland Ltd., this master's thesis is part of an effort to obtain new calculation methods for the dimensioning of airflow rates in large scale parking space ventilation. It is done in parallel with CFD analysis simulations ordered by SRV Ltd. for the Tampereen Kansi parking space, carried out by Niklas Söderholm who is also the thesis advisor from Ramboll. The thesis supervisor from Aalto University is Professor Risto Kosonen.

The objectives of this thesis are to construe a calculation tool for the simulation of transient airborne contaminant concentration in large scale parking spaces; surpass the accuracy of conventional averaged pen-and-paper calculations that treat the whole parking space as a single control volume; calibrate this calculation tool with the best simulated and researched data currently at hand. As the main outcome of this thesis work, Ramboll is left with a customizable calculation tool that provides valuable, justifiable quantitative data to back decision making in future parking space ventilation designs. The thesis work is funded by Ramboll as an internal R&D project.

I would personally like to thank my thesis advisor Niklas Söderholm for all the advice, for lending his copies of reference material and for the bits of his work I have been able draw benefit from in this master's thesis. Reciprocally, the simulations carried out by Niklas have utilized much of the input data researched by yours truly. From Ramboll I would also like to thank the rest of the Building Energy Efficiency team and my direct forepersons who have been considerate in allowing me the time I've needed to concentrate on this thesis fully. Thank you Hannu Martikainen for the experience and contacts you shared with myself and Niklas at the beginning of this project.

A word of thanks to my thesis supervisor Risto Kosonen who was prompt in communications even during the summer and provided valuable comments during the work.

Finally, a special thank you to university lecturer Tommi Mikkola who was generous with his time and patience in advising the implementation of the pressure correction method, both live and by e-mail.

Espoo 16.08.2018

Mats Böök

# Table of contents

# Nomenclature

| | |
|---|---|
| $A$ | area |
| $A_{section,1-4}$ | cross-sectional areas of pipe sections measured from architect drawings |
| $C$ | concentration |
| $C_{1hmax,i}$ | maximum one-hour CO concentration average found on deck $i$ during 24-hour simulation |
| $C_{target}$ | target CO concentration |
| $D_t$ | turbulent diffusivity |
| $E$ | total energy |
| $\vec{F}$ | external body force vector |
| $F_{JF}$ | thrust produced by jet fan |
| $G_k$ | generation rate of turbulent kinetic energy due to the mean velocity gradients |
| $G_b$ | generation rate of turbulent kinetic energy due to buoyancy |
| $I$ | unit tensor |
| $\vec{J}_i$ | diffusion flux of species $i$ |
| $K_{ij}$ | lumped pressure loss coefficient for pipe between nodes $i$ and $j$ |
| $K'_{ij}$ | dimensional friction factor for pipe between nodes $i$ and $j$ |
| $N_{DA}$ | number of arriving diesel driven vehicles with engines running |
| $N_{DL}$ | number of leaving diesel driven vehicles with engines running |
| $N_{DS}$ | number of arriving diesel driven engine starts |
| $N_{GA}$ | number of arriving gasoline driven vehicles with engines running |
| $N_{GL}$ | number of leaving gasoline driven vehicles with engines running |
| $N_{GS}$ | number of arriving gasoline driven engine starts |
| $R_i$ | net rate of production of species $i$ |
| $S_{ij}$ | cross-sectional area of duct |
| $Sc_t$ | Schmidt number |
| $S_h$ | source term for heat |
| $S_i$ | source term for production of species $i$ |
| $S_k$ | source term for k |
| $S_m$ | source term for mass |
| $S_\epsilon$ | source term for $\epsilon$ |
| $T$ | temperature |
| $T_{ref}$ | reference temperature |
| $V_i$ | cell volume for cell $i$ |
| $\dot{V}$ | volumetric flow |
| $Y_j$ | mass fraction of species $j$ |
| $Y_M$ | contribution of the fluctuating dilatation in compressible turbulence to the overall dissipation rate |
| $c_p$ | specific heat capacity |
| $dt, \Delta t$ | length of timestep |
| $\vec{g}$ | gravitational body force vector |
| $h$ | sensible enthalpy |
| $i$ | as subscript, denotes value at node point $i$ |

| | |
|---|---|
| $ij$ | as subscript, denotes value between node points $i$ and $j$ |
| $k$ | turbulent kinetic energy |
| $k_{eff}$ | effective conductivity |
| $l$ | length |
| $l_m$ | length of measurement area |
| $l_{zone}$ | length of calculation cell in Excel model |
| $\dot{m}$ | mass-flow |
| $n$ | as superscript, denotes intermediate result of previous pressure correction iteration round |
| $n$ | as subscript, denotes value at the n:th timestep |
| $p$ | pressure |
| $q$ | volumetric flow |
| $q_i$ | deck specific air flow rate |
| $q_{in}$ | incoming volumetric flow |
| $q_{out}$ | outgoing volumetric flow |
| $q'_{DS,i}$ | deck specific air flow rate per unit of floor area |
| $q'_{DSO,i}$ | deck specific optimal air flow rate per unit of floor area |
| $t$ | time |
| $u$ | flow velocity |
| $\vec{v}$ | velocity vector |
| $\Phi$ | CO concentration |
| $\Phi_0$ | ambient CO concentration |
| $\Phi_{in}$ | incoming CO concentration |
| $\Delta$ | denotes difference or error term |
| $\Delta p_{ana}$ | pressure difference derived analytically |
| $\Delta p_{JF}$ | pressure difference produced by jet fan in Excel model |
| $\Delta p_{sim}$ | simulated pressure difference |
| $\alpha$ | pressure correction alpha term |
| $\epsilon$ | dissipation of turbulent kinetic energy |
| $\mu$ | molecular viscosity |
| $\mu_t$ | turbulent viscosity |
| $\rho$ | density of fluid |
| $\sigma_k$ | turbulent Prandtl number for k |
| $\sigma_\epsilon$ | turbulent Prandtl number for $\epsilon$ |
| $\bar{\bar{\tau}}$ | stress tensor |
| $*$ | as superscript, denotes most up-to-date intermediate result of pressure correction iteration |
| $'$ | as superscript, denotes a correction term |

# Abbreviations

| | |
|---|---|
| ASHRAE | The American Society of Heating, Refrigerating and Air-Conditioning Engineers |
| CFD | Computational fluid dynamics |

| | |
|---|---|
| CO | Carbon monoxide |
| CSEE | Cold start extra emissions |
| EU | The European Union |
| HVAC | Heating, ventilation and air conditioning |
| IFC | Industry foundation classes |
| P01-04 | Parking decks below ground |
| P1-4 | Parking decks above ground |
| VAV | Variable air volume |
| VBA | Visual Basic for Applications -programming language |
| VTT | Technical Research Centre of Finland Ltd |
| YM | Finnish Ministry of The Environment |

| | |
|---|---|
| $ppm_V$ | parts per million, volumetric, equal to $\frac{cm^3}{m^3}$ |

# 1 Introduction

Guidelines for the design and dimensioning of ventilation systems in parking spaces, as defined in the Finnish Building Code D2, have until recently remained nearly identical since 1978. A specification allowing for the limiting of air flow rates outside of operating hours for ventilation systems controlled by carbon monoxide (CO) concentration, was added in the 1987 update of the building code, but other than that the instructions have remained identical, including the formulas for determining sufficient extract air flow rates. [1, 2, 3, 4, 5]

Meanwhile, emissions from the Finnish motor vehicle stock have declined due to improving emission standards, the advent of catalyzers and overall advancements in automotive technology. In particular, as seen in Figure 1, carbon monoxide emissions have declined drastically, with the 2016 level constituting a fraction of the 1980 level. The decline in CO emissions for the average motor vehicle is even more pronounced, since the number of motor vehicles registered for Finnish road traffic has increased by 184.1 % during the same time period depicted in Figure 1. [6] It follows that the formulas for determining sufficient extract air flow rates defined in 1978 have been rationalized by expected emission levels far higher than those produced by typical motor vehicles today.

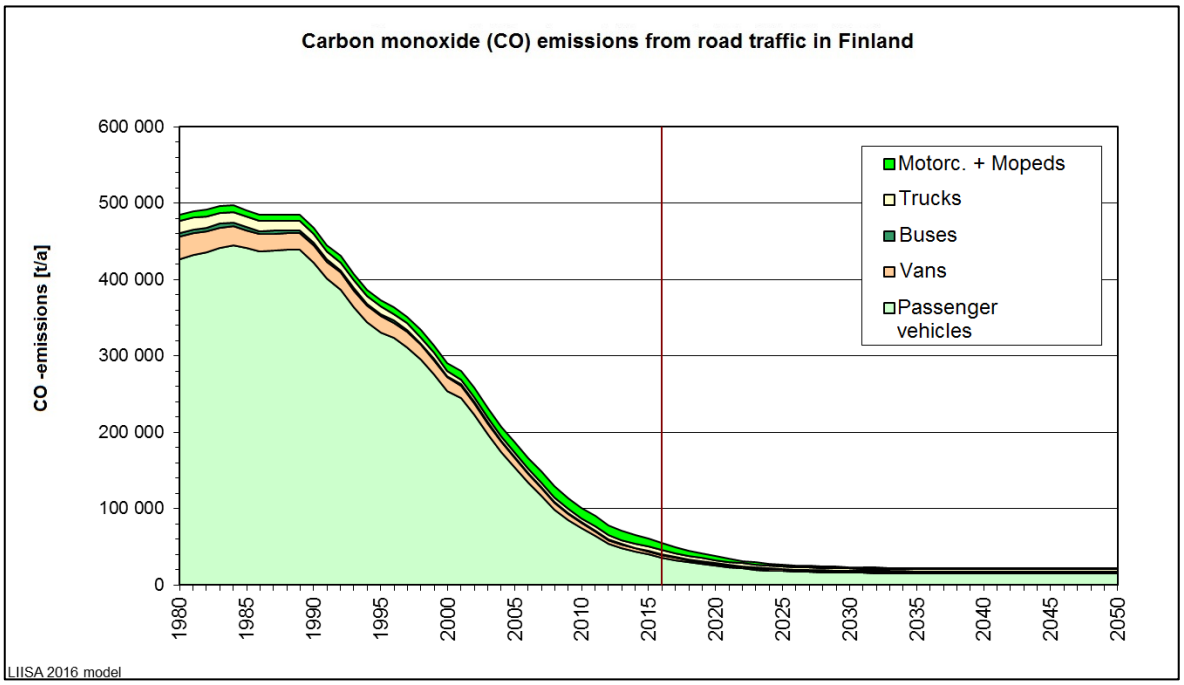


*Figure 1. Historical development of carbon monoxide emissions from road traffic in Finland [7]*

Subsequently, the sentiment at the engineering and design bureau Ramboll is that air flow rates in parking space ventilation systems have been systematically over-dimensioned in recent years. Since vehicle emission levels have declined, the possibility arises to design for smaller air flow rates without compromising indoor air quality or safety within the parking space. Parking spaces often have several large scale air handling units dedicated to serving them. Reducing air flow rates in parking spaces can thereby mean averting the instalment of

whole air handling units, leading to significant savings in capital expenditure, further savings in operational costs and a reduction in energy consumption.

Methods of calculating sufficient extract air flow rates based on the contaminant balance of the parking space air volume have been published e.g. in the ASHRAE Handbook – HVAC Applications. [8] The method published by ASHRAE uses CO concentration as the governing variable. Extract airflow rates are dimensioned in such a way that a pre-defined permissible concentration (or below) is maintained throughout the parking space. A method based on a lumped contaminant balance for the whole parking space presupposes the assumption of *fully mixed* air within the whole parking space i.e. any contaminant generated within the space is assumed instantly and uniformly distributed in the parking space air volume. Since parking spaces often contain a multitude of obstacles hindering air flow such as columns, walls, bends and the parked vehicles, pockets of limited air flow and subsequent areas of uneven contaminant concentration are easily formed. For this reason, the *fully mixed* -assumption can be thought of as problematic in parking spaces.

Section D2 of the building code has recently been repealed, and the statement about dimensioning air flow rates for parking spaces in the currently applied building code is quite broad: the decisive dimensioning factor is that the average CO concentration for a one-hour period should not exceed 35 $mg_{CO}/m^3_{air}$, which equates to 30 $ppm_V$. [9] It follows that any calculation method construed for dimensioning air flow rates for parking space ventilation should be able to estimate these averages. A more detailed manual specifically for the dimensioning of air flow rates in parking spaces titled "*Moottoriajoneuvosuojan ilmanvaihdon mitoitusopas. Ympäristöministeriö. 2017"* is currently being written by Finnish Ministry of The Environment (YM) and various experts from the industry, but this manual has not been published as of yet.

The aim of the present work is to study what rates the extract air flows can be safely reduced to assuming a present-day vehicle stock. Tampereen Kansi, a civil engineering project where a parking space is currently designed by Ramboll, is examined as a case-in-point. The commercial CFD software Ansys Fluent has been utilized at Ramboll for modelling the flow field of air within the parking space of Tampereen Kansi, including ventilation system components and vehicles as contaminant sources. Due to limits in computational resources, the CFD calculation carried out in Fluent is static in nature, and represents an averaged situation. A transient time-accurate Fluent calculation that captures the detailed geometry of the parking space and the flow phenomena within, would simply not be possible with current available computational resources. Ideally, transient CO concentration would be useful to model, since the new dimensioning rules for parking space ventilation involve a limit for the *one-hour-average* CO concentration, something that a static calculation cannot accurately solve for because the traffic that produces the CO load is transient and impulsive in nature.

This problem acts as the motivation and background for building a simplified, MS Excel based model for calculating transient contaminant concentration. To that end, a program is construed using the Visual Basic for Applications (VBA) programming language. A simplified *pressure correction method* is implemented, wherein the decks of the parking space are modeled as a 1-D flow system of rectangular pipes, which the shapes of the decks in the example case of Tampereen Kansi resemble. Being one-dimensional in nature, the Excel based calculation loses much of the details of the geometry and details of the flow field compared to the Fluent model – e.g. backward facing flow is not possible, each pipe segment

contains flow in one direction only – and computes averaged flow-quantities but, importantly, the Excel based model is able to model transient CO concentrations within the parking space. It assumes fully mixed air within zones (also to be called cells and control volumes) that the parking space is divided into and subsequently achieves a greater level of detail than a lumped contaminant balance calculation for the whole parking space. The Excel model loses geometrical details, but some of these losses of information are mitigated by calibrating the Excel model with data acquired from the more intricate Fluent CFD simulations. The aim is to combine the best of both worlds, from the geometrically accurate but static Fluent calculation and from the geometrically simplified but time-accurate Excel based calculation. In effect, the aim of the present work is to produce well-founded information, and most importantly a new calculation tool, to support decision making in future designs of parking space ventilation.

In addition to the calculation methodology, emphasis is put into finding appropriate input values for the simulations. The emission rates of the modeled vehicles are of particular interest as items of input data since their quality in part determines the quality of the results for simulated CO concentration. An ill-made choice of input values for the emission rates would result in erroneous results for CO concentration even if the flow field is modeled correctly. With this reasoning in mind, multiple studies measuring hot and cold engine emissions are examined.

The main research questions are:

1. What factors influence the dimensioning of air flow rates for parking spaces?
2. What is the optimal dimensioning for air flow rates in the Tampereen Kansi parking space, based on a known diurnal carbon monoxide load?
3. How do results computed via time-averaged static Ansys Fluent CFD analysis compare with those computed via transient time-accurate MS Excel based calculations?
4. How does the ventilation system of Tampereen Kansi perform with an example VAV configuration controlled by CO-concentration?

The hypothesis is that a sizing based on known carbon monoxide load from a modern vehicle fleet is smaller than a sizing based on conventional uniform air flow rates per square meter of floor area and that by simulating the transient CO concentration of the Tampereen Kansi parking space, smaller air flow rates per square meter of floor area can be justified than those mandated by Building Code D2.

Left outside of the scope of the present work is the role of the ventilation system during emergency situations such as fires and smoke control. Also left outside of the scope, but recognized, is the possibility that carbon monoxide might no longer be the most significant or dangerous emission from modern motor vehicles and that it might be prudent to use the concentration of another contaminant all together (e.g. particles) as the air flow rate dimensioning criteria. Both the Fluent and Excel models could with relative ease be modified to host multiple emissions species, but their ranking in terms of harmfulness to human health is not commented on as the topic belongs to the realm of medicine. As the current YM regulation on air flow rate dimensioning is based on CO concentration, it will be the focus of the present work as well. The present work studies ventilation design within the scope of mechanical ventilation. Designs involving natural ventilation are mentioned briefly but left out of any calculations or comparisons for contaminant removal.

# 2 Description of case subject

## 2.1 Description of Tampereen Kansi

Designed by Ramboll and to be built by SRV, Tampereen Kansi is a building complex that consists of a multi-purpose arena, a hotel, apartment buildings and commercial space. The building complex is built on a deck erected on top of the railroad that runs through the city of Tampere in the south-north direction. The extent of the project is all-together approximately 120 000 m² of floor area. The project is carried out in phases. Depicted in teal in Figure 2, the first phase consists of the arena and three multi-storied buildings, set to be completed in 2022. Depicted in orange, the high-rise apartment buildings and with them the project all-in-all is set to be completed in 2024. Figure 3 shows a photorealistic rendition of an aerial view of the completed building complex. [10, 11, 12, 13]

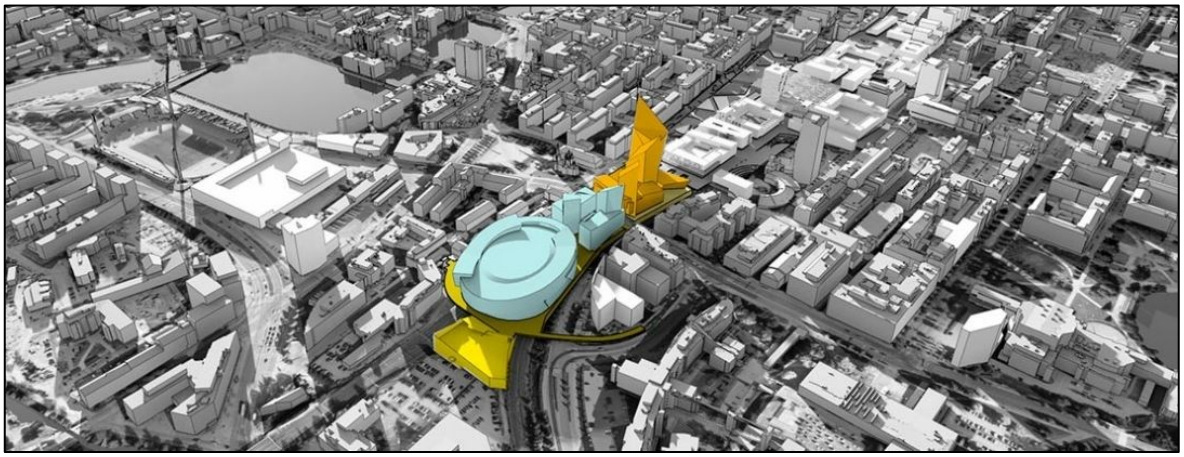

*Figure 2. Conceptual image of the planned Tampereen Kansi building complex, seen from the south-east[10]*

*Figure 3. 3D rendition of the planned Tampereen Kansi building complex, seen from the south [10]*

The parking space to be modelled is located underneath the multi-purpose arena. The parking space consists of eight decks, out of which four are enclosed spaces completely underground and four are semi-enclosed, located above ground level. The underground decks receive their supply air through a dedicated shaft, whereas the above ground decks receive their supply air as fresh air through a screen in the southern gable wall. Air is extracted through a shaft that runs vertically through all of the decks.

The parking space entrances are equipped with heating to keep the entrance slips from freezing. Other than that, the parking space has no installed heating or cooling systems. [14] Therefore temperatures within the space will closely mimic ambient outside air temperatures. During winter, temperatures inside the parking space will often reach minus degrees. As the vehicles using the parking space are prone to produce more emissions when started and driven with cold engines [15], the worst-case-scenario in terms of pollution source strength within the space is likely to occur during the cold season.

## 2.2 Tampereen Kansi parking space geometry

The geometry of the Tampereen Kansi parking space is shown in architect drawings in Figure 4, Figure 5, Figure 6, Figure 7 and Figure 8. The configuration of the ventilation system is marked into floor plan drawings in Figures 5-8. Ordered from highest to lowest above sea-level, decks P4, P3, P2 and P1 are located above ground and decks P01, P02, P03, P04 are located below ground. Seen in a section in Figure 4, the decks are located in a staggered manner where the adjacent decks are 1.5 m apart from each other in height and connected by two two-lane slips.

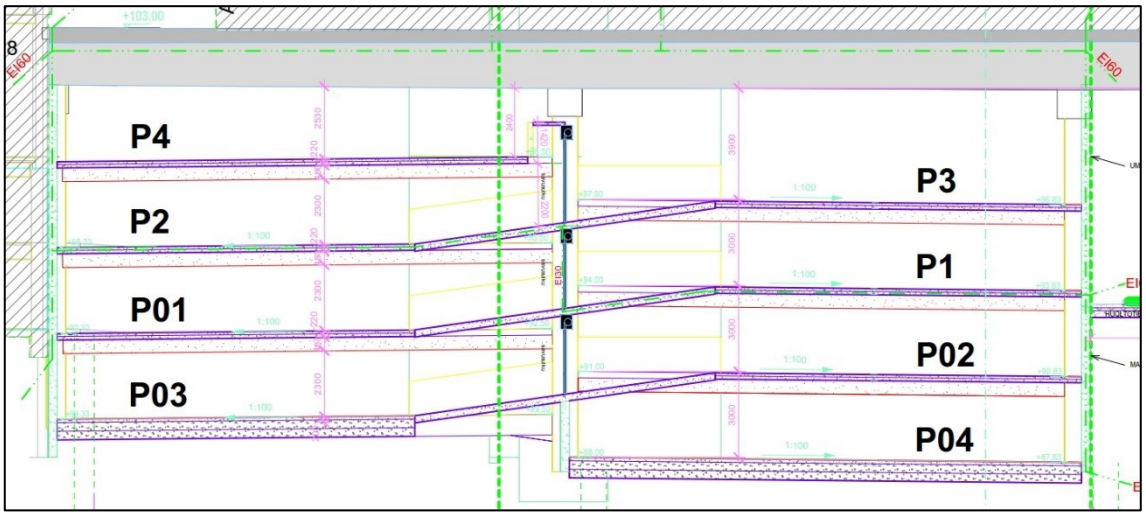


*Figure 4. Section view of the parking space*

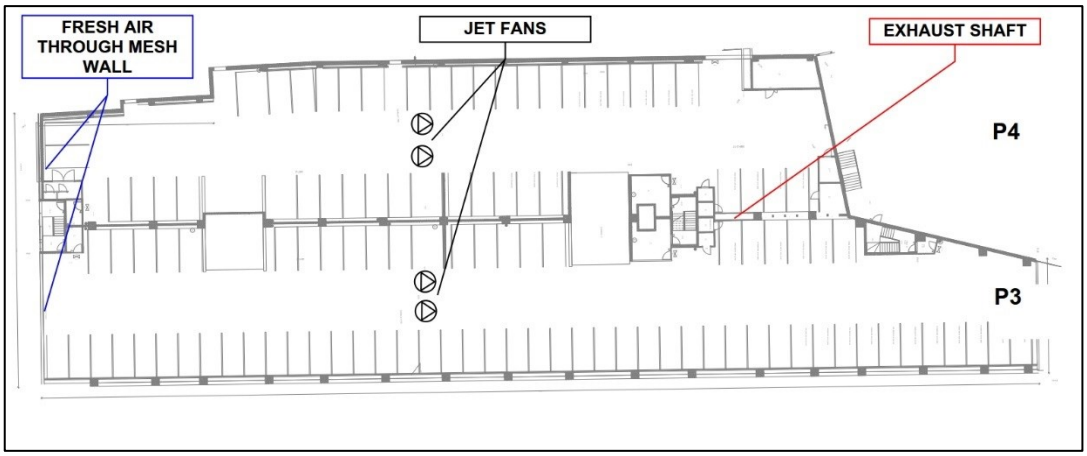


*Figure 5. Floor plan and ventilation configuration for decks P4, P3*

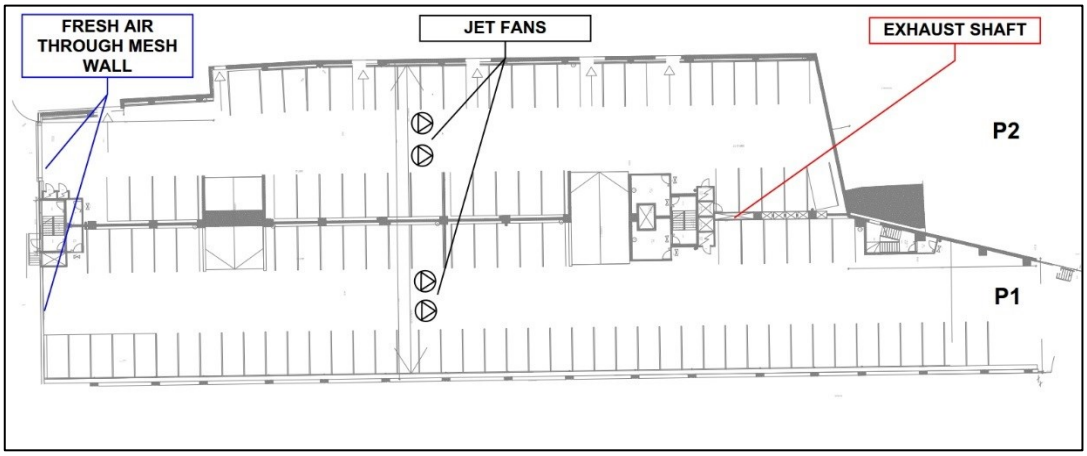


*Figure 6. Floor plan and ventilation configuration for decks P2, P1*

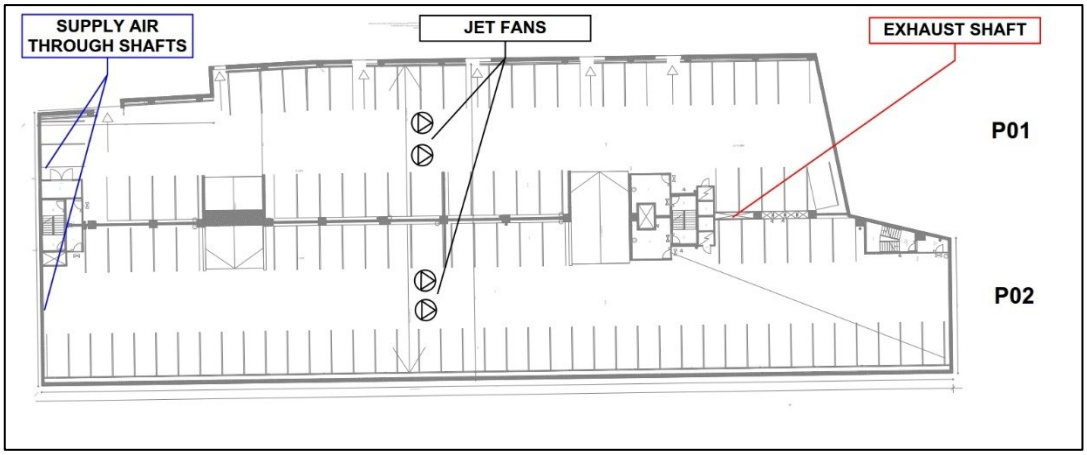


*Figure 7. Floor plan and ventilation configuration for decks P01, P02*

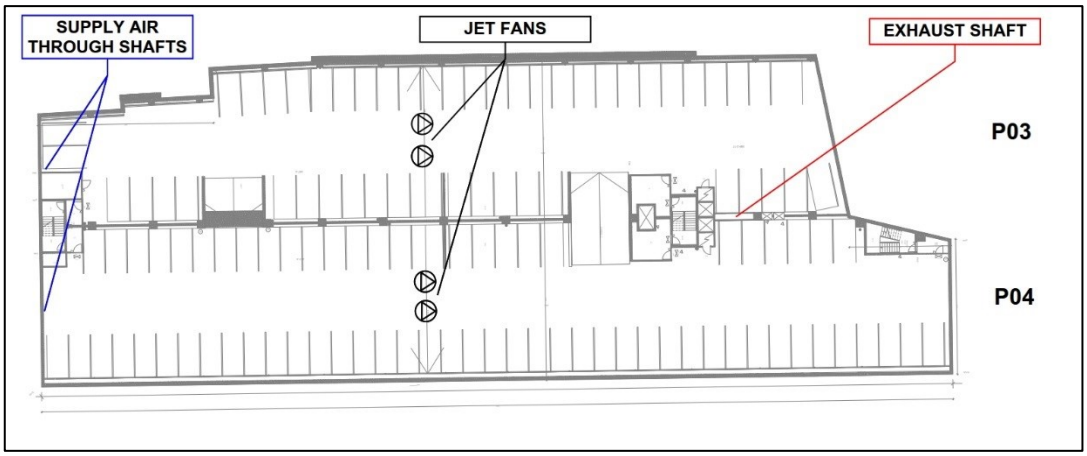


*Figure 8*. Floor plan and ventilation configuration for decks P03, P04

## *2.3 The Finnish vehicle stock*

### 2.3.1 CO emission levels associated with the Finnish vehicle stock

Emission levels from the Finnish vehicle stock have declined dramatically during the last three decades. An examination of statistics on carbon monoxide emissions from Finnish road traffic, found in the LIISA 2016 data published by VTT and statistics on the number of motor vehicles registered for Finnish road traffic found in a database compiled by Tilastokeskus, is done. Contrasting these two datasets reveals that annual carbon monoxide emissions from the average passenger vehicle are today around 3 % of what their counterparts produced in 1980. Table 1 shows the aforementioned comparison. The reader should note the difference to Figure 1, which encompasses all motor vehicles in road traffic. Here passenger vehicles are chosen for examination as they will be the most common vehicle type to utilize the Tampereen Kansi parking space. [6, 7]

*Table 1. Average carbon monoxide emissions from passenger vehicles registered for road traffic in Finland, vehicle count according to [6] and emissions according to [7]*

| Year | Passenger vehicles [count] | CO emissi-ons [t/a] | Average emissions per vehicle [t/a,vechicle] | Difference to 1980 emission level [%] |
|---|---|---|---|---|
| **1980** | 1225931 | 425 950 | 0.34745 | 0 % |
| **1981** | 1279192 | 432 171 | 0.33785 | -2.8 % |
| **1982** | 1352055 | 435 905 | 0.32240 | -7.2 % |
| **1983** | 1410438 | 441 898 | 0.31331 | -9.8 % |
| **1984** | 1473975 | 445 215 | 0.30205 | -13.1 % |
| **1985** | 1546094 | 440 847 | 0.28514 | -17.9 % |
| **1986** | 1619848 | 436 596 | 0.26953 | -22.4 % |
| **1987** | 1698671 | 438 406 | 0.25809 | -25.7 % |
| **1988** | 1795908 | 439 428 | 0.24468 | -29.6 % |
| **1989** | 1908971 | 439 618 | 0.23029 | -33.7 % |
| **1990** | 1938856 | 422 317 | 0.21782 | -37.3 % |
| **1991** | 1922541 | 401 453 | 0.20881 | -39.9 % |
| **1992** | 1936345 | 386 549 | 0.19963 | -42.5 % |
| **1993** | 1872933 | 363 852 | 0.19427 | -44.1 % |
| **1994** | 1872588 | 344 350 | 0.18389 | -47.1 % |
| **1995** | 1900855 | 330 827 | 0.17404 | -49.9 % |
| **1996** | 1942752 | 323 071 | 0.16630 | -52.1 % |
| **1997** | 1948126 | 311 596 | 0.15995 | -54.0 % |
| **1998** | 2021116 | 294 503 | 0.14571 | -58.1 % |
| **1999** | 2082580 | 275 769 | 0.13242 | -61.9 % |
| **2000** | 2134728 | 254 098 | 0.11903 | -65.7 % |
| **2001** | 2160603 | 244 514 | 0.11317 | -67.4 % |
| **2002** | 2194683 | 222 537 | 0.10140 | -70.8 % |
| **2003** | 2274577 | 196 634 | 0.08645 | -75.1 % |
| **2004** | 2346726 | 174 176 | 0.07422 | -78.6 % |
| **2005** | 2430345 | 154 504 | 0.06357 | -81.7 % |
| **2006** | 2505543 | 133 605 | 0.05332 | -84.7 % |
| **2007** | 2570356 | 116 808 | 0.04544 | -86.9 % |
| **2008** | 2700492 | 98 816 | 0.03659 | -89.5 % |
| **2009** | 2776664 | 85 216 | 0.03069 | -91.2 % |
| **2010** | 2877484 | 73 876 | 0.02567 | -92.6 % |
| **2011** | 2978729 | 63 942 | 0.02147 | -93.8 % |
| **2012** | 3057484 | 53 333 | 0.01744 | -95.0 % |
| **2013** | 3127399 | 47 770 | 0.01527 | -95.6 % |
| **2014** | 3194950 | 43 454 | 0.01360 | -96.1 % |
| **2015** | 3257581 | 39 745 | 0.01220 | -96.5 % |
| **2016** | 3346005 | 35 127 | 0.01050 | -97.0 % |

### 2.3.2 Representative vehicles

Emissions are dominantly dependent on the vehicle engine type and the fuel used.[16] Gasoline- and diesel-powered vehicles have a somewhat different emission profile so a distinction between the two fuel types needs to be made in the modelled vehicles as well. Furthermore, the age and level of maintenance of the vehicle; engine displacement; whether the vehicle is equipped with a catalyzer or not; operating temperature of the engine; the speed of the vehicle influence CO emissions.[17, 18] To correctly model the vehicles and their emissions inside the parking space we need to define the types of vehicles that are to be included in the model. To save computational resources and for simplicity, a choice is made to define one median gasoline-powered vehicle and one median diesel-powered vehicle, that represent the bulk of the Finnish vehicle stock.

Figure 9 shows the historical development of the share of diesel powered vehicles according to data gathered by TRAFI and Verohallinto and published by Autoalan Tiedotuskeskus. The latest information from 2017 is that the share of diesel powered vehicles in traffic use is 27.5 %. Hence this proportion of diesel powered vehicles will be modelled as well, but with the fraction of diesel vehicles expected to decrease in the near future, the percentage is rounded down and defined such that a quarter of the modelled vehicles populating the parking space will produce emissions at rates associated with diesel vehicles and the rest at rates associated with gasoline vehicles.

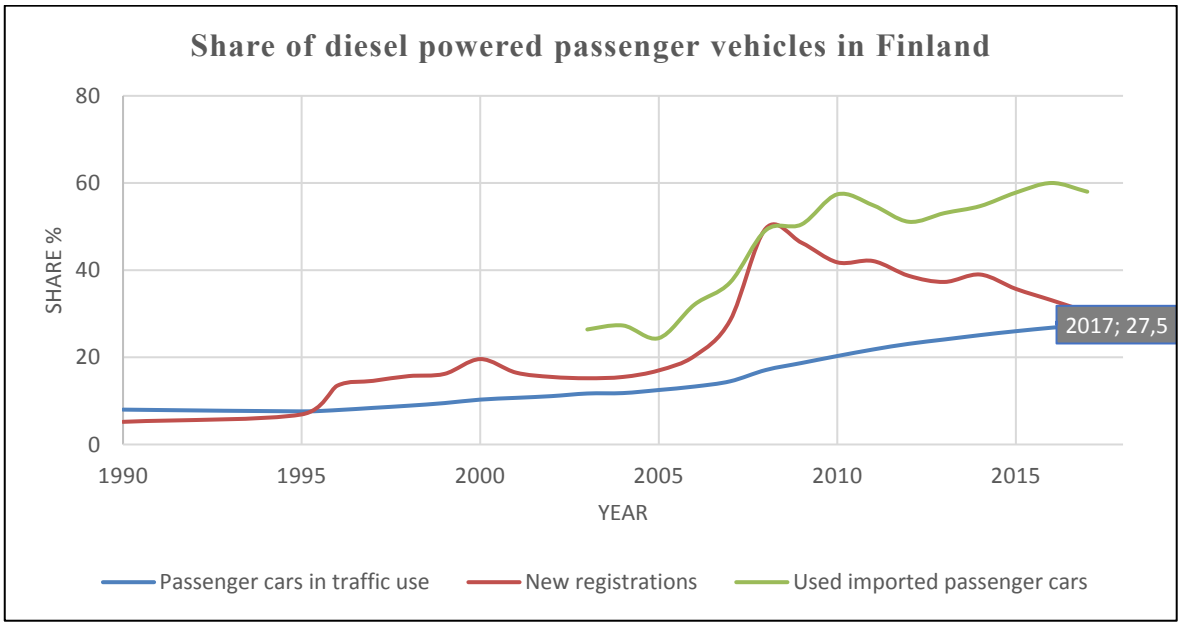


*Figure 9. Historical development of the share of diesel powered passenger vehicles in Finland [19]*

The age of the modelled median vehicles is chosen based on data gathered and published by TRAFI and Tilastokeskus. The graph in Figure 10 shows the historical development of the mean age of vehicles registered for Finnish road traffic. Since vehicles registered as museum vehicles are relatively rare and it is unlikely that such vehicles will often visit the Tampereen Kansi parking space, museum vehicles are left out of the examination and the red line depicting mean age without museum vehicles is applied.

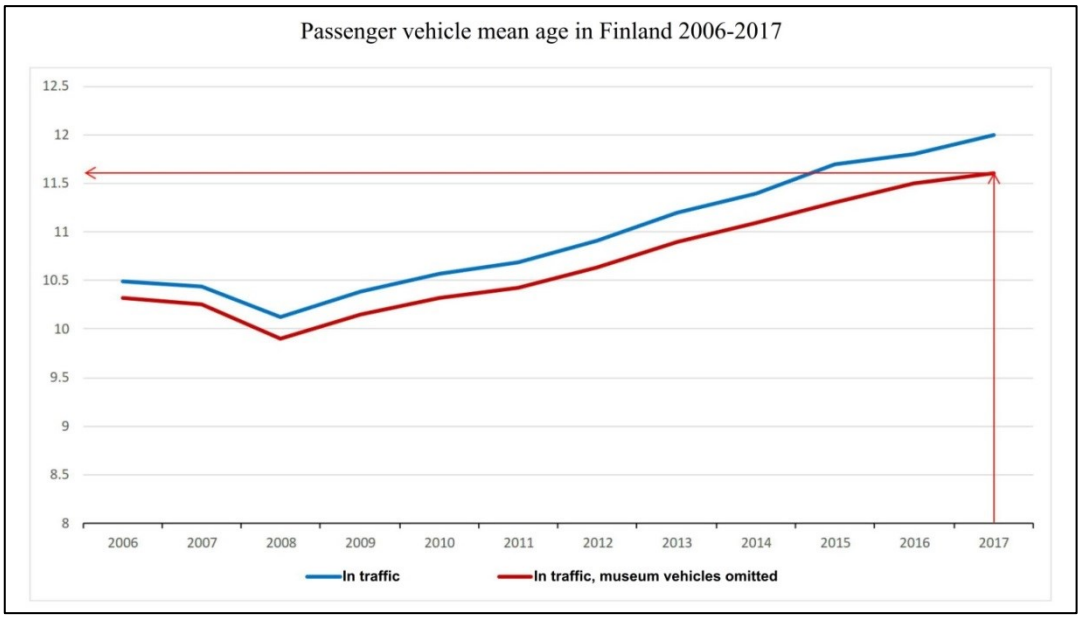


*Figure 10. Historical development of the mean age of Finnish passenger vehicles [20]*

From the graph in Figure 10 it can be read that the latest data on the vehicle fleet mean age is from 2017, when the mean age was approx. 11.6 years. It follows that the average passenger vehicle in Finnish road traffic has been manufactured 2005-2006.

Within the EU, acceptable limits for exhaust emissions for new sold vehicles are defined by European Union directives. The EU defines classifications according to maximum allowable emissions and these classifications are updated every few years. The classifications are named "Euro x" where x denotes the successive update of acceptable emission levels. Once a Euro emission level has been put into effect, all newly registered vehicles must comply to it, with a year-long transition phase applied. To cut down on emissions from European traffic each update makes the allowable levels increasingly stringent. The classification has reached Euro 6. [21]

For vehicles manufactured and registered 2005-2006, the classification applied at the time was Euro 4. Euro 4 defines the acceptable limit for carbon monoxide as 1.0 g/km and 0.5 g/km for gasoline and diesel vehicles respectively. These values have since remained the same, also in the currently applied Euro 6. These values cannot be used as input values in the parking space ventilation simulations as such, since the values are defined as grams per kilometer of driving in a specific standardized test cycle that does equate to the short distances driven at low speeds within the parking space – with the effect of cold temperature accentuating the error that would be made. For the simulation input values, what is needed are transient mass flow rates of carbon monoxide in either [kg/s] or in the combined knowledge of exhaust gas contaminant concentration in [ppm] and exhaust gas volumetric flow in [$m^3/s$]. [22]

Emission values in the sought-after units are found in a computer software called *IDA Road Tunnel Ventilation,* developed by the Swedish EQUA Ltd. for modelling longitudinal road tunnel ventilation [23]. The software in turn derives its emission values from emission data published by the World Road Association PIARC. The PIARC data features CO emission rates for both gasoline and diesel driven Euro 4 vehicles in units of [g/h], easily convertible

into [kg/s] which is perfect for the task at hand. The emission rates are given as a function of driving speed and slope. The two emission tables for gasoline and diesel driven vehicles respectively are presented as screen-captures in Figure 11.

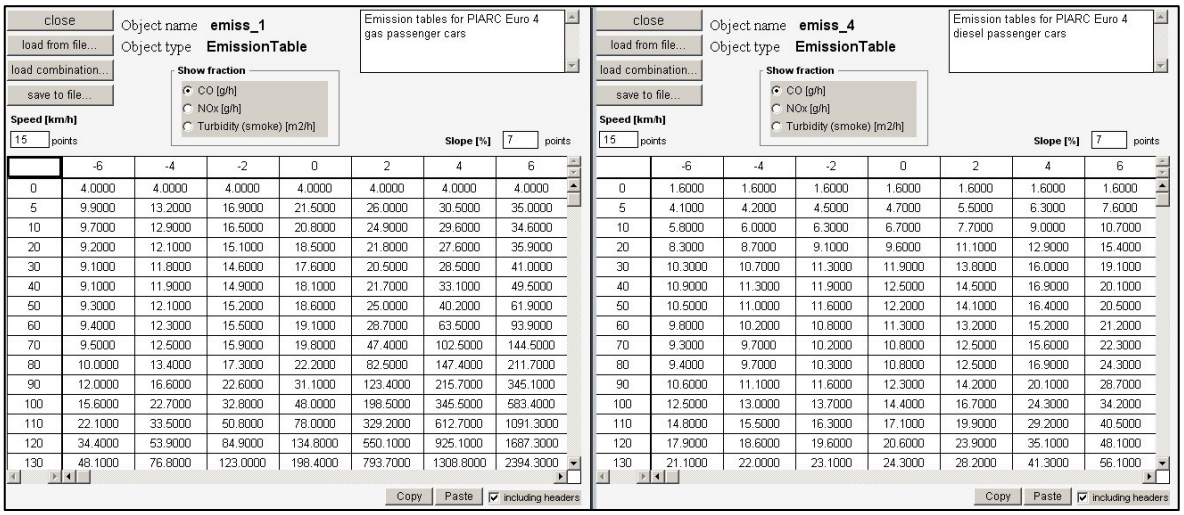
close
load from file...
load combination...
save to file...
Object name emiss_1
Object type EmissionTable
Emission tables for PIARC Euro 4 gas passenger cars
Show fraction
CO [g/h]
NOx [g/h]
Turbidity (smoke) [m2/h]
Speed [km/h]
15 points
Slope [%] 7 points

| | -6 | -4 | -2 | 0 | 2 | 4 | 6 |
|---|---|---|---|---|---|---|---|
| 0 | 4.0000 | 4.0000 | 4.0000 | 4.0000 | 4.0000 | 4.0000 | 4.0000 |
| 5 | 9.9000 | 13.2000 | 16.9000 | 21.5000 | 26.0000 | 30.5000 | 35.0000 |
| 10 | 9.7000 | 12.9000 | 16.5000 | 20.8000 | 24.9000 | 29.6000 | 34.6000 |
| 20 | 9.2000 | 12.1000 | 15.1000 | 18.5000 | 21.8000 | 27.6000 | 35.9000 |
| 30 | 9.1000 | 11.8000 | 14.6000 | 17.6000 | 20.5000 | 28.5000 | 41.0000 |
| 40 | 9.1000 | 11.9000 | 14.9000 | 18.1000 | 21.7000 | 33.1000 | 49.5000 |
| 50 | 9.3000 | 12.1000 | 15.2000 | 18.6000 | 25.0000 | 40.2000 | 61.9000 |
| 60 | 9.4000 | 12.3000 | 15.5000 | 19.1000 | 28.7000 | 63.5000 | 93.9000 |
| 70 | 9.5000 | 12.5000 | 15.9000 | 19.8000 | 47.4000 | 102.5000 | 144.5000 |
| 80 | 10.0000 | 13.4000 | 17.3000 | 22.2000 | 82.5000 | 147.4000 | 211.7000 |
| 90 | 12.0000 | 16.6000 | 22.6000 | 31.1000 | 123.4000 | 215.7000 | 345.1000 |
| 100 | 15.6000 | 22.7000 | 32.8000 | 48.0000 | 198.5000 | 345.5000 | 583.4000 |
| 110 | 22.1000 | 33.5000 | 50.8000 | 78.0000 | 329.2000 | 612.7000 | 1091.3000 |
| 120 | 34.4000 | 53.9000 | 84.9000 | 134.8000 | 550.1000 | 925.1000 | 1687.3000 |
| 130 | 48.1000 | 76.8000 | 123.0000 | 198.4000 | 793.7000 | 1308.8000 | 2394.3000 |

Copy Paste including headers

close
load from file...
load combination...
save to file...
Object name emiss_4
Object type EmissionTable
Emission tables for PIARC Euro 4 diesel passenger cars
Show fraction
CO [g/h]
NOx [g/h]
Turbidity (smoke) [m2/h]
Speed [km/h]
15 points
Slope [%] 7 points

| | -6 | -4 | -2 | 0 | 2 | 4 | 6 |
|---|---|---|---|---|---|---|---|
| 0 | 1.6000 | 1.6000 | 1.6000 | 1.6000 | 1.6000 | 1.6000 | 1.6000 |
| 5 | 4.1000 | 4.2000 | 4.5000 | 4.7000 | 5.5000 | 6.3000 | 7.6000 |
| 10 | 5.8000 | 6.0000 | 6.3000 | 6.7000 | 7.7000 | 9.0000 | 10.7000 |
| 20 | 8.3000 | 8.7000 | 9.1000 | 9.6000 | 11.1000 | 12.9000 | 15.4000 |
| 30 | 10.3000 | 10.7000 | 11.3000 | 11.9000 | 13.8000 | 16.0000 | 19.1000 |
| 40 | 10.9000 | 11.3000 | 11.9000 | 12.5000 | 14.5000 | 16.9000 | 20.1000 |
| 50 | 10.5000 | 11.0000 | 11.6000 | 12.2000 | 14.1000 | 16.4000 | 20.5000 |
| 60 | 9.8000 | 10.2000 | 10.8000 | 11.3000 | 13.2000 | 15.2000 | 21.2000 |
| 70 | 9.3000 | 9.7000 | 10.2000 | 10.8000 | 12.5000 | 15.6000 | 22.3000 |
| 80 | 9.4000 | 9.7000 | 10.3000 | 10.8000 | 12.5000 | 16.9000 | 24.3000 |
| 90 | 10.6000 | 11.1000 | 11.6000 | 12.3000 | 14.2000 | 20.1000 | 28.7000 |
| 100 | 12.5000 | 13.0000 | 13.7000 | 14.4000 | 16.7000 | 24.3000 | 34.2000 |
| 110 | 14.8000 | 15.5000 | 16.3000 | 17.1000 | 19.9000 | 29.2000 | 40.5000 |
| 120 | 17.9000 | 18.6000 | 19.6000 | 20.6000 | 23.9000 | 35.1000 | 48.1000 |
| 130 | 21.1000 | 22.0000 | 23.1000 | 24.3000 | 28.2000 | 41.3000 | 56.1000 |

Copy Paste including headers

*Figure 11. PIARC Euro 4 passenger vehicle CO emission rates, captures from IDA RTV simulation software [23]*

Since most of the driving done inside the parking space is on flat decks – the slips connecting the decks are relatively short – the effect of slope is omitted from the modeling and emission values are selected from the *Slope = 0 %* column. These values are converted into [kg/s] and used as such for the arriving vehicles with warmed up engines.

A distinction is made between arriving and leaving vehicles. The leaving vehicles are assumed to have cold engines and will have significantly higher emission rates, due to what are known as cold-start extra emissions (CSEE's). The CSEES's make for a notable increase in emissions, stemming from the fact that the catalyzers of the vehicles work at a diminished efficiency during the warm-up phase of the engine. The catalysts require typically an exhaust temperature of 300 °C to be effective. The most pronounced emission is made at the ignition of a cold engine. [15, 24]

For determining emission rates to be used in the models for the leaving vehicles, data from measurements performed in cold climate for cold engines is needed. Now, even if data reported in units [g/km] cannot be used as such as initial information in the simulations, an assumption is made that ratios measured between cold-engine emissions in [g/km] and hot-engine emissions in [g/km] apply to rates in [kg/s] as well. It is then possible to use [g/km] measurement data to compute factors that can be used to multiply the previously found hot-engine emission rates (Figure 11) to arrive at satisfactory estimates for cold-engine esmissions in [kg/s]. This approach is chosen since emission data from cold engines measured at temperatures that reflect the Finnish winter and measured directly in [kg/s] was not found. Measurement results vary notably from study to study. Factors for cold-engine emission are computed from several studies. The chosen emission rates can be easily switched as initial values in the simulations, absolute values presented in this chapter are not final but are to be taken as options when using the Excel model.

A Swiss 2009 study carried out by Weilenmann et al. measured cold-start emissions of Euro 4 passenger vehicles at three different ambient temperatures, 23 °C, -7 °C and -20 °C. The study features passenger vehicles from European and Asian manufacturers that are very common in the Finnish vehicle stock as well. Table 2 features a summary of their results relevant to the calculation of cold-engine emission factors. [24]

*Table 2. Results by Weilenmann et al. with Factor column added*

| 2009, Cold-start emissions of modern passenger cars at different low ambient temperatures and their evolution over vehicle legislation categories | | | | |
|---|---|---|---|---|
| Temperature -7 °C | | | | |
| Vehicle model | Engine type | CO-emission hot engine (g/start) | CO-emission cold engine (g/start) | Factor (cold emis./hot emis.) |
| Seat Ibiza 1.2 | Gasoline | 4.17 | 23.25 | 5.57 |
| Volkswagen Polo 1.4 | Gasoline | 6.61 | 17.34 | 2.63 |
| Audi A3 1.6 | Gasoline | 8.62 | 32.22 | 3.74 |
| Mazda 3 2.0 | Gasoline | 6.45 | 40.66 | 6.30 |
| Opel Zafira 2.2 | Gasoline | 10.31 | 77.54 | 7.52 |
| Mercedes Benz S 350 L 3.7 | Gasoline | 3.78 | 14.98 | 3.96 |
| **AVERAGE** | | **6.66** | **34.33** | 4.95 |

The 2012 LIISA report by VTT reports generalized cold-start emissions for both gasoline and diesel driven vehicles, presented in Table 3. [25]

*Table 3. Values from VTT LIISA 2012 with Factor column added*

| 2012, LIISA Raportti Liite E | | | | |
|---|---|---|---|---|
| Temperature -10 °C | | | | |
| Vehicle model | Engine type | CO-emission hot engine (g/start) | CO-emission cold engine (g/start) | Factor (cold emis./hot emis.) |
| HA Bens. Kat + ei-kat | Gasoline | 9.0 | 92.00 | 10.22 |
| **AVERAGE** | | **9.00** | **92.00** | 10.22 |
| Vehicle model | Engine type | CO-emission hot engine (g/start) | CO-emission cold engine (g/start) | Factor (cold emis./hot emis.) |
| HA dies. ei-kat | Diesel | 4.0 | 8.00 | 2.00 |
| **AVERAGE** | | **4.00** | **8.00** | 2.00 |

A joint study by Tekniikan Maailma and VTT measured CO-emissions of gasoline driven passenger vehicles and one plug-in hybrid in cold climate temperature -7 °C, as a part of a larger comparison of performance in winter conditions. Table 4 sums up the results relevant for the present work. The factors calculated are to be taken as approximative and are not absolutely accurate, since many of the values marked 0.01 were actually presented as "< 0.01". To compute factors and estimate cold engine emissions, they are handled as exactly 0.01. It follows that the factors listed on these rows might be higher in reality, based on these results. Choosing input values based on the results in Table 4 is problematic, since the test cycle driven in this study includes the emission from engine start into the [g/km] values. [26]

*Table 4. Results from joint study of TM and VTT with Factor column added*

| Tekniikan Maailma 04 2018 21.02.2018 | | | | |
|---|---|---|---|---|
| Temperature -7 °C | | | | |
| Vehicle model | Engine type | CO-emission hot engine (g/km) | CO-emission cold engine (g/km) | Factor (cold emis./hot emis.) |
| BMW 530e iPerformance | Gasoline + e hybrid | 0.01 | 0.53 | 53.00 |
| Kia Stonic 1,0 T-GDI EX | Gasoline | 0.01 | 0.56 | 56.00 |
| Hyundai i30 Fastback 1,4 T-GDI Style | Gasoline | 0.01 | 0.62 | 62.00 |
| Seat Arona 1.0 EcoTSI 115 Xcellence DSG | Gasoline | 0.01 | 0.98 | 98.00 |
| Skoda Karoq 1.5 TSI Exclusive DSG | Gasoline | 0.01 | 1.03 | 103.00 |
| Honda Civic 5D 1.0 Turbo Elegance CVT | Gasoline | 0.01 | 2.00 | 200.00 |
| Volkswagen T-Roc Style 1.0 TSI | Gasoline | 0.01 | 2.01 | 201.00 |
| Nissan Micra IG-T 90 N-Connecta | Gasoline | 0.04 | 2.68 | 67.00 |
| Ford Fiesta 1.0 Ecoboost Titanium | Gasoline | 0.06 | 3.61 | 60.17 |
| Mazda CX-5 2.0 Skyactiv-G Premium Plus | Gasoline | 0.05 | 3.91 | 78.20 |
| Renault Scenic Tce 130 Bose | Gasoline | 0.01 | 5.56 | 556.00 |
| Opel Insignia Grand Sport Innovation 1.5 Turbo A | Gasoline | 0.85 | 7.30 | 8.59 |
| Opel Grandland X Enjoy 1.2 Turbo A | Gasoline | 0.14 | 9.80 | 70.00 |
| Citroen C3 Aircross Puretech 110 Shine A | Gasoline | 0.14 | 10.30 | 73.57 |
| **AVERAGE** | | **0.10** | **3.64** | 120.47 |

A 2018 study by Suarez-Bertoa and Astorga at the European Commission Joint Research Centre measured emissions in 23 °C and -7 °C for Euro 6 classified gasoline and diesel driven passenger vehicles, Table 5. [15]

*Table 5. Results by Suarez-Bertoa & Astorga, with Factor column added*

| 2018, Impact of cold temperature on Euro 6 passenger car emissions | | | | |
|---|---|---|---|---|
| Temperature -7 °C | | | | |
| Vehicle model | Engine type | CO-emission hot engine (g/km) | CO-emission cold engine (g/km) | Factor (cold emis./hot emis.) |
| GV1 | Gasoline | 0.567 | 0.791 | 1.40 |
| GV2 | Gasoline | 0.154 | 0.206 | 1.34 |
| GV3 | Gasoline | 0.158 | 0.92 | 5.82 |
| GV4 | Gasoline | 5.766 | 10.111 | 1.75 |
| GV5 | Gasoline | 0.972 | 2.604 | 2.68 |
| **AVERAGE** | | **1.52** | **2.93** | 2.60 |
| Vehicle model | Engine type | CO-emission hot engine (g/km) | CO-emission cold engine (g/km) | Factor (cold emis./hot emis.) |
| DV1 | Diesel | 0.126 | 0.199 | 1.58 |
| DV2 | Diesel | 0.46 | 0.138 | 0.30 |
| DV3 | Diesel | 0.41 | 0.88 | 2.15 |
| DV4 | Diesel | 0.22 | 0.3 | 1.36 |
| DV5 | Diesel | 0.41 | 0.45 | 1.10 |
| **AVERAGE** | | **0.33** | **0.39** | 1.30 |

From these studies it can be gathered that when measured in -7 °C the hot to cold emission factors ranged from 2.6 all the way up to 120 for gasoline driven vehicles, whereas for diesel driven vehicles CO emissions are lower to start with and the effect of a cold engine is not as pronounced with cold emissions reported on average 1.3 times higher than hot emissions when driving and a mere 2 times higher at engine start. The results from the Tekniikan Maailma study are an outlier by a significant margin.

To find emission rates suitable for temperatures colder than the available measurement data, extrapolations have been made based on measurement results by Weilenmann et al. Extrapolations have been made for engine start emissions utilizing the mean emissions measured from six gasoline riven and six diesel driven Euro 4 vehicles in three different temperatures. A trendline has been fitted to these data-points and the behavior of CO emissions with decreasing temperature is found to be close to exponential growth. The extrapolation is displayed in Figure 12.

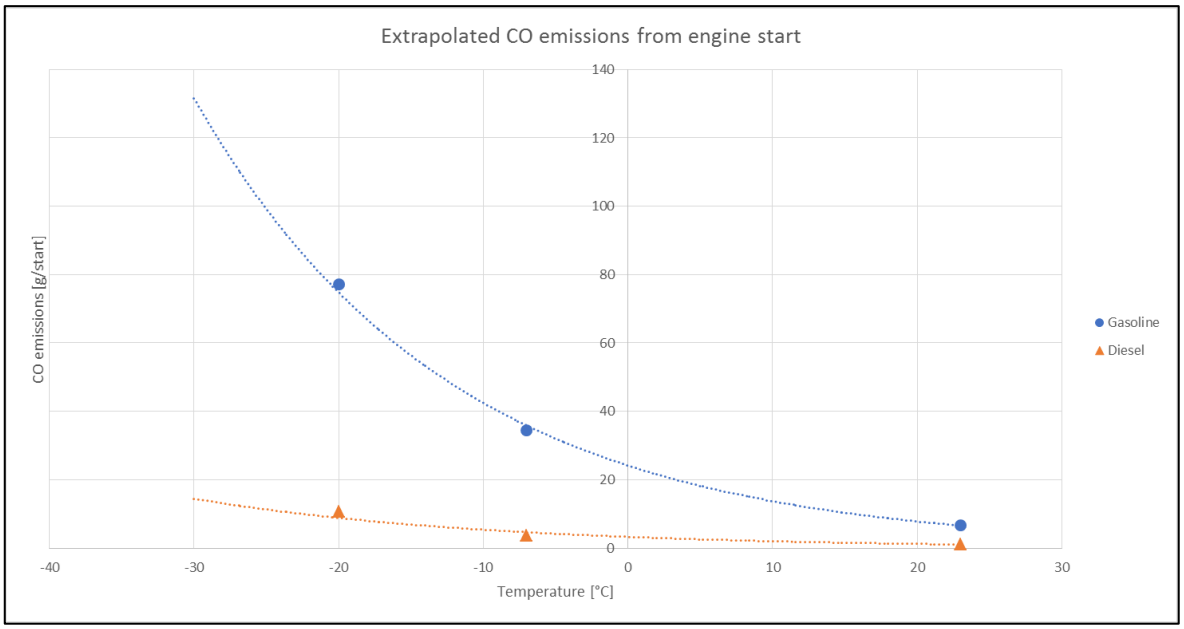


*Figure 12. Extrapolation of measurement results for CO emissions at engine start of Euro 4 vehicles*

## 2.4 Common parking space ventilation designs and current code of practice in parking space ventilation design

Parking spaces can be open, semi-enclosed or enclosed, generally depending on their location with respect to ground level. What is meant by open is an envelope with either no walls or walls consisting of a loose grid or mesh like structure that allows free airflow through the envelope. Examples of what is meant by semi-enclosed spaces are an underground tunnel that is a dead end on one side and open on the other side or a parking space with both enclosed decks below ground and open decks above ground. By enclosed, a space with a complete closed envelope is meant. A parking space that resides completely underground is an enclosed space by condition. Parking space ventilation can be carried out via natural ventilation based on natural convective airflow induced by density differences or natural wind blowing through the space; by mechanical ventilation; by a combination of the two. An open parking space with decks above ground might rely completely on natural wind for ventilation, whereas an underground closed space will require mechanical ventilation.[8]

Common designs for mechanical ventilation include air distribution and removal via ductwork and more recently designs based on jet fans (aka impulse ventilation) have been adopted from longitudinal tunnel ventilation. Generally, the air distribution works either by the principal of mixing ventilation or by the principal of displacement ventilation. Figure 13 and Figure 14 illustrate the operating principle of channelized ventilation (with ductwork) and jet fan ventilation (without ductwork) in a simple parking space architecture.

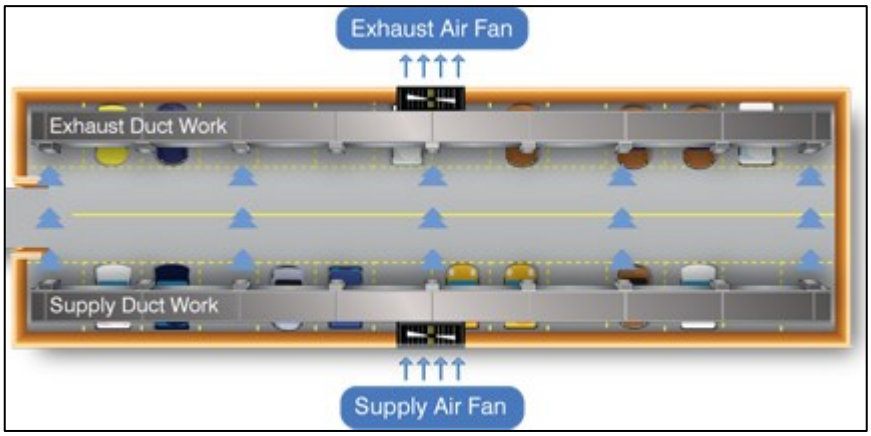


*Figure 13. Channelized ventilation principle [27]*

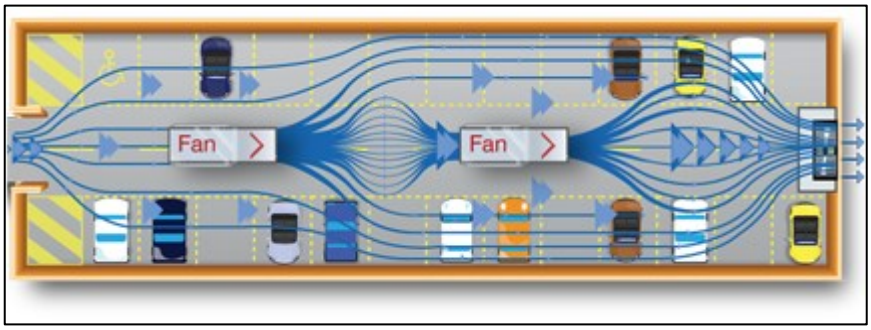


*Figure 14. Jet fan ventilation principle [27]*

The currently applied regulation for the design of parking space ventilation published by YM states that air flow rates in parking space ventilation must be dimensioned in such a way that airborne contaminants do not pose a health threat to the users of the parking space. The governing dimensioning criterion to be used is that average CO concentration for a one-hour period should not exceed 35 $mg/m^3$ which equates to 30 $ppm$. For constantly manned areas, airflows are to be dimensioned in such a way that instantaneous CO concentration does not exceed 7 $mg/m^3$ (6 $ppm$). [9]

In addition to the YM regulation, an instructional text on the interpretation of the YM regulation has been written by Talotekniikkainfo [28]. The instructional text specifies that when the contaminant load of the parking space is unknown, the dimensioning of air flow rate should be done using square-meter-based minimum values according to Eq. 1

$$q_v = n\ x\ 0.9 \frac{dm^3}{s,m^2} \quad (1)$$

where $n$ is a factor dependent on the type of the building the parking space serves. Eq. 1 is also the dimensioning equation from the recently repealed Building Code D2. The instructional text goes on to specify that alternatively, the dimensioning of air flow rate can be done based on a known contaminant load and air flow rates smaller than those suggested by Eq. 1 can be justified to the local construction supervision if a number of conditions including specifications on the monitoring of CO concentration are met. The instructional text specifies instances where the reduction of air flow rates using VAV-control is justified:

- Ventilation can be switched off outside of parking space operating hours if CO concentration is below 6 ppm.
- Ventilation can be reduced to a minimum of e.g. 30 % of maximum air flow rate if CO concentration during operating hours is below 9 ppm.
- Ventilation can be controlled on an on-demand basis e.g. 30 %-100 % of maximum air flow rate when CO concentration is 9-50 ppm.
- Ventilation at maximum air flow rate when CO concentration exceeds 50 ppm.
- Alarm when CO concentration exceeds 70 ppm.

Notably, the instructional text written by Talotekniikkainfo references the manual "*Moottoriajoneuvosuojan ilmanvaihdon mitoitusopas. Ympäristöministeriö. 2017"* which is still in draft stage and has not yet been published. This attests to the fact that the situation with official instructions for ventilation design for parking spaces is alive and not very consolidated at the moment of writing, which further adds to the motivation of researching novel ways of calculating optimal air flow rates as part of parking space ventilation design.

## *2.5 Ambient CO concentration*

Measurements of a range of contaminants in the ambient air have been carried out in Tampere by city officials, but the monitoring of carbon monoxide levels specifically has been discontinued 2009. [29] More recent data is available from measurements carried out by HSY in Helsinki. [30] Appendix 1 contains a cited page of measurement data with annual average ambient CO concentrations in the Helsinki region. The value 0.5 ppm is chosen to be the simulated ambient CO concentration $\Phi_0$, from the high end of reported ambient CO concentrations.

# 3 Theoretical basis for the used methodology

## *3.1 MS Excel based simulation*

### 3.1.1 Pressure Correction Method

For the purpose of the MS Excel based calculation, the decks of the Tampereen Kansi parking space are modelled as a large system of ducts with varying rectangular cross-sections, interconnecting at the slips that connect the decks. The Excel based calculation relies on the pressure correction method laid out by Ptankar, 1980 [31] and Siikonen, 2014 [32]. The pressure correction method is an iterative algorithmic sequence that is well suited for determining pressures and flow-rates in branching and interconnecting systems of ducts. The pressure correction method was likely one of the first elementary CFD algorithms [32]. The pressure correction method is implemented into an Excel VBA program i.e. an Excel macro, the structure of which can be found as a block diagram in Appendix 3. In the following description of the pressure correction method, intermediate results of the pressure correction iteration are denoted with a star " $*$ ", results from the previous iteration round with " $n$ ", correction terms are denoted with an apostrophe " $'$ " and the error term in mass-flows is denoted by capital delta " $\Delta$ ". A singular subscript e.g. " $i$ " denotes a value at a node point $i$ and a twin subscript e.g. " ij " denotes a value between nodes $i$ and j.

The flow between two nodes $i$ and $j$ can be described in a simplified manner by the equation

$$\frac{1}{2}K_{ij}\rho u_{ij}|u_{ij}| = p_i - p_j \tag{2}$$

wherein $K_{ij}$ is a lumped pressure loss coefficient between points $i$ and $j$ that includes the friction loss and minor losses incurring between these points. Equation 2 is modified into

$$\frac{1}{2}K'_{ij}\dot{m}_{ij}|\dot{m}_{ij}| = p_i - p_j \tag{3}$$

where the velocities $u_{ij}$ are now replaced by corresponding mass flows $\dot{m}_{ij}$ and $K'_{ij} = K_{ij}/\rho S_{ij}^2$ is described by Siikonen as a dimensional friction factor, $S_{ij}$ being the cross-sectional area of the duct that connects nodes $i$ and $j$. After linearization, Eq. 3 becomes

$$\Delta\dot{m}_i^* = \left[-\frac{1}{2}K'_{ij}|\dot{m}_{ij}^n| + \left(p_i^n - p_j^n\right)\right]/(K'_{ij}|\dot{m}_{ij}^n|) \tag{4}$$

It proves useful in simplifying the equations to write the denominator (in normal brackets) as *alpha terms* [33]

$$\alpha_{ij} = K'_{ij}|\dot{m}_{ij}^n| \tag{5}$$

For time-accurate calculation and to take into account the inertia of the fluid, a term is added into the square brackets yielding

$$\Delta\dot{m}_i^* = \left[-\frac{1}{2}K'_{ij}|\dot{m}_{ij}^n| + \left(p_i^n - p_j^n\right) - l_i * \frac{\dot{m}_{ij}^* - \dot{m}_{ij}^n}{\rho * S_{ij} * dt}\right] / (K'_{ij}|\dot{m}_{ij}^n|) \quad (6)$$

, which written using the alpha term notation becomes

$$\Delta\dot{m}_i^* = \left[-\frac{1}{2}K'_{ij}|\dot{m}_{ij}^n| + \left(p_i^n - p_j^n\right) - l_i * \frac{\dot{m}_{ij}^* - \dot{m}_{ij}^n}{\rho * S_{ij} * dt}\right] / \alpha_{ij} \quad (7)$$

, where $l_i$ is the length of the control volume and $dt$ is the chosen length of time step. [33] For the control volumes that host the jet fans, the head they produce is also added into Eq. 7 as a source term, added into the square brackets as summation. Eq. 7 is the momentum equation for the pressure correction method. In addition to the momentum equation, for every node point $i$ the continuity equation

$$\sum_{i \neq j} \dot{m}_{ij} = 0 \quad (8)$$

must hold. Finally, the core of the pressure correction method is the pressure correction equation

$$\sum_{j \neq i} \frac{p'_i - p'_j}{K'_{ij}|\dot{m}_{ij}^*|} = -\Delta\dot{m}_i^* \quad (9)$$

where again we make use of the alpha term simplification such that

$$\sum_{j \neq i} \frac{p'_i - p'_j}{\alpha_{ij}} = -\Delta\dot{m}_i^* \quad (10)$$

The alpha term simplification proves very useful when writing out the system of equations produced by Eq. 9. For example for node 2 that has two neighboring nodes 1 and 3, if we expand Eq. 9 we obtain

$$\frac{p'_1 - p'_2}{K'_{12}|m_{12}^*|} + \frac{p'_2 - p'_3}{K'_{23}|m_{23}^*|} = -\Delta m_2^*$$

$$=> p'_2 = \frac{-\Delta m_2^* K'_{12}|m_{12}^*|K'_{23}|m_{23}^*| - p'_1 K'_{23}|m_{23}^*| + p'_3 K'_{12}|m_{12}^*|}{K'_{12}|m_{12}^*| - K'_{23}|m_{23}^*|} \quad (11)$$

And for node 5 that has three neighboring cells 4, 6 and 12 we obtain

$$\frac{p'_4 - p'_5}{K'_{45}|m_{45}^*|} + \frac{p'_5 - p'_6}{K'_{56}|m_{56}^*|} + \frac{p'_5 - p'_{12}}{K'_{512}|m_{512}^*|} \quad (12)$$

$$=> p'_5$$
$$= (-\Delta m_5^* K'_{45}|m_{45}^*|K'_{56}|m_{56}^*|K'_{512}|m_{512}^*| - p'_4 K'_{56}|m_{56}^*|K'_{512}|m_{512}^*| +$$
$$p'_6 K'_{45}|m_{45}^*|K'_{512}|m_{512}^*| + p'_{12} K'_{45}|m_{45}^*|K'_{56}|m_{56}^*|)$$
$$/ (K'_{45}|m_{45}^*|K'_{512}|m_{512}^*| + K'_{45}|m_{45}^*|K'_{56}|m_{56}^*| + K'_{56}|m_{56}^*|K'_{512}|m_{512}^*|) \quad (13)$$

It is easy to foresee that writing the pressure correction equations for a large quantity of nodes in this expanded form becomes overwhelmingly tedious and error-prone. Instead, by utilizing the simplification into alpha terms, the pressure correction equations for the same example nodes simplify into

$$p_2' = \frac{-\Delta m_2^* + \frac{p_1'}{\alpha_{12}} + \frac{p_3'}{\alpha_{23}}}{\frac{1}{\alpha_{12}} + \frac{1}{\alpha_{23}}} \tag{14}$$

and

$$p_5' = \frac{-\Delta m_5^* + \frac{p_4'}{\alpha_{45}} + \frac{p_6'}{\alpha_{56}} + \frac{p_{12}'}{\alpha_{512}}}{\frac{1}{\alpha_{45}} + \frac{1}{\alpha_{56}} + \frac{1}{\alpha_{512}}} \ . \tag{15}$$

The equations utilized in the pressure correction method describe flow behavior within and between control volumes defined around node points: pressure is calculated at a node point in the middle of a control volume and mass flows are calculated at the edges of the control volumes in what is known as a staggered grid approach. The pressure correction method iterates for pressure values at node points and mass flow values at control volume interfaces that satisfy both the momentum equation Eq. 7 and the continuity equation Eq. 8 simultaneously for every control volume in the calculation domain. Figure 15 depicts the modeled pipe system and staggered grid approach. The dashed red lines depict control volumes and the black circles depict nodes that the momentum equation and continuity equation are describing. Black lines are the pipes connecting the nodes. Horizontal lines represent the parking space in longitudinal direction. Vertical lines represent the slips that connect decks.

Where supply air is fed into the system, the mass flow values are marked with a blue “S”. Where fresh air is freely taken into the system, the mass flows are marked with a blue “F”. Where air is exhausted out of the system, the mass flow values are marked with a red “E”.

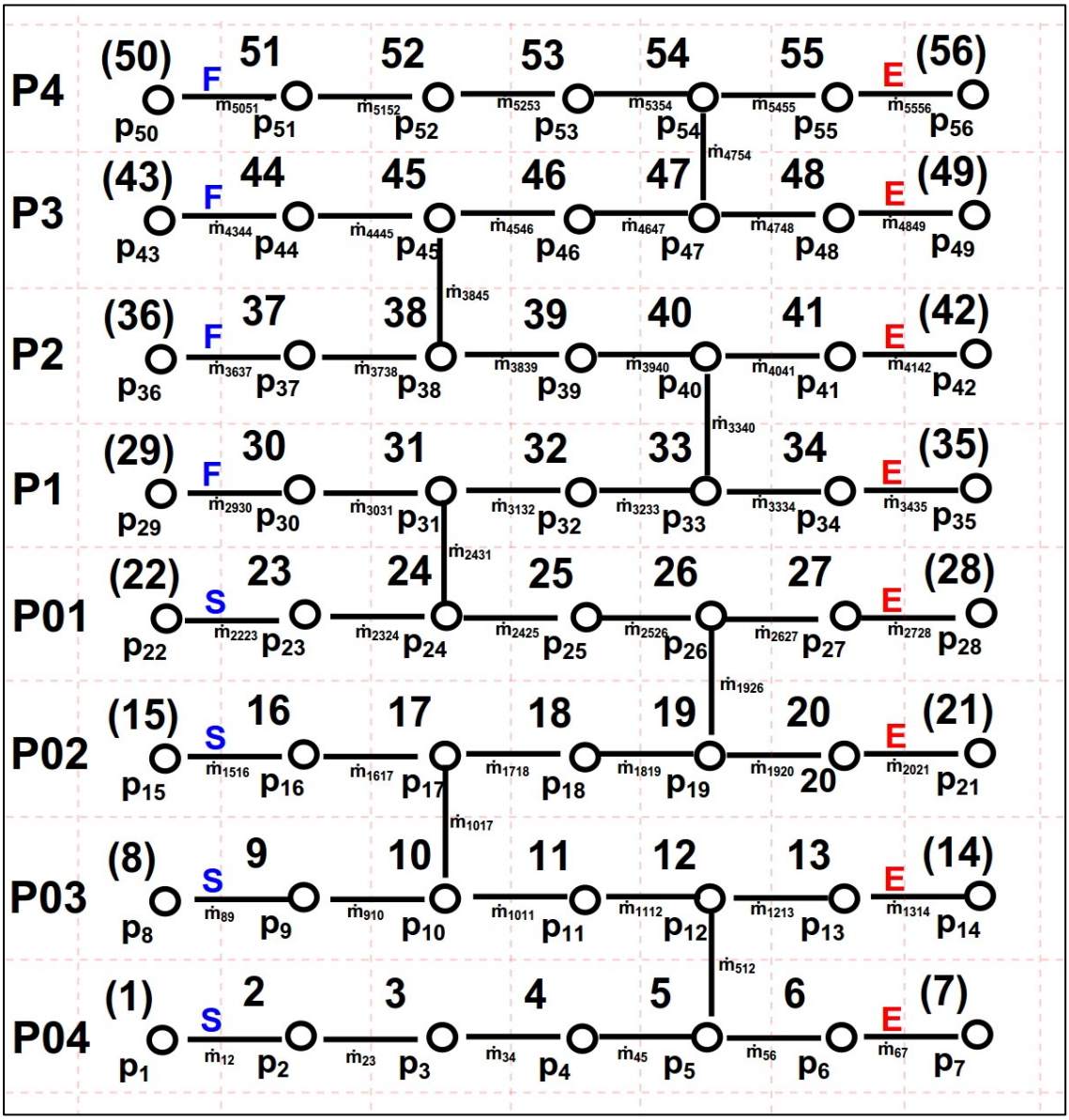


*Figure 15. Decks P01 to P4 modelled as a pipe system.*

Ghost cells, written in brackets in Figure 15, are used to produce the necessary boundary conditions for the pressure correction scheme. It is also through the boundary conditions for mass flow that the user-defined supply and exhaust air flow rates are given to the calculation. The desired boundary conditions are created by modifying equations for pressure correction and mass balance for the ghost cells. The cells that are assigned boundary conditions, their physical representations and the modifications these cells receive are listed in Table 6. Continuity is not monitored for in the ghost cells – it can't be since the ghost cells have no neighbouring cells on the other side. For a more detailed view on how the nodes are placed in relation to the parking space geometry, see Figure 20.

*Table 6. Cells assigned boundary conditions and boundary condition treatments*

| Cells | Represent | Boundary condition | Modifications made |
|---|---|---|---|
| 50, 43, 36, 29 | Outside air | For pressure | Pressure is always the inverse of pressure at nodes 51, 44, 37, 30 respectively. Hence reference pressure 0 is always found between these 50-51, 43-44 etc. |
| 1, 8, 15, 22 | Inside air right outside of supply air shaft | For pressure and mass flow | Pressure is always equal to pressure at nodes 2, 9, 16, 23 respectively. Mass flow values are fixed and not updated during the pressure correction iteration. |
| 7, 14, 21, 28, 35, 42, 49, 56 | Inside air right outside of exhaust shaft | For pressure and mass flow | Pressure is always equal to pressure at nodes 6, 13, 20, 27, 34, 41, 48, 55 respectively. Mass flow values are fixed and not updated during the pressure correction iteration. |

The iteration algorithm, as described by Siikonen, proceeds as follows

1. The pressure values from the last iterations cycle are used to compute mass-flows according to momentum equation Eq 7. In the case of the first iteration cycle, initial guess values are used, typically 0 for all pressure nodes except known boundary pressures.

2. The error in mass balance $\Delta\dot{m}_i^* = \sum_{i\neq j} \dot{m}_{ij}^*$ is computed for each node except for the ghost cells. If the absolute value of $\Delta\dot{m}_i^*$ is below a pre-defined accuracy for each calculated node, the continuity equation holds, the pressure correction iteration is complete and the sequence is terminated. If not, move to phase 3.

3. The linear system of equations formed by the pressure correction equation Eq. 10 is solved. In the implementation of the present work, Gauss-Seidel iteration is applied for numerical solving of the system of equations.

4. Pressure values $p_i$ are corrected with the newly found correction terms $p_i'$ such that $p_i = p_i^* + \beta p_i'$ where $\beta$ is an optional under-relaxation factor. Mass flow corrections are calculated such that $\dot{m}_{ij}' = \frac{p_i' - p_j'}{\alpha_{ij}}$. Mass-flow values are updated according to $\dot{m}_{ij} = \dot{m}_{ij}^* + \dot{m}_{ij}'$. The sequence is then looped back to step 1.

### 3.1.2 Gauss-Seidel iteration

The Gauss-Seidel iteration method is applied in the numerical solving of the linear system of pressure correction equations in step 3 of the pressure correction iteration sequence i.e. this is an iteration within an iteration. The Gauss-Seidel -method is chosen since it is relatively simple to implement into VBA code and makes for a short and elegant While-loop structure.

The principle of the Gauss-Seidel iteration is laid out by Kreyszig, 2003. [34] The general formulas for Gauss-Seidel iteration, written in matrix form are quoted from Kreyszig.

It is assumed that $a_{jj} \neq 1$ for $j = 1, \ldots n$. Starting with

$$\boldsymbol{A} = \boldsymbol{I} + \boldsymbol{L} + \boldsymbol{U} \tag{16}$$

and

$$\boldsymbol{Ax} = \boldsymbol{b} \tag{17}$$

where $\boldsymbol{I}$ is the $n\ x\ n$ unit matrix, $\boldsymbol{L}$ and $\boldsymbol{U}$ are the lower and upper triangular matrices with zero main diagonals respectively, $\boldsymbol{A}$ is a square $n \times n$ matrix for which $a_{jj} \neq 0$ for all $j = 1, \ldots, n$. Substituting Eq. 17 into Eq. 16 yields

$$\boldsymbol{Ax} = (\boldsymbol{I} + \boldsymbol{L} + \boldsymbol{U})\boldsymbol{x} = \boldsymbol{b} \tag{18}$$

Moving $\boldsymbol{Lx}$ and $\boldsymbol{Ux}$ to the right side of Eq. 18 leads to

$$\boldsymbol{x} = \boldsymbol{b} - \boldsymbol{Lx} - \boldsymbol{Ux} \tag{19}$$

Since $\boldsymbol{Ix} = \boldsymbol{x}$.

The Gauss-Seidel method is defined by the iteration formula

$$\boldsymbol{x}^{(m+1)} = \boldsymbol{b} - \boldsymbol{L}\boldsymbol{x}^{(m+1)} - \boldsymbol{U}\boldsymbol{x}^{(m)} \tag{20}$$

where $\boldsymbol{x}^{(m)} = [x_j^{(m)}]$ is the $m$th approximation and $\boldsymbol{x}^{(m+1)} = \left[x_j^{(m+1)}\right]$ is the $(m+1)$st approximation.

Put verbally in the form of an algorithm, descriptive of how the Gauss-Seidel method is implemented in the present work since matrix calculation is not utilized:

1. An initial quess of $p_i' = 0$ is made for all pressure correction terms that are treated as variables
2. Each equation from the linear system of equations that results from Eq. 10 is solved for one of the variables
3. Values are calculated for each variable
4. Calculated values are substituted into the remaining equations immediately upon being calculated
5. Once every variable has a value, the newest values are compared to their previous values. While the difference of two subsequent values is greater than a pre-defined convergence criterion, the sequence is looped back to step 2 and new values are calculated for each variable, always utilizing the newest available values in the remaining equations. When the convergence criterion is met, the iteration is stopped and the resulting pressure correction term $p_i'$ values are stored and used for correcting pressure terms.

### 3.1.3 Contaminant balance

The supply air entering the parking space is always carrying the ambient CO concentration $\Phi_0$ with it and before the first time step at $t = 0$ the zones are all filled with air containing this concentration. From $t = 1$ onwards the space is populated by vehicles according to an hourly diurnal schedule estimated by Ramboll Traffic & Infrastructure department. The hourly traffic data is distributed to correspond with the second based flow calculation. To realistically simulate CO concentration inside the parking space, the movement of the vehicles and their transient CO emissions must be accounted for. Hence the *routes* that the vehicles drive when parking into or diving out from each zone are built separately. Each zone in the Excel model is assigned a probability that a vehicle will park there. The same probabilities are applied for vehicles leaving the parking space. Importantly, the arriving and leaving vehicles are handled separately, since their emissions are different due to the leaving vehicles starting with cold engines. Also, gasoline and diesel driven vehicles are handled separately due to varying emissions.

The sequence of code that takes place when the program arrives at a simulated second that contains the event of an arriving / leaving vehicle (see Appendix 3), achieves the following:

1. Draw a lottery for whether the vehicle is gasoline or diesel driven. The probabilities for this lottery are derived from the data presented in Figure 9 that describes the Finnish vehicle stock.
2. Draw a lottery for which zone the vehicle is going to park in / leave from.
3. Based on the lottery results, a route is built in either the $N_{DA}$ , $N_{DL}$ , $N_{GA}$ or $N_{GL}$ column by incrementing the cell values by 1 for the duration of seconds (= number of rows) that it takes to drive through each zone. In case of a leaving vehicle, the first second of departure also receives an incrementation by 1 in the $N_{DS}$ or $N_{GS}$ column, that represent the engine start for diesel and gasoline vehicles respectively. Since the slips are not control volumes of their own, when passing through a slip, half of the emission from driving through the slip is assigned to the cell that precedes the slip and half is assigned to the cell that follows the slip. In the Excel spreadsheet, the routes are visible in the *Calculation* sheet as vertical successions of entries in the aforementioned columns that describe the number of running engines and their types in each cell.

For each cell, one to three mass flow rates are associated with the mass balance of the cell. A series of IF-statements is utilized to determine which flows are towards the cell node, counted as incoming flow $q_{in}$ and which are counted as outflow $q_{out}$. Likewise, the same series of IF-statements are utilized to determine for each cell, from which neighboring cell or cells the incoming concentration $\Phi_{in}$ is flowing from. The terms for incoming mass flow of CO for each cell are then calculated by summing $\Sigma q_{in,i}\Phi_{in,i}$.

The CO concentration for the ghost cells at the entrance is always equal to $\Phi_0$, meaning that air carrying the ambient concentration is always flowing into the space to replace the dirtier air within. The ghost cells at the exhaust shafts will always receive the same value for concentration as the last cell located on the deck right before the shaft. For the rest of the cells, concentration at the $n$:th time step is solved for by Eq. 21

$$\Phi_{i,n} = \Phi_{i,n-1} + \frac{\Delta t}{V_i}(\Sigma q_{in,i,n}\Phi_{in,i,n-1} - q_{out,i,n}\Phi_{i,n-1} + N_{GA} * \dot{m}_{CO,GA} + N_{DA} * \dot{m}_{CO,DA} + N_{GL} * \dot{m}_{CO,GL} + N_{DL} * \dot{m}_{CO,DL} + N_{GS} * \dot{m}_{CO,GS} + N_{DS} * \dot{m}_{CO,DS}) \quad (21)$$

, where

$q_{in}$ and $q_{out}$ are the flow rates in and out of the cell $[q] = \frac{m^3}{s}$
$\Phi_{in,i,n}$ is the incoming CO concentration for node i at time step n $[\Phi] = \frac{kg}{m^3}$
$\Phi_{i,n}$ is CO concentration for node i at time step n
$\Delta t$ is the length of the timestep $[\Delta t] = s$
$V_i$ is the air volume of cell i $[V] = m^3$
$N_{GA}$ is the number of arriving gasoline driven vehicles with engines running
$N_{GL}$ is the number of leaving gasoline driven vehicles with engines running
$N_{DA}$ is the number of arriving diesel driven vehicles with engines running
$N_{DL}$ is the number of leaving diesel driven vehicles with engines running
$N_{GS}$ is the number of arriving gasoline driven engine starts
$N_{DS}$ is the number of arriving diesel driven engine starts
$\dot{m}_{CO,GA}$ is the emission rate of CO from arriving gasoline vehicle $[\dot{m}] = \frac{kg}{s}$
$\dot{m}_{CO,GL}$ is the emission rate of CO from leaving gasoline vehicle
$\dot{m}_{CO,DA}$ is the emission rate of CO from arriving diesel vehicle
$\dot{m}_{CO,DL}$ is the emission rate of CO from leaving diesel vehicle
$\dot{m}_{CO,GS}$ is the emission rate of CO from a gasoline driven engine start
$\dot{m}_{CO,DS}$ is the emission rate of CO from a disel driven engine start

Concentration values are printed both in $\frac{kg_{CO}}{m^3_{air}}$ and in $ppm$. As each $ppm$ is one cubic centimeter of CO in one cubic meter of air, the $\frac{kg_{CO}}{m^3_{air}}$ value that corresponds to a $ppm$ value is found by multiplying the $ppm$ value by $10^{-6}$ (in essence how many cubic meters of CO in a cubic meter of air) then multiplying by the density of CO (how much does the CO in a cubic meter of air weigh). The resulting value is still per cubic meter of air, which is exactly what was sought after. Put as a formula, values are converted from $ppm$ to $\frac{kg}{m^3}$ by Eq. 22

$$x\ ppm_{CO} * 10^{-6}\frac{m^3_{CO}}{cm^3_{CO}} * \rho\frac{kg_{CO}}{m^3_{CO}} = x\frac{cm^3_{CO}}{m^3_{air}} * 10^{-6}\frac{m^3_{CO}}{cm^3_{CO}} * \rho\frac{kg_{CO}}{m^3_{CO}} = y\ \frac{kg_{CO}}{m^3_{air}} \quad (22)$$

and correspondingly form $\frac{kg_{CO}}{m^3_{air}}$ to $ppm$ by Eq. 23

$$(\ y\ \frac{kg_{CO}}{m^3_{air}} /\ \rho_{CO}\ )\ *\ 10^6\ \frac{cm^3_{CO}}{m^3_{CO}} = x\ ppm_{CO} \quad (23)$$

## 3.2 Ansys Fluent simulation

### 3.2.1 Description of CFD as a research tool

Computational fluid dynamics combines the fields of fluid mechanics, mathematics and computer science, in order to produce numerical simulations of fluid flow behavior. In essence, mathematical expressions usually in the form of partial differential equations describing physical characteristics of fluid motion are solved iteratively by software packages running on high-speed digital computers to obtain a numerical solution for a flow field. Experimental and analytical methods have commonly been used in industrial product and process design problems involving fluid flow. The numerical simulations made possible by modern computers running CFD software are gaining in favor and being increasingly relied upon as a complimentary and sometimes alternative method. Compared to analytical and experimental methods, CFD offers a cost-effective method of studying and obtaining information on flow situations that can be either hard, expensive or impossible to accurately recreate in an experimental setting – as is the case for a building project still in its planning stage. In cases where empirical methods in the form of physical measurements and direct experimentation are possible, CFD can provide an unmatched level of detail in the visualization of results and can thus supplement the empirical methods. For these reasons CFD is being applied in an increasingly widespread array of engineering problems and the trend is likely to continue as the diminishing cost of computational resources makes extensive CFD analysis increasingly affordable. CFD simulations always contain some numerical error, however, and as the numerical calculations are iterative and approximative in nature, some differences between the computed results and measured reality are likely to occur and the numerically calculated results are not to be taken as a perfect representation of the flow domain in reality. [35]

For the purposes of the present work, an established and validated CFD software Ansys Fluent is utilized in the calculation of pressure loss coefficients for pipe sections in the Excel model. Results computed by the Excel model are also compared to results computed via Fluent simulations. The benefit of comparing the two models is two-fold. On the other hand the comparison acts as validation for the Excel model and on the other hand the Excel model produces transient data that can be used in improving the time-averaging done in future Fluent models of parking spaces.

Ansys Fluent combines comprehensive flow modelling capabilities with the readiness to model complex geometries. The software includes options for accurate turbulence modelling and near-wall treatment, encompassing the effects of physical phenomena such as buoyancy. [36] The Ansys software will be utilized for all steps of the CFD analysis carried out for the parking space ventilation: geometry modelling, meshing, simulation runs and post-processing.

### 3.2.2 Governing equations

The Fluent CFD software predicts a forming flow field – in this case the flow of air within the parking space – by solving a set of fundamental flow equations derived from the study area of fluid dynamics. The set of equations relevant to the simulation of the parking space ventilation is well documented in the Ansys Fluent 17 Documentation [36] and the following formulae and their descriptions have been selectively quoted from the said documentation. These equations include:

1. Equation of continuity i.e. an equation for mass conservation

$$\frac{\partial \rho}{\partial t} + \nabla \cdot (\rho \vec{v}) = S_m \tag{24}$$

where $\rho$ denotes density, $t$ time, $\vec{v}$ is the velocity vector and $S_m$ is a source term for mass added to the continuous phase from the dispersed second phase (applicable for multi-phase flow) and/or any user-defined sources.

2. Conservation equation for momentum in the three coordinate directions of three-dimensional space

$$\frac{\partial}{\partial t}(\rho \vec{v}) + \nabla \cdot (\rho \vec{v} \vec{v}) = -\nabla p + \nabla \cdot (\bar{\bar{\tau}}) + \rho \vec{g} + \vec{F} \tag{25}$$

where $p$ denotes static pressure, $\rho \vec{g}$ and $\vec{F}$ are the gravitational and external body forces respectively and $\bar{\bar{\tau}}$ is the stress tensor

$$\bar{\bar{\tau}} = \mu \left[ (\nabla \vec{v} + \nabla \vec{v}^T) - \frac{2}{3} \nabla \cdot \vec{v} I \right] \tag{26}$$

with $\mu$ denoting molecular viscosity, $I$ is the unit tensor and the second term on the right-hand side is the effect of volume dilation.

3. Equation for energy conservation

$$\frac{\partial}{\partial t}(\rho E) + \nabla \cdot \left( \vec{v}(\rho E + p) \right) = \nabla \cdot \left( k_{eff} \nabla T - \sum_j h_j \overrightarrow{J_j} + \left( \bar{\bar{\tau}}_{eff} \cdot \vec{v} \right) \right) + S_h \tag{27}$$

where $k_{eff}$ denotes the effective conductivity, $\overrightarrow{J_j}$ is the diffusion flux of species $j$ and $S_h$ includes the heat of chemical reaction and any other volumetric heat sources defined by the user. The first three terms on right-hand side represent energy transfer due to conduction, species diffusion and viscous dissipation, respectively. In equation (27)

$$E = h - \frac{p}{\rho} + \frac{v^2}{2} \tag{28}$$

where sensible enthalpy h is defined for an ideal gas as

$$h = \sum_j \ Y_j h_j \tag{29}$$

and for incompressible flow as

$$h = \sum_j \ Y_j h_j + \frac{p}{\rho} \tag{30}$$

$Y_j$ denotes the mass fraction of species $j$ and

$$h_j = \int_{T_{ref}}^{T} c_{p,j} dT \tag{31}$$

The value used for $T_{ref}$ in the enthalpy calculation depends on the solver and models in use. For the pressure based solver $T_{ref} = 298{,}15\ K$ except for PDF models in which case $T_{ref}$ is a user input for the species.

4. For the distribution of the CO in the parking space, Fluent predicts the local mass fraction of the species through the solution of a convection-diffusion equation

$$\frac{\partial}{\partial t}(\rho Y_i) + \nabla \cdot (\rho \vec{v} Y_i) = -\nabla \cdot \vec{J}_i + R_i + S_i \tag{32}$$

where $Y_i$ is the $i^{th}$ species, $R_i$ is the net rate of production of species $i$ by chemical reaction and $S_i$ is the rate of creation by addition from the dispersed phase plus any user-defined sources. In equation (32) $\vec{J}_i$ is the diffusion flux of species $i$, which arises due to gradients of concentration and temperature. In turbulent flows, Ansys Fluent computes the mass diffusion in the following form

$$\vec{J}_i = -\left(\rho D_{i,m} + \frac{\mu_t}{Sc_t}\right)\nabla Y_i - D_{T,i}\frac{\nabla T}{T} \tag{33}$$

where $Sc_t$ is the turbulent Schmidt number ($\frac{\mu_t}{\rho D_t}$ where $\mu_t$ is the turbulent viscosity and $D_t$ is the turbulent diffusivity). The default $Sc_t$ is 0.7.

5. The modelling of turbulence using the Realizable $k-\epsilon$ model introduces transport equations for the turbulent kinetic energy $k$ and the dissipation of turbulent kinetic energy $\epsilon$ respectively

$$\frac{\partial}{\partial t}(\rho k) + \frac{\partial}{\partial x_j}(\rho k u_j) = \frac{\partial}{\partial x_j}\left[\left(\mu + \frac{\mu_t}{\sigma_k}\right)\frac{\partial}{\partial x_j}\right] + G_k + G_b - \rho\epsilon - Y_M + S_k \tag{34}$$

and (35)

$$\frac{\partial}{\partial t}(\rho \epsilon) + \frac{\partial}{\partial x_j}(\rho \epsilon u_j) = \frac{\partial}{\partial x_j}\left[\left(\mu + \frac{\mu_t}{\sigma_\epsilon}\right)\frac{\partial \epsilon}{\partial x_j}\right] + \rho C_1 S\epsilon - \rho C_2 \frac{\epsilon^2}{k+\sqrt{\nu\epsilon}} + C_{1\epsilon}\frac{\epsilon}{k}C_{3\epsilon}G_b + S_\epsilon$$

where

$$C_1 = \max\left[0.43, \frac{\eta}{\eta+5}\right], \eta = S\frac{k}{\epsilon}, S = \sqrt{2S_{ij}S_{ij}} \quad (36)$$

In these equations $G_k$ represents the generation of turbulence kinetic energy due to the mean velocity gradients. $G_b$ is the generation of turbulence kinetic energy due to buoyancy. $Y_M$ represents the contribution of the fluctuating dilatation in compressible turbulence to the overall dissipation rate. $C_2$ and $G_{1\epsilon}$ are constants. $\sigma_k$ and $\sigma_\epsilon$ are the turbulent Prandtl numbers for $k$ and $\epsilon$ respectively. $S_k$ and $S_\epsilon$ are user-defined source terms.

This set of equations is a coupled set of partial differential equations, meaning that all the equations must be solved simultaneously and iteratively at each point of the flow field. Direct solving of the equations usually results in a demand of computational resources that far exceeds the capabilities of even high-performance computers, certainly so in a case like the parking space ventilation, which involves complex turbulent flow in a large flow domain. [36, 37]

### 3.2.3 Settings

In all of the Fluent simulations examined in the present work, the solver algorithm used is the pressure based SIMPLE algorithm. The turbulence model utilized is the *Realizable* $k-\epsilon$ model, together with scalable wall functions. Further specifications for solution methods and under-relaxation factors are listed in Table 7.

*Table 7. Specifications for solution methods and under-relaxation factors used in Ansys Fluent simulations*

| **Solution Methods** | |
|---|---|
| **Solver algorithm** | |
| Pressure Velocity Coupling: | SIMPLE |
| **Spatial Discretization schemes** | |
| Gradient | Least Squares Cell Based |
| Pressure Velocity Coupling: | PRESTO! |
| Momentum | Second Order Upwind |
| Turbulent Kinetic Energy | Second Order Upwind |
| Tubulent dissipation rate | Second Order Upwind |
| Species | Second Order Upwind |
| Energy | Second Order Upwind |
| **Under-Relaxation Factors** | |
| Pressure | 0.2 |
| Density | 1 |
| Body Forces | 1 |
| Momentum | 0.5 |
| Turbulent Kinetic Energy | 0.5 |
| Turbulent Dissipation rate | 0.5 |
| Turbulent Viscosity | 1 |
| Species | 0.99 |
| Energy | 0.99 |

# 4 Modelling

## 4.1 Modelled parking space geometry

For the Ansys Fluent model the geometry of the structures of the parking space is extracted from an IFC (Industry Foundation Classes) model and inverted to obtain a body that resembles the air volume inside the parking space. The vehicle geometries and jet fan geometries are then distributed to their appropriate locations and cut out of the air volume body. The resulting body is displayed in Figure 16 and Figure 17.

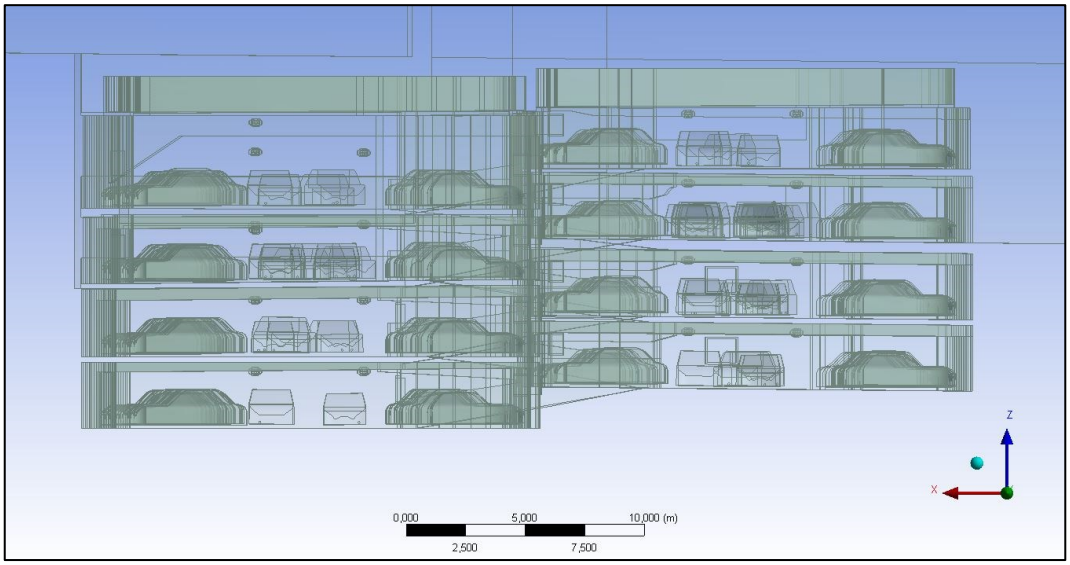


*Figure 16. Complete parking space Geometry for Fluent simulation, transparent side view*

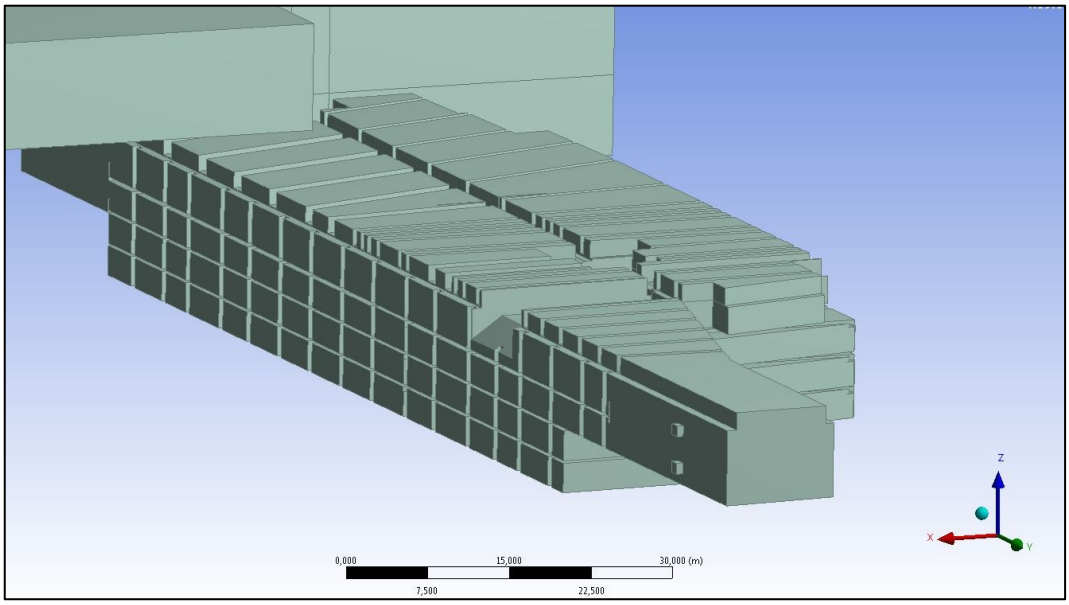


*Figure 17. Complete parking space Geometry for Ansys Fluent simulation, solid*

The geometry displayed in Figure 16 and Figure 17 defines the calculation domain for the Fluent simulations. Next the calculation domain is meshed, i.e. it is divided into small control volumes, for which the governing equations listed in Chapter 3.2.2 are solved. The sizing specifications for the meshing are listed in Table 8. Five inflation layers were added to wall, ceiling, floor and vehicle chassis surfaces, which means that the mesh density is increased by a factor of 1.2 five times, to better capture the details of flow phenomena at these surfaces.

*Table 8. Mesh sizing specifications*

| Mesh sizing | |
|---|---|
| Large straight wall, floor and ceiling surfaces | 3.00E-01 |
| Ventilation ducts | 5.00E-02 |
| Supply and exhaust grilles | 5.00E-02 |
| Jet fan details | 1.00-5.00E-02 |
| Vehicle surfaces | 1.00E-01 |
| Vehicle tailpipes | 1.50E-02 |
| Defeature size | 1.00E-04 |
| Curvature minimum size | 2.50E-03 |
| Global minimum element size | 3.00E-03 |
| Global maximum element size | 6.00E-01 |

The resulting mesh consists of 63.9 million tetrahedral cells. A cross-section of the mesh is displayed in Figure 18 and Figure 19. Figure 19 shows as a detail the inflation layers on floor, ceiling and vehicle chassis surfaces.

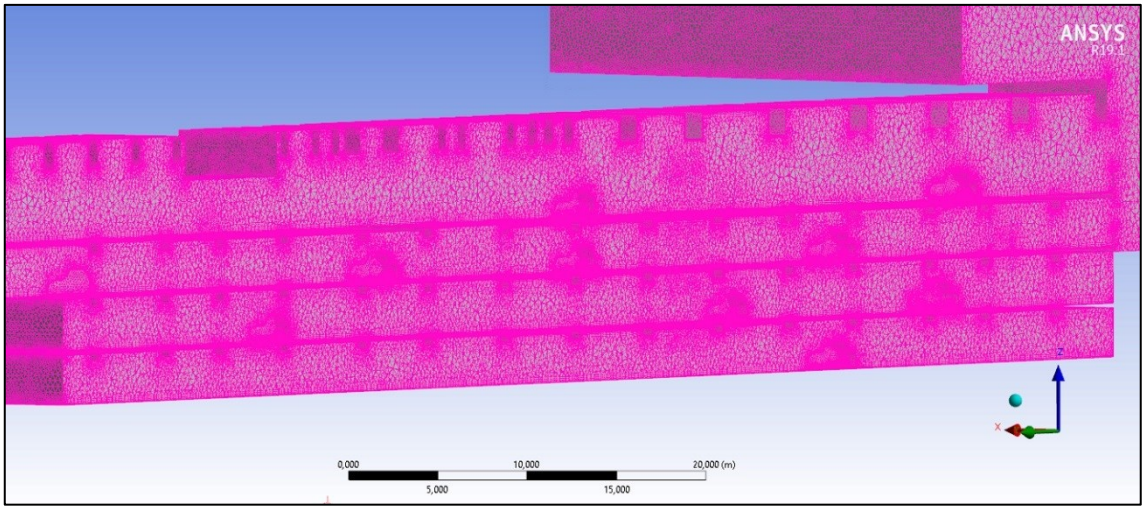


*Figure 18. The tetrahedral mesh of the Ansys Fluent model, cross-section view*

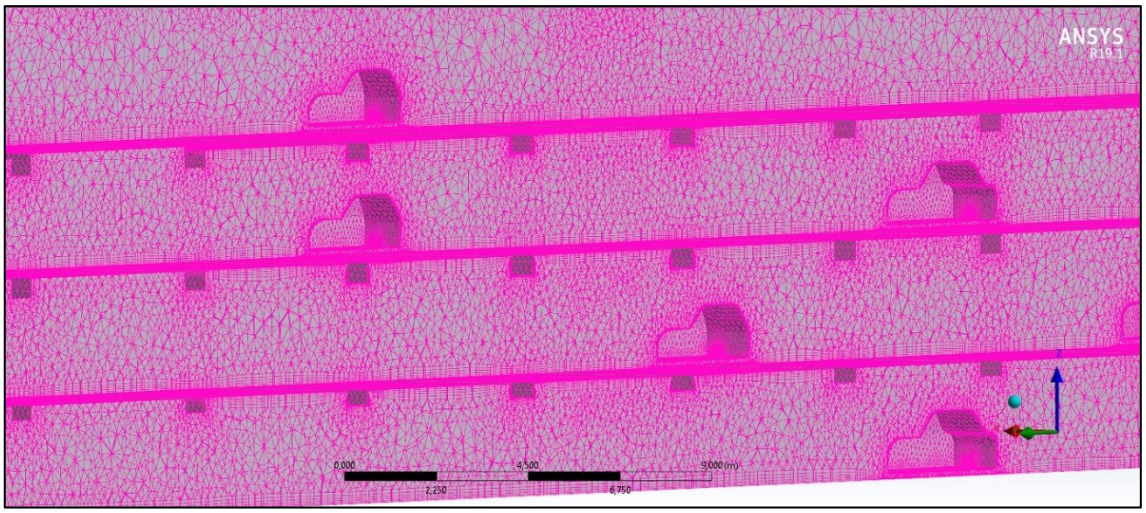


*Figure 19. Mesh details, cross-section view*

In the Excel model the parking space decks are modelled as a system of pipes with varying rectangular cross-section. Figure 20 shows the node placement and overall relation of the modelled pipe system to the actual parking space geometry by overlaying a schematic drawing of the pipe system on the floor plan drawings of the parking space decks. Note that the schematic drawing shows the principal of node placement but the lengths of the pipes are not exact.

Due to unexpected convergence issues when using a varying control volume length $l_i$, the control volume length had to be fixed. To that end, the actual length of the decks was measured from the architect drawings and divided onto the number of control volumes per parking space deck. The control volume length was fixed to $l_i = l_{zone} = 20\ m$ whereby the resulting air volume, now a uniform 4639.6 m³ for every deck in the Excel model, is close to equal to the air volume of deck P1 in the Ansys model. The cross-sectional areas of the deck have been measured from architect drawings, with some averaging applied to exclude small narrowings and widenings of the deck. The cross-sectional areas used in the calculations are listed in Table 9.

*Table 9. Deck cross-sectional areas used in Excel model*

| | | | **Applied for length of cells** |
|---|---|---|---|
| $A_{section,1}$ | 31.23 | m² | 2 and similar |
| $A_{section,2}$ | 47.95 | m² | 3, 4, 5 and similar |
| $A_{section,3}$ | 38.95 | m² | 6 and similar |
| $A_{section,4}$ | 17.95 | m² | slips, between 5 and 12 and similar |

Some error is therefore made in the air volumes – of the smaller underground decks in particular – in the Excel model, but by fixing the control volume length to a uniform value, the convergence issue was averted. Furthermore, since the fact that deck P3 has a larger room height than the other decks is not accounted for in the Excel model, the total air volume of the parking space is close to equal in the Excel and Ansys models, 37117 m³ and 38064 m³

respectively, the difference of which is ~2.5 %. Although the air volume for every deck is uniform in the Excel model, the air volume for each control volume is not uniform due to varying cross-sectional area of the rectangular pipes.

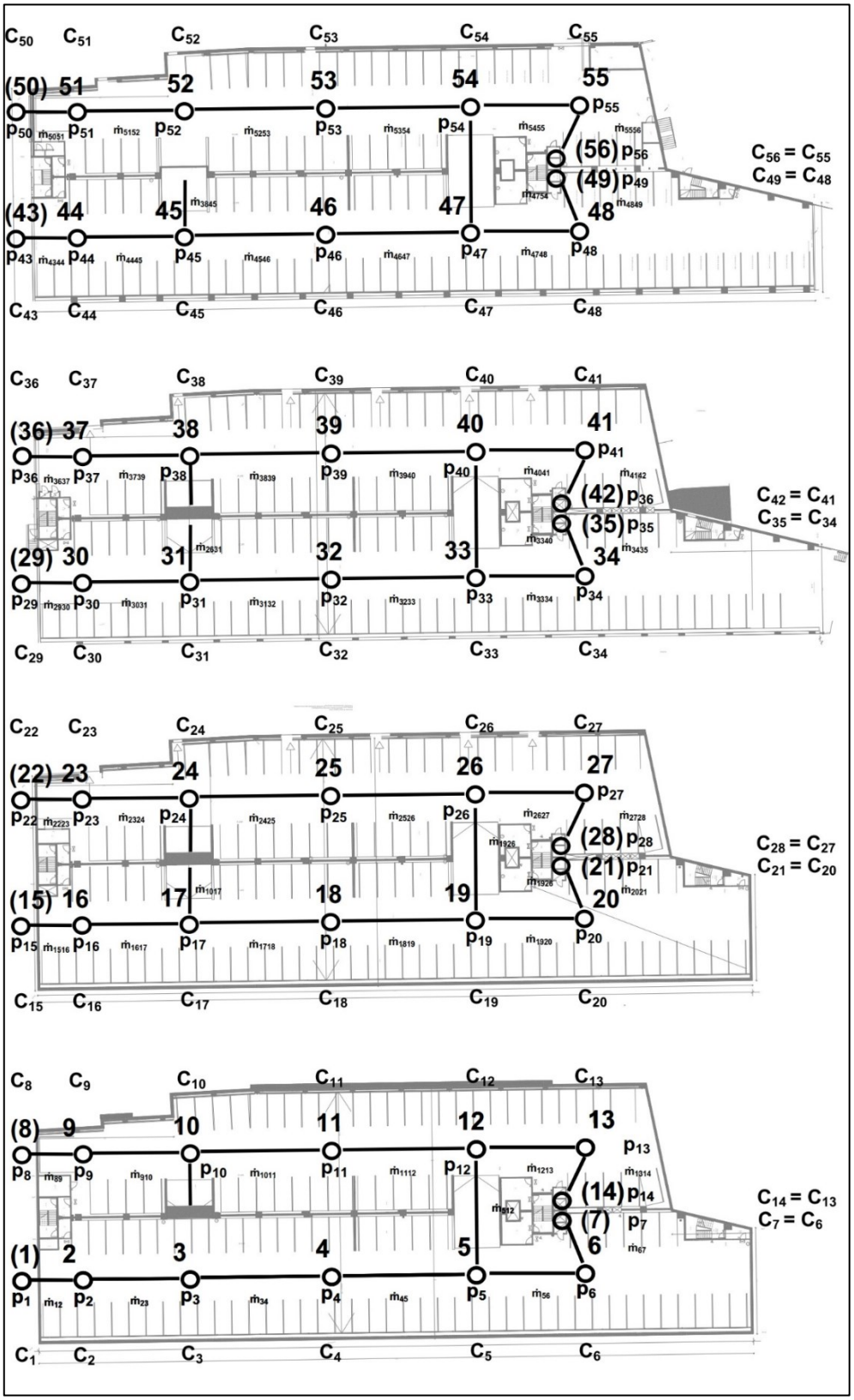


*Figure 20. The parking space modeled as a pipe system, node placement*

Another source of difference between the two models is the modelled geometry of the slips that connect the decks. In the Excel model, the slips are rectangular pipes that are true to the actual geometry of the structure in the sense that their cross-sectional area is measured from architect drawings, but the length of the pipe is longer than in the actual geometry. As can be seen in the node placement in Figure 20, the pipes that represent the slips run from the middle of one deck to the middle of the deck that the slip connects to, making for some extra length at both sides of the actual length of the slip. In the system of nodes and pipes that the pressure correction method solves for, this deviation from the actual parking space geometry was unavoidable. Every node must be connected to another node by a pipe for the iteration to converge. Placing extra nodes exactly at the actual edges of the slip surfaced as a possibility, but in that case, what would be the cross-sectional area for the pipe from the middle of the deck to the edge of the slip? That would essentially be the cross-sectional area of the whole deck in longitudinal direction, and it would be farfetched to assume flow developing throughout the whole deck towards one slip. With this reasoning in mind, the only rational option was to place nodes at the middle of the decks at both sides of the slips and connect them with a rectangular pipe where the cross-sectional area is that of the actual slip and accept the deviation in slip length.

### 4.1.1 Ventilation components

The supply air is provided into the underground parking decks through a shaft and moved by Systemair AXC 630-6/32°-2 axial fans. What is relevant to the simulations, the openings from the shaft to the parking space are rectangular grilles, 1200x1000 mm in dimensions. The Ansys modelled geometry does not contain the axial fans nor any ductwork, only the grilles modelled as surfaces to which *velocity inlet* boundary conditions are applied and assigned positive velocity values (velocity vectors point perpendicularly into the room space) that when multiplied by the grille areas produce the volumetric air flow rates that are to be simulated. The pressure loss of the grilles is not accounted for, because the flow domain of the model does not contain the ventilation ductwork. The extract air is likewise moved by axial fans, the type of which is Fläkt Woods KM Aerofoil. The air is extracted through rectangular grilles with dimensions 1200x800 mm. The exhaust grilles are likewise modelled as surfaces in the Ansys model, with *velocity inlet* boundary conditions applied and assigned negative velocity values (velocity vectors point perpendicularly out from the room space) on the exhaust side to simulate outflow.

In the Excel model, the grilles are represented by ghost cells where fixed mass-flows are assigned as boundary conditions. The situation with pressure losses is the same as in the Ansys model: the pressure losses of the grilles are not accounted for, because duct work before them is outside of the flow domain.

The jet fans responsible for diluting contaminants and moving contaminated air towards the exhaust grille are of the type Fläkt Woods Low Profile. Appendix 2 shows a schematic drawing, dimensions and technical specifications of the jet fan. The close to horizontal flap depicted at both openings in the schematic, can be used to direct the flow pattern produced by the jet fan. The jet fans will be fixed to the ceiling between beams that are orthogonal to the direction the jet fans are blowing. To avoid the jet colliding into or attaching to the side or

bottom of the adjacent beam (and from there to the ceiling) the jet must be guided downwards by assigning the flaps an angle. Figure 21 shows the modelled jet fans in the Ansys model geometry. In the Excel model, jet fans are accounted for as source terms in the momentum equation Eq. 7. The jet fans reside in cells 4, 11, 18 etc. and the head they produce is calculated by dividing the thrust they produce onto the cross-sectional area of the pipe at cells 4, 11, 18 etc.

$$\Delta p_{JF} = \frac{F_{JF}}{A_{section,2}} = \frac{22\ N}{47.95\ m^2} = 0.46\ Pa \tag{37}$$

Calculating the source term $\Delta p_{JF}$ that is added into Eq. 7 like this leads to a miniscule pressure difference before and after the jet fan and a negligible effect of the jet fans in the Excel modelling. This is attributable to the main weakness of the Excel model: it is 1-dimensional in nature and very coarse in resolution, it is simply incapable of capturing flow phenomena as local as the jet produced by a jet fan.

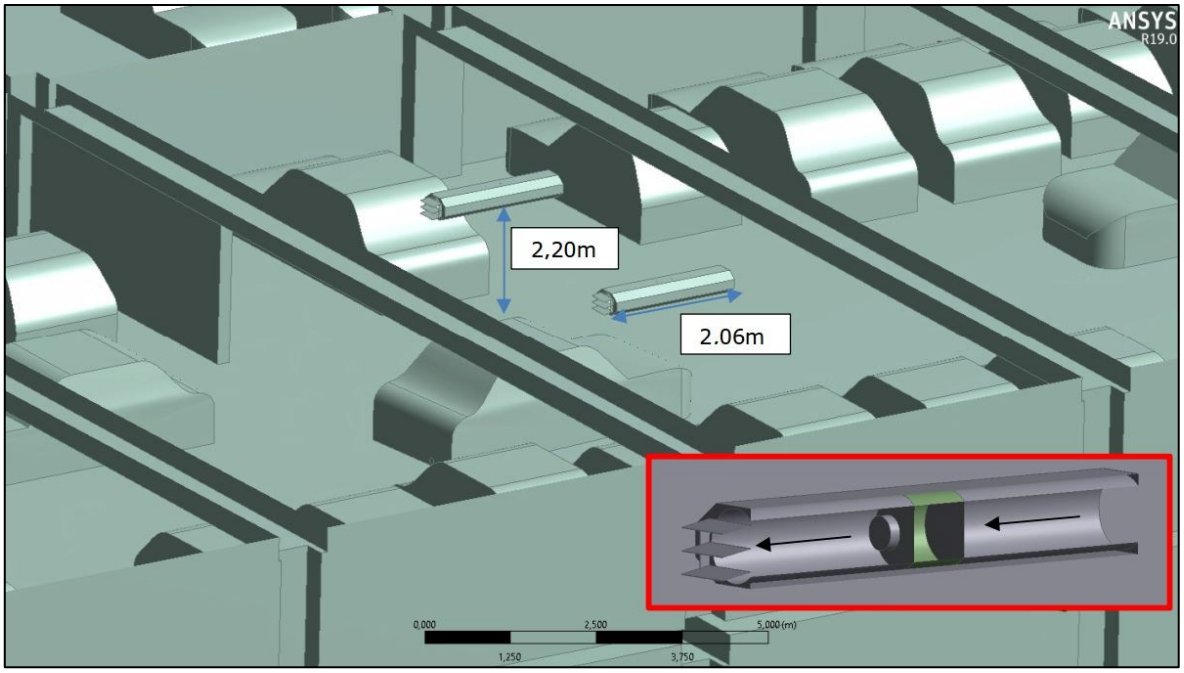


*Figure 21. Jet fan geometry detail screen capture from Ansys Fluent model*

The mesh walls at the gable walls of the above-ground decks P1-P4 are modelled in the Ansys model as being completely open: the mesh wall is assumed to be so loose that its pressure loss is negligible and left outside of examination. A volume of outside air is however modelled outside of the mesh walls and their edges are assigned *pressure outlet* boundary conditions. This is done to correctly simulate the free inflow of air driven by the small underpressure inside the space. Assigning *velocity inlet* conditions at the mesh walls would be erroneous because then flow phenomena related to the air flowing *around* the edges of the opening (like "bubbles" of backward facing flow) would likely be lost. In the Excel model the mesh walls are again represented by ghost cells, but this time not assigned fixed

mass flows. Instead, the mass flows through the mesh wall are computed in the pressure correction iteration sequence as part of the rest of the pipe system: the mass flow through the mesh walls is indirectly determined by the mass flows at exhaust nodes and other inlet nodes and the overall flow field that forms, emulating free inflow. For the Excel model, a lumped pressure loss coeffiecient that encompasses the whole entrance area is computed in Chapter 4.2.

In both of the models, the effect of wind is omitted. The supply and exhaust air flow rates are assumed to be in exact balance for every deck

### 4.1.2 Vehicles

In the Ansys model, the vehicles are modelled with a semi-accurate profile geometry to produce a realistic wake in the flow field. The modeled geometry of the vehicles is short of any details like mirrors, door handles, window frames etc. so as to save computational resources in the meshing phase and in running the simulations. Two types of vehicles are modeled, a sedan type chassis and a hatch-back type chassis. The latter is produced from the former simply by cutting off the tail end of the sedan. Figure 22 displays the vehicle geometries in the midst of the parking space geometry.

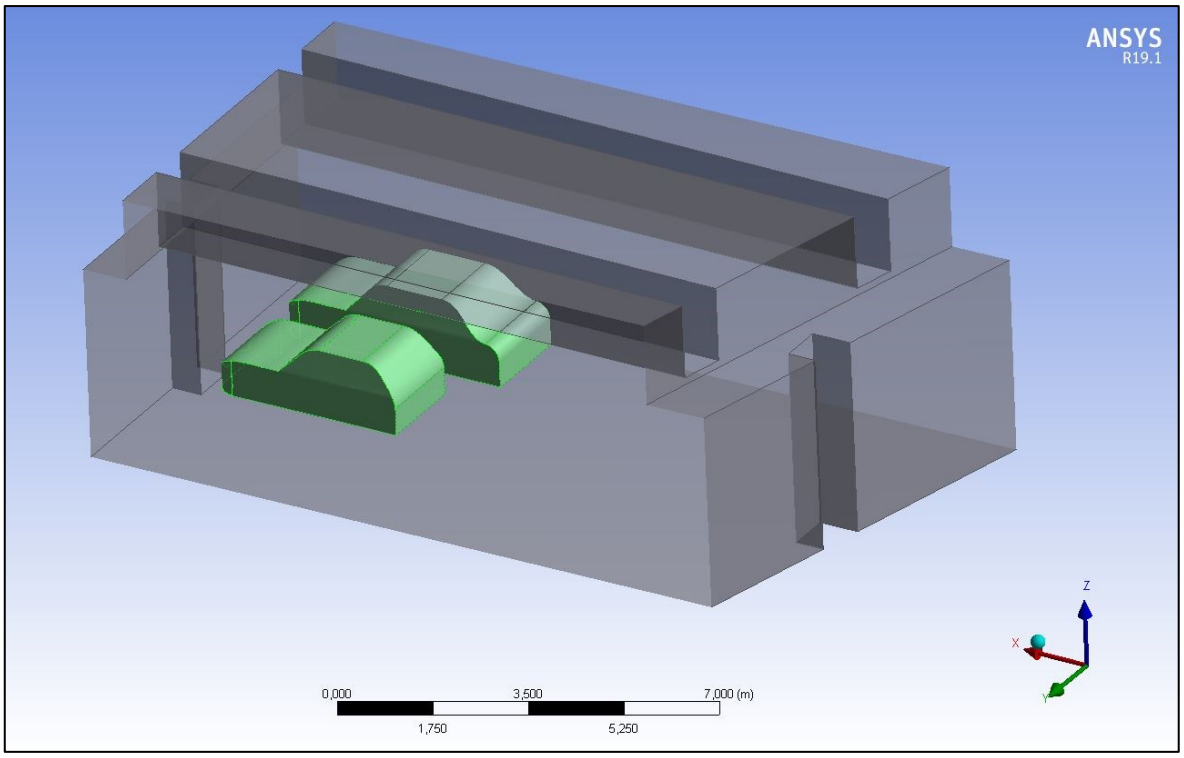


*Figure 22. Vehicle geometry detail screen-capture*

The vehicles are located both at the sides of the decks as parked vehicles and on the lanes as moving vehicles. The tailpipes of the vehicles are modelled as circular surfaces. For the vehicles with running engines, the influx of exhaust gas is assigned in the form of *velocity*

*inlet* boundary conditions. The matter flowing in through the tailpipe velocity inlets, the exchaust gas, is assigned a composition. The velocity value assigned to the exhaust gas is such that when multiplied by the area of the tailpipe circular surface, produces a volumetric flow of 20 $dm^3/s$. The volumetric flow rate of exhaust gas 20 $dm^3/s$ is chosen based on a published CFD study on a shopping center carpark by Al-Waked, R. 2017 [18]

In the Ansys model the chassis surfaces of moving cars are assigned *moving wall* boundary conditions, meaning that they produce a semi-realistic wake pattern in the flow field. The vehicles in the Excel are modelled as moving transient point sources, to which a contaminant generation rate is assigned. In the Excel model, the vehicles do not influence the flow field of air by producing wake nor thrust. Similar to the effect of the jet produced by jet fans, local multi-dimensional flow phenomena such as wake or thrust produced by vehicles would be either impossible or quite meaningless to model due to the one-dimensional and coarse nature of the Excel model.

## 4.2 Calibrating the Excel based model

For each connected node pair $ij$, the lumped pressure loss coefficient $K_{ij}$ in Eq. 2 could be estimated by summing conventional tabulated minor loss coefficient values associated with the bends and cross-section changes etc. happening between nodes $i$ and $j$ and estimating the friction loss by using the Moody diagram. Since a detailed Fluent model of the parking space exists, however, the choice is made to calculate $K_{ij}$ values via simulation using the Fluent model. Three representative parts of a parking space deck – the entrance, the middle and a slip that connects two decks – are cut out from the complete model and airflow through them is simulated. The detailed Fluent model accurately captures the geometry of the parking space including shapes of parked cars, beams in the ceiling and the walls, partitioning walls etc. and solves for fluid behavior around them. The surfaces are assigned surface roughness values that correspond to their materials. Done in this way, more accurate estimates for $K_{ij}$ values can be computed than when using tabulated values. Combining information from the Fluent model with the Excel model in this manner can be thought of as calibration of the Excel model using the best available simulated data.

The geometries of the three characteristic parts of the parking space, cut out and modified from the complete parking space geometry, are shown in Figure 23, along with streamlines associated with computing the $K_{ij}$ values and boundary conditions chosen for the simulation. Each of the three displayed parts outlines a calculation domain of its own, there will be no flow or interaction between the parts. The parts represent the air volume inside the parking space, hence the geometry is inverted, such that the beams, vehicles and other shapes residing inside the space are *cut out* of the geometry. It follows that their shapes are visible as outlines, but from the viewpoint of the calculation, their interior is not part of the flow domain. In the meshing phase, their surfaces will be meshed, but their interior is excluded. Each part contains some free air space before and after the streamline intended for loss coefficient calculation: before to let the flow develop, and after so as to not have the boundary condition control the solution. The boundary condition *velocity inlet* defines a face as the inlet of the flow, where a velocity magnitude, direction and temperature of the fluid are assigned. Here the velocity direction is assigned as normal to the face. The *pressure outlet*

boundary condition mimics the flow being able to continue unhindered into a large space after the face that the boundary condition is assigned to. For the rest of the faces, the default boundary condition *wall* is applied, meaning that the *no-slip* condition applies and velocity is zero at the wall. For the part that resembles the entrance of the parking space, the *velocity inlet* boundary condition is utilized with a negative value – the direction points out from the part – to simulate the air being sucked in from the innermost end and *pressure outlet* is utilized at the entrance to simulate free flow of air into the parking space through the opening in the entrance wall.

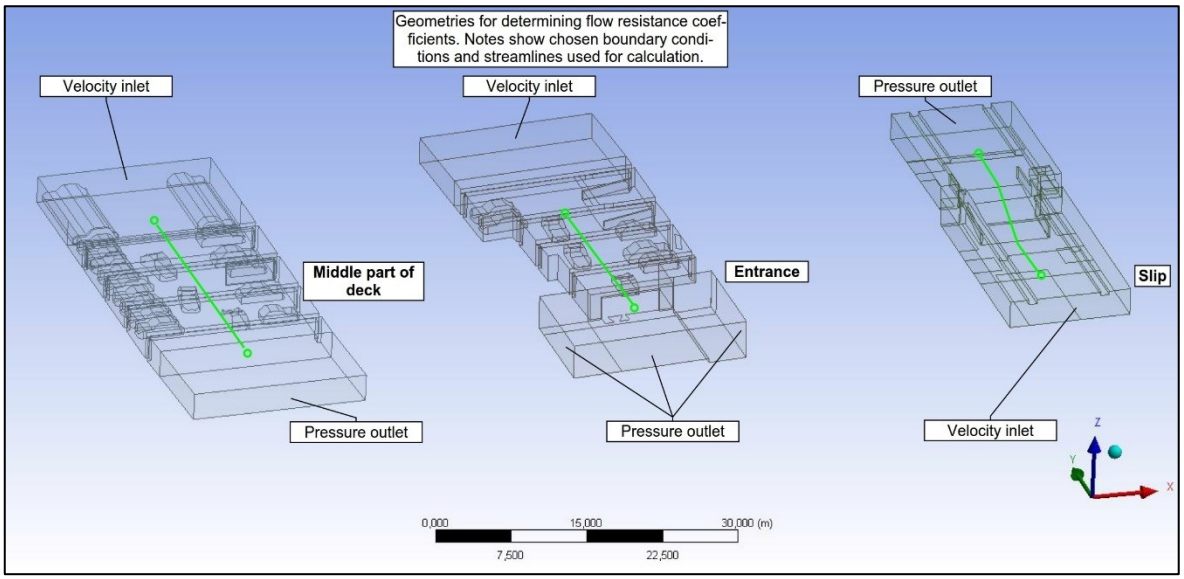


*Figure 23. Geometries and boundary conditions for calculation of loss coefficients*

Next the parts are meshed, using the sizing specifications shown in Table 10. For calculating the loss coefficients, it is not necessary to capture all intricate flow phenomena so to save computational resources mesh density is diminished by defining a large cell size where possible. Large straight surfaces receive a less dense mess and faces that belong to details in the geometry receive a denser mesh. For the air volume itself, the meshing algorithm scales the cells appropriately between a global minimum and maximum element size.

Table 10. *Mesh sizing specifications, calibration of Excel model*

| **Mesh sizing** | **[m]** |
|---|---|
| Large straight wall and ceiling surfaces | 0.12 |
| Floor surfaces | 0.08 |
| Details: beams, narrowings, partitioning walls etc. | 0.06 |
| Vehicle chassis surfaces | 0.06 |
| Vehicle bottom surfaces | 0.06 |
| Defeature size | 5E-04 |
| Curvature minimum size | 0.03 |
| Global minimum element size | 0.02 |
| Global maximum element size | 0.5 |

Given these specifications the resulting mesh consists of approximately 27 million tetrahedral cells. A section of the resulting mesh, from the deck-middle part, is shown in Figure 24.

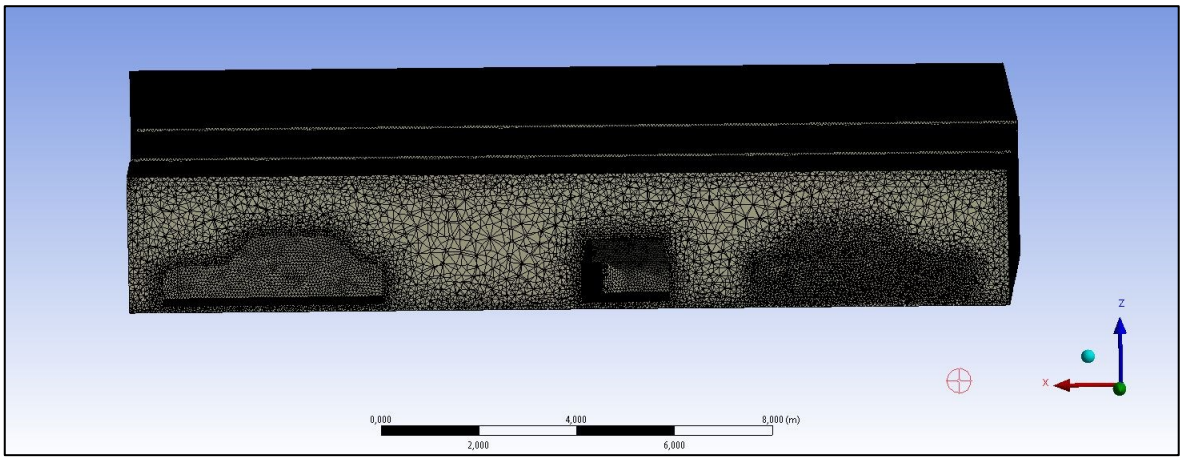


*Figure 24. Section of the mesh for the deck middle part*

Values for loss factor $K_{ij}$ are computed by running the above case with three different inlet velocities, resulting in three distinct volumetric flows. Figure 25, Figure 26 and Figure 27 depict the resulting velocity and pressure fields respectively for the entrance, middle part and slip respectively, from the simulation run with the highest inlet velocity. Note that the scales at the left-hand sides of the contours differ for each contour, as the range depicted in the scale colormap has been fitted for information value.

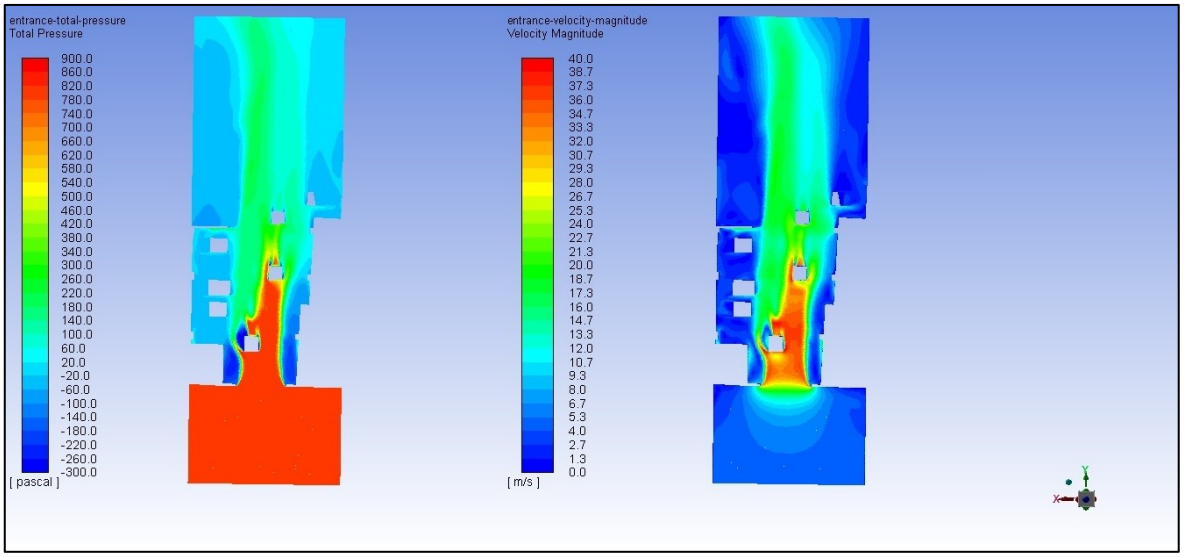


*Figure 25. Resulting contours of total pressure and velocity magnitude, entrance*

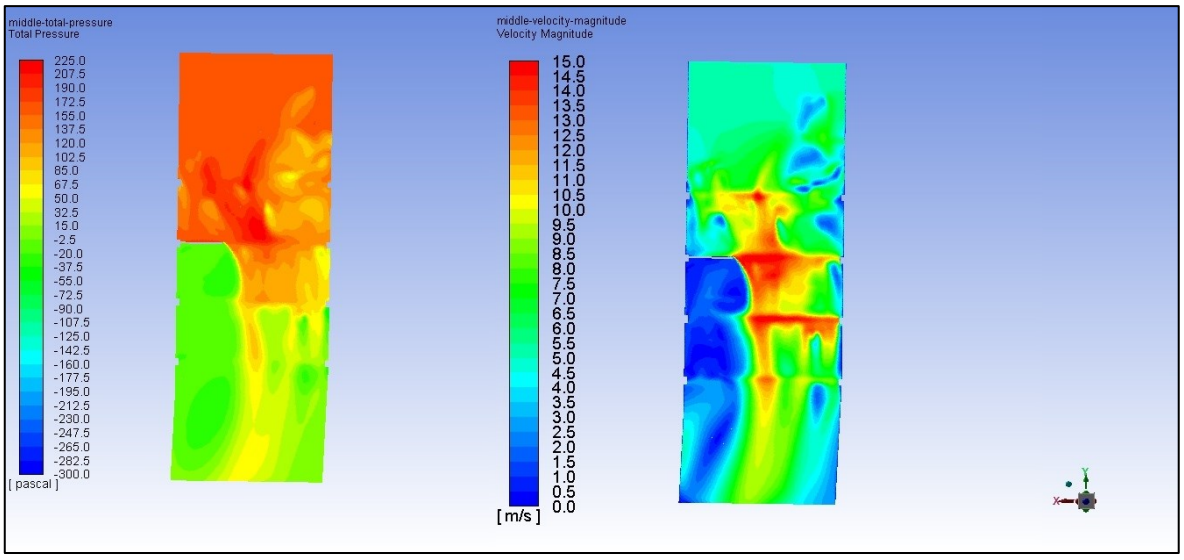


*Figure 26. Resulting contours of total pressure and velocity magnitude, middle part of deck*

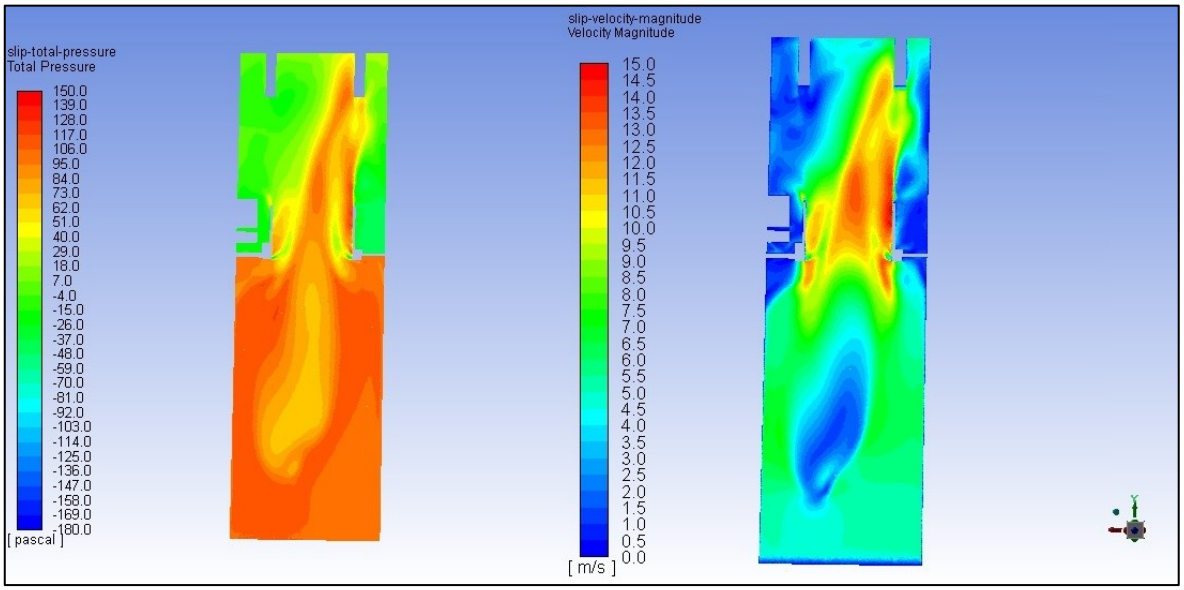


*Figure 27. Resulting contours of total pressure and velocity magnitude, slip*

The volumetric flows are computed within Fluent as surface integrals along section planes that are set perpendicular to the mean flow direction, located at the end-points of the streamlines depicted in Figure 23. Pressure and pressure differences are computed also within Fluent, at the same end-points. From the three cases run at different inlet velocities, three points are calculated onto a $\dot{V}, \Delta p$ -graph and a power-law type trendline is fitted onto the three points.

The Excel model handles simplified geometry. The pipes of the Excel model are as such empty, meaning that they do not contain parked or moving cars that would diminish their free cross-sectional area. The Excel model takes into account the parked and moving vehicles through the $K_{ij}$ value that is simulated by the Fluent model that contains the vehicles. The cross-sectional areas of the pipes in the Excel model have been averaged to leave out

small narrowing's/widenings and hence varies slightly from the more intricate geometry of the Fluent model. For this reason, before computing $K_{ij}$ values, $\dot{V}$ values measured from the Fluent simulations are divided by respective cross-sectional areas that are used in the Excel model. The resulting velocities are more correct to use in calculating $K_{ij}$, they are the velocities that the Fluent-simulated volumetric flows would produce in the pipes of the Excel model, were they to run through them.

These velocities are substituted into the left hand side of Eq. 2 to compute a pressure difference by analytical solution. The analytical pressure difference and the simulated pressure difference are then compared. Excels solver utility is used to minimize the difference between the analytical pressure difference and the simulated pressure difference, by changing the value of $K_{ij}$ in Eq. 2. When the difference between analytical and simulated solution is minimized, $K_{ij}$ has been obtained. The obtained $K_{ij}$ value is then divided by the length of the distance between the points from which the simulated pressure difference was measured in the Fluent model, to produce a loss factor per meters. In the Excel calculation, this loss factor per meters is then multiplied by the zone length and divided by $\rho A_{section}$ to obtain $K'_{ij}$ values to be used in the momentum equation Eq. 7.

### 4.2.1 Loss factor for middle part of deck

Table 11 shows the steps and intermediate results of the calculation procedure for obtaining the pressure loss factor for the middle part of the deck. The length of the streamline (see Figure 23) is $l_m = 21\ m$. The ends of the streamline are regarded as points $i$ and $j$. Volumetric flows measured from the simulations at the ends of the streamline are denoted $\dot{V}$. Velocity values are denoted $v$ and are computed by dividing $\dot{V}$ values by $A_{section,2}$ in the case of the middle part of the deck, see Table 9.

$\Delta p_{sim}$ values are differences of pressure values measured from the simulation at the ends of the streamline. $\Delta p_{ana}$ values are pressure differences obtained analytically by substituting the velocity values $v$ and the value of the $K_{ij}$ cell into the left hand side of Eq. 2. The summed difference between the analytical $\Delta p_{ana}$ values and the simulated $\Delta p_{sim}$ values is then minimized by changing the value of the $K_{ij}$ cell using Excels solver utility. Essentially what is being done is solving for the $K_{ij}$ value that best satisfies the equation

$$\Delta p_{ana} = \frac{1}{2} K_{ij} \rho v |v| = \Delta p_{sim} \tag{38}$$

for all of the simulation cases at the three different inlet velocities. Finally the found $K_{ij}$ value is divided by the length of the measurement area $l_m$. The resulting $K_{ij}$ value per meter is used for the same zones in the Excel model as the cross sectional area $\mathrm{A_{section,2}}$ , see Table 9. The corresponding dimensional loss factor value $K'_{ij}$ used in the momemntum equation Eq. 7, is computed in the Excel model by Eq. 39

$$K'_{ij,middle} = \frac{l_{zone} * \frac{K_{ij,middle}}{l_{m,middle}}}{\rho A^2_{section,2}} \tag{39}$$

For the zones in Table 9 where the cross-sectional area $\mathrm{A_{section,3}}$ is used, $\mathrm{K'_{ij}}$ values are computed by

$$K'_{ij,end} = \frac{l_{zone} * \frac{K_{ij,middle}}{l_{m,middle}}}{\rho A^2_{section,3}} \tag{40}$$

*Table 11. Calculation of pressure loss factor for middle part of deck*

variable
minimized
result

Length of measured area $l_m$ 21

| Simulation case, inlet velocity | $\dot{V}$ | v | $\Delta p_{sim}$ | $\Delta p_{ana}$ |
|---|---|---|---|---|
| 5 m/s | 205.00 | 4.28 | 143.20 | 143.20 |
| 2.25 m/s | 92.30 | 1.92 | 30.37 | 29.03 |
| 0.5 m/s | 20.51 | 0.43 | 1.48 | 1.43 |

$K_{ij}$
10.84

$\Sigma|\Delta p_{sim} - \Delta p_{ana}|$ to be minimized
1.39

$K_{ij}$ / $l_m$
0.52

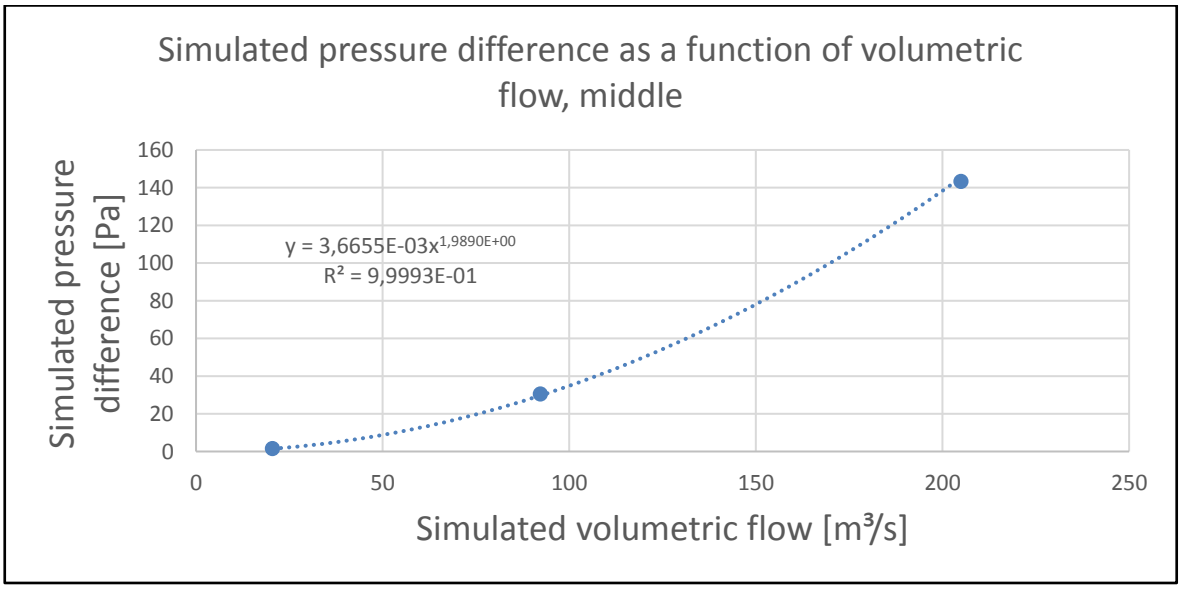


*Figure 28. The power-law type curve formed by the simulated pressure difference as a function of volumetric flow*

### 4.2.2 Loss factor for entrance

Table 12 shows the steps and intermediate results of the calculation procedure for obtaining the pressure loss factor for the entrance part of the deck. The procedure is identical to that of the middle part of the deck, but the length of the streamline (see Figure 23) is now $l_m = 19\ m$. Velocity values are computed by dividing $\dot{V}$ values by $A_{section,1}$ in the case of the entrance part of the deck, see Table 9. Note that the streamline starts inside of the entrance. The pressure loss of the entrance itself (the hole in the wall) will be omitted, since the wall is comprised of a loose mesh.

The summed difference between the analytical $\Delta p_{ana}$ values and the simulated $\Delta p_{sim}$ values is again minimized by changing the value of the $K_{ij}$ cell using Excels solver utility. The resulting $K_{ij}$ value per meter is used for the same zones in the Excel model as the cross sectional area $A_{section,1}$ , see Table 9. The corresponding dimensional loss factor value $K'_{ij}$ used in the momemntum equation Eq. 7, is computed in the Excel model by equation 41

$$K'_{ij,entrance} = \frac{l_{zone} * \frac{K_{ij,entrance}}{l_{m,entrance}}}{\rho A^2_{section,1}} \tag{41}$$

*Table 12. Calculation of loss factor for entrance*

variable
minimized
result

**Length of measured area** $l_m$ 19

| Simulation case, inlet velocity | $\dot{V}$ | v | $\Delta p_{sim}$ | $\Delta p_{ana}$ |
|---|---|---|---|---|
| 5 m/s | 236.28 | 7.57 | 57.44 | 57.44 |
| 2.25 m/s | 106.35 | 3.41 | 10.66 | 11.64 |
| 0.5 m/s | 23.63 | 0.76 | 0.48 | 0.57 |

$K_{ij}$
1.39

$\Sigma|\Delta p_{sim} - \Delta p_{ana}|$ to be minimized
1.07

**Loss factor / m**
**0.07**

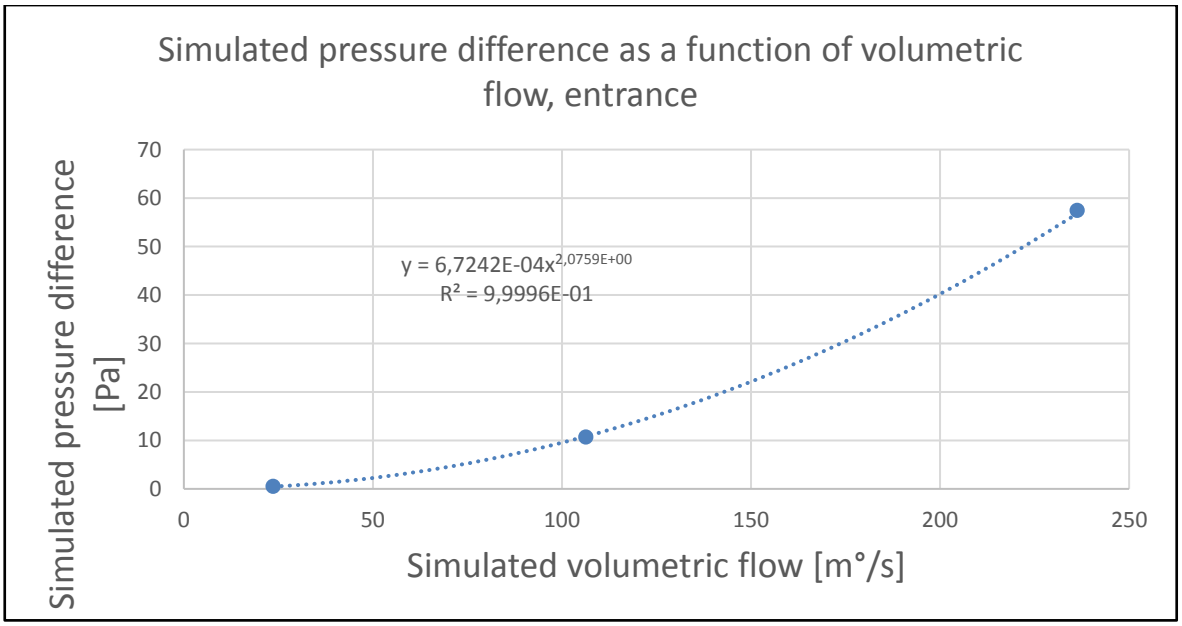


*Figure 29. The power-law type curve formed by the simulated pressure difference as a function of volumetric flow*

### 4.2.3 Loss factor for slip

Table 13 shows the steps and intermediate results of the calculation procedure for obtaining the pressure loss factor for a slip. The procedure is nearly identical to those of the middle and entrance parts of the decks, but the length of the streamline is this time not measured and the resulting $K_{ij}$ is not divided by the length of the streamline. This is because the streamline ranges exactly between the points that the slip is located at in the Excel model – from the middle of one deck to the middle of the deck that the slip connects to. Velocity values are computed by dividing $\dot{V}$ values by $A_{section,4}$ in the case of the slip, see Table 9.

The summed difference between the analytical $\Delta p_{ana}$ values and the simulated $\Delta p_{sim}$ values is again minimized by changing the value of the $K_{ij}$ cell using Excels solver utility. The resulting $K_{ij}$ value is used as such for all of the slips. The corresponding dimensional loss factor value $K'_{ij}$ used in the momemntum equation Eq. 7, is computed in the Excel model by equation 42

$$K'_{ij,slip} = \frac{K_{ij,slip}}{\rho A_{section,4}} \tag{42}$$

*Table 13. Calculation of loss factor for slip*

variable
minimized
result

| Simulation case, inlet velocity | $\dot{V}$ | v | $\Delta p_{sim}$ | $\Delta p_{ana}$ |
|---|---|---|---|---|
| 5 m/s | 170.99 | 9.52 | 97.74 | 97.74 |
| 2.25 m/s | 79.98 | 4.46 | 22.00 | 21.38 |
| 0.5 m/s | 17.10 | 0.95 | 0.92 | 0.98 |

$K_{ij}$
1.49

$\Sigma|\Delta p_{sim} - \Delta p_{ana}|$ to be minimized
0.67

Loss factor
1.49

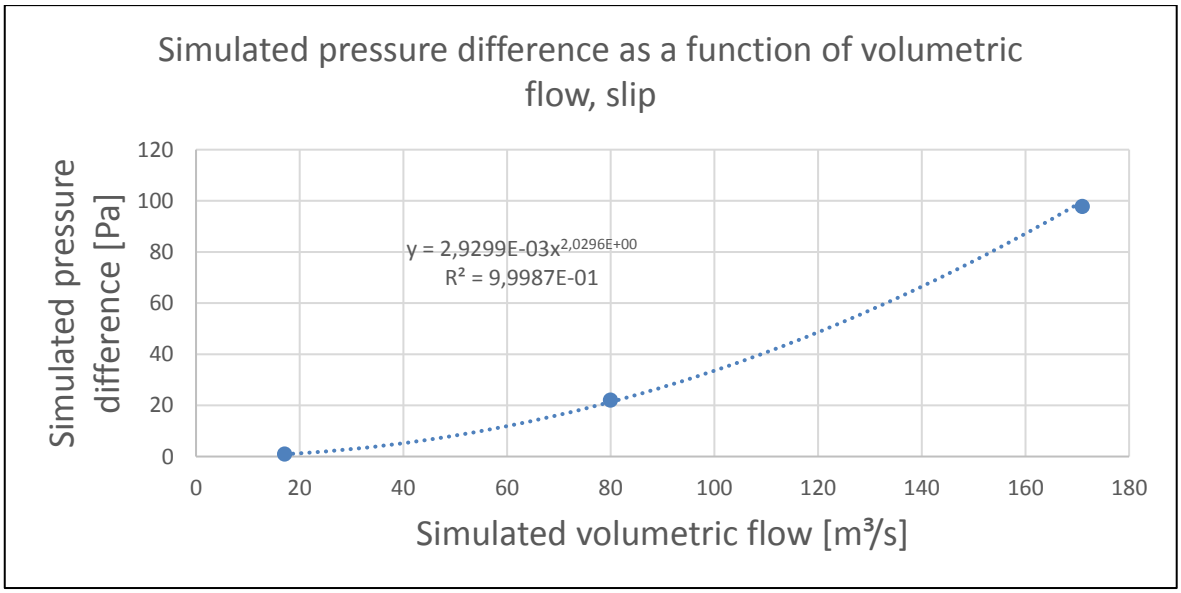


*Figure 30. The power-law type curve formed by the simulated pressure difference as a function of volumetric flow*

# 5 Simulation runs for computing optimal air flow rates

The calibrated Excel-based calculation tool is used to simulate transient CO concentrations inside the Tampereen Kansi parking space in various temperature conditions and with a range of air flow rates as boundary conditions. A 24-hour period is simulated in three distinct temperature conditions. Emphasis is put on finding out wether the simulated air flow rates result in adequate contaminant removal so as to satisfy the currently applied official dimensioning criteria of one-hour average CO concentrations not exceeding 30 ppm throughout the parking space, in the examined temperature. On the other hand, the one-hour average concentrations need not be below 30 ppm by a large margin for the official criteria to be satisfied. $30 \pm 5$ ppm is used as a target for maximum one-hour average CO concentrations found within the simulated 24-hour period.

For compactness, the maximum one-hour average found during the simulated 24-hour period is assigned the notation $C_{1hmax,i}$ where $i$ denotes the deck. The target concentration $30 \pm 5$ ppm is assigned the notation $C_{target}$. Deck specific air flow rate (as opposed to a uniform air flow rate throughout the parking space) is assigned the notation $q'_{DS,i}$, with $i$ again denoting the deck and the asterix in superscript is added to remind the reader that these are flow rates per square meter of floor area. Deck specific *optimal* air flow rate is assigned the notation $q'_{DSO,i}$. A value for $q'_{DS,i}$ is deemed optimal if

$$C_{1hmax,i} = C_{target} = 30 \pm 5\ ppm \tag{43}$$

for deck $i$ using that $q'_{DS,i}$ value. The optimal $q'_{DSO,i}$ values are sought by first simulating uniform air flow rates, then adjusting air flow rates based on the resulting $C_{1hmax,i}$ values of those runs, either lower if $C_{1hmax,i}$ was lower than $C_{target}$, or higher if $C_{1hmax,i}$ was higher than $C_{target}$. Hence the varying traffic in each deck is taken into account, whereas in the first runs the air flow rates are uniform throughout the parking space, regardless of traffic count. Within the context of one simulated temperature, if only the air flow rates are changed, the resulting CO concentrations can be expected to behave close to proportionally. Notably the behavior of the CO concentrations will not be *exactly* linearly proportional to the selected airflow rates across different simulation runs due to the stochastic nature of the spreading of the traffic. None the less, a reasonable guess towards $q'_{DSO,i}$ values can be formed by taking the resulting $C_{1hmax,i}$ values from previous simulation runs, dividing them individually by the target concentration of $C_{target}$ and using this ratio to scale the airflow rate up or down. Then, to prevent over-adjusting and going too far the other way, the average is taken from the previous guess and the value suggested by scaling by the aforementioned ratio. The procedure is as follows

$$q'_{DS,i,new} = \left(\left[\frac{C_{1hmax,i,previous}}{C_{target}} * q'_{DS,i,previous}\right] + q'_{DS,i,previous}\right)/2 \tag{44}$$

The guessing procedure is repeated and new $q'_{DS,i}$ values are simulated until optimal $q'_{DSO,i}$ values have been found (Eq. 43 is satisfied) for all of the decks.

Definitions for the simulated scenarios and input data that is common to Simulations 1-3 are laid out in Table 14. The listed probabilities of parking in a specific deck are important in that they directly govern the share of traffic received by each deck and subsequently the share of emission load received by each deck.

The reasoning behind the listed probabilities is an assumption that visitors of the parking space prefer to park immediately close to the entrance of the parking space and will not drive around in vain to park far from the entrance if a free slot can be found in the deck that hosts the entrance. Therefore, the probability is the highest for parking at the deck that hosts the entrance, P2 and probabilities diminish the further a visitor would need to drive before parking. The probability mass of each deck is evenly distributed to the (real) cells that the deck hosts, meaning that e.g. for deck P01 which all-in-all has a 14 % chance of being parked into, the cells 23, 24, 25, 26 and 27 located on P01 all receive 14 % / 5 = 2.8 % chance of being parked into. The sum of the probabilities listed is 100 %.

Figure 31 and Figure 32 constitute the traffic data used in the simulations. The data includes clear peaks in traffic in the morning as well as in the afternoon and a decline in traffic towards night-time. For the simulations, numbers of vehicles in Figure 31 have been scaled up by a safety factor 1.72 so that during the peak traffic hour from 4 to 5 pm 200 vehicles drive in total and values for other hours are adjusted proportionally, multiplying by 1.72. The shape of the diurnal traffic profile is none the less the same.

In the Fluent model, the static situation that resembles the peak traffic hour ranging from 4 pm to 5 pm is created by reading the average amount of running engines from Figure 32 at the peak traffic hour. The amount is then multiplied by the safety factor 1.72. The resulting amount of vehicles with engines running inside the parking space, is 6.7 vehicles in total. To avoid controlling the resulting distribution of CO concentration too much by choosing the locations of the vehicles, the emission load of vehicles with engines running is divided onto several virtual vehicles, in effect the emission load from the vehicles is divided more evenly into the parking space decks. The total emission load is the same as from 6.7 vehicles. Importantly, the amount of virtual vehicles in the Fluent model is divided onto the parking space decks in exactly the same ratios as the probabilistic wheights of parking in the decks are divided in the Excel model, so that the traffic count for each deck matches in the two models.

In the Fluent model, the share of diesel vehicles is factored into an average emission rate that all vehicles share in common, whereas in the Excel model gasoline and diesel driven vehicles have their respective emission rates and the engine type of an arriving/leaving vehicle is chosen by lottery, probabilities of either engine type are in accordance with Figure 9.

The main results extracted from the simulations are the instantaneous cell CO concentrations graphed as a function of simulated time; one-hour average CO concentrations for each cell graphed as a function of time; deck and cell specific maximum average concentration for a one-hour-period. The results presented in this chapter are developed further in Chapter 6.

During the calculation, the results are visualized by printing them onto the architect drawings of the parking space. Convergence plotting is shown for Simulations 1 and 4.

*Table 14. Simulation scenario definitions, common input data and calculation settings*

| **Simulated scenario definitions** | | |
|---|---|---|
| 1. Zone II Heat loss calculation dimensioning temperature | -29 | °C |
| 2. Summer conditions | +23 | °C |
| 3. Comparison to Ansys Fluent CFD analysis | -10 | °C |
| **Calculation Settings** | | |
| Simulated time | 86400 | seconds |
| Timestep | 1 | seconds |
| Accuracy | 1.00E-06 | |
| Pressure Under-relaxation | 0.2 | |
| Average concentration for | 3600 | seconds |
| **Probability of parking into or leaving from deck** | | |
| **Deck** | | |
| P4 | 2.00 | % |
| P3 | 8.00 | % |
| P2 | 33.00 | % |
| P1 | 23.00 | % |
| P01 | 14.00 | % |
| P02 | 12.00 | % |
| P03 | 6.00 | % |
| P04 | 2.00 | % |

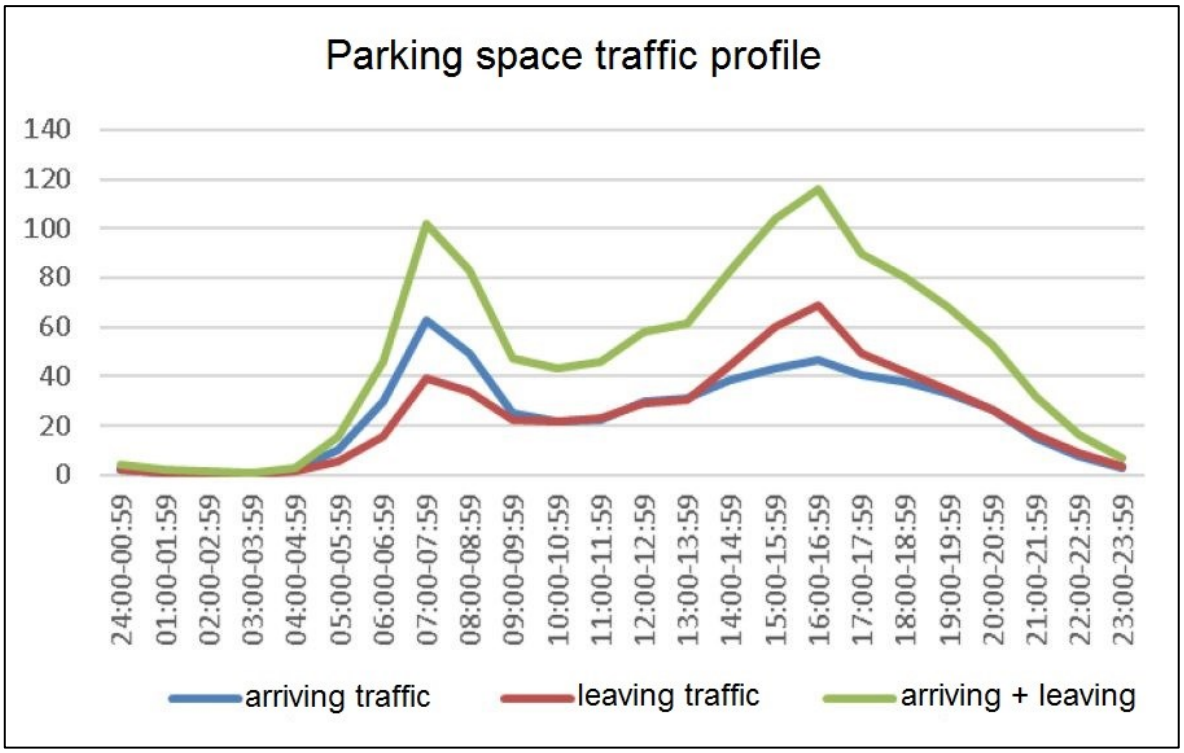


*Figure 31. Traffic data estimated by Ramboll Traffic & Infrastructure department, amounts of arriving and leaving traffic*

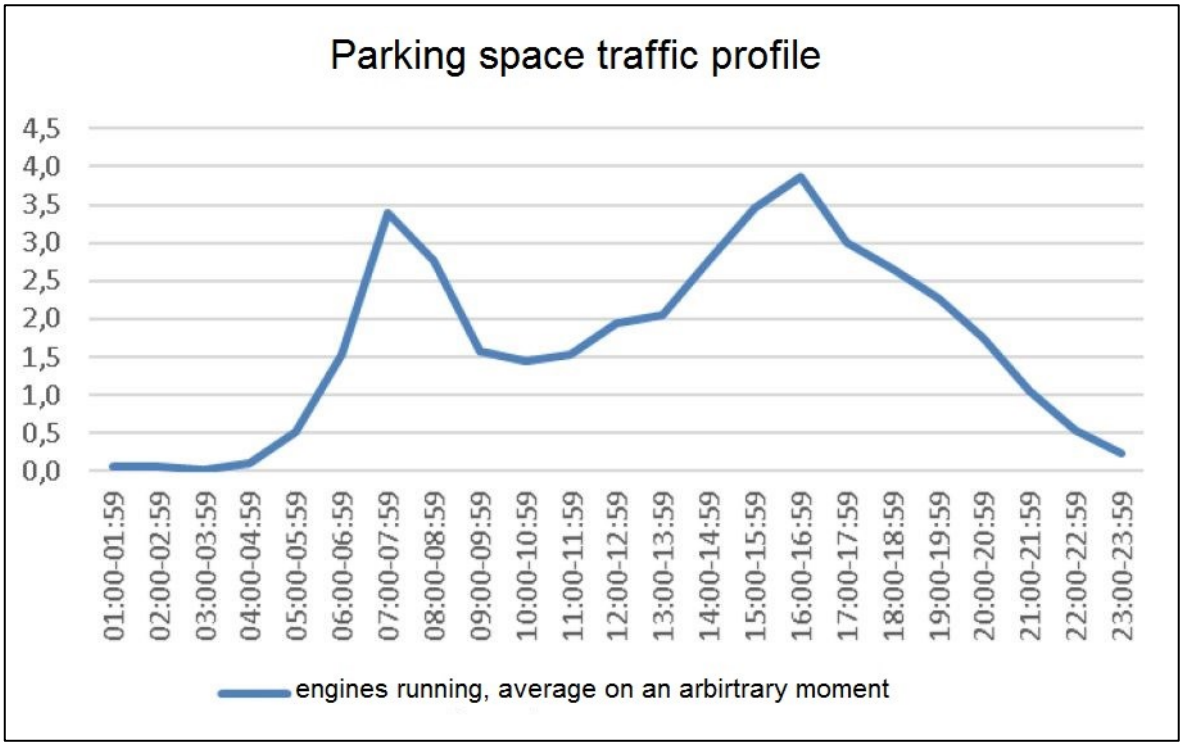


*Figure 32. Traffic data estimated by Ramboll Traffic & Infrastructure department, number of running engines*

## 5.1 Simulation 1: Zone II Dimensioning Temperature -29 °C

A 24-hour period resembling a cold winters day with an outside temperature of -29 °C is simulated. This simulation is construed as a worst case scenario in terms of temperature and subsequently in terms of emission rates and contaminant load. The temperature -29 °C is chosen as an appropriate worst case scenario to examine, since it is also used as the dimensioning temperature in heat loss calculations in the Tampere region. [38] The used traffic data for the 24-hour period is an estimation provided by Ramboll Traffic & Infrastructure department. The run-time for simulating a 24-hour period is approximately two hours.

### 5.1.1 Input data

Three sets of air flow rates are examined. The first chosen airflow rate, a uniform 3.6 $\frac{l}{s,m^2}$ is the minimum airflow rate defined for a multi-purpose parking space in the recently repealed Building Code D2. The second air flow rate simulated is the D2 minimum doubled, 7.2 $\frac{l}{s,m^2}$. The third set of air flow rates is the set of $q'_{DSO,i}$ values in temperature -29 °C, computed by repeatedly adjusting air flow rates according to Eq. 44, beginning by using $C_{1hmax,i}$ results and simulated air flow rates from the first two runs.

*Table 15. Input data specific for Simulation 1*

| Simulation 1 Zone II Dimensioning Temperature -29 °C Input data | | |
|---|---|---|
| Temperature | -29 °C | °C |
| Air density | 1.45 | kg/m³ |
| Carbon monoxide density | 1.40 | kg/m³ |
| Ambient CO Concentration | 0.5 | ppm |
| Average driving speed | 10 | km/h |
| CO emiss., gasoline, arriving | 5.78E-06 | kg/s |
| CO emiss., gasoline, leaving | 2.89E-05 | kg/s |
| CO emiss., diesel, arriving | 1.86E-06 | kg/s |
| CO emiss., diesel, leaving | 9.31E-06 | kg/s |
| CO emiss., start, gasoline | 1.30E-01 | kg |
| CO emiss., start, diesel | 1.70E-02 | kg |

| Deck | Airflow rate | |
|---|---|---|
| P4 | 3.6 ; 7.2 ; 6.1 | l/s,m² |
| P3 | 3.6 ; 7.2 ; 3.0 | l/s,m² |
| P2 | 3.6 ; 7.2 ; 21.5 | l/s,m² |
| P1 | 3.6 ; 7.2 ; 5.5 | l/s,m² |
| P01 | 3.6 ; 7.2 ; 6.4 | l/s,m² |
| P02 | 3.6 ; 7.2 ; 4.0 | l/s,m² |
| P03 | 3.6 ; 7.2 ; 2.2 | l/s,m² |
| P04 | 3.6 ; 7.2 ; 2.0 | l/s,m² |

For simulating a worst-case scenario, ambient CO concentration is chosen from the high end of measurement data logged in Appendix 1. Average driving speed inside the parking space is chosen as 10 km/h. The chosen driving speed directly influences emission rates and also determines the time the vehicles drive through cells and through the whole parking space.

Vehicle CO emissions are chosen based on the findings listed in Chapter 2.3.2. The findings are somewhat differing from one another in absolute numbers, but unified in that the cold engine emissions are multiple times higher than hot engine emissions. For worst-case scenario simulation the view is taken that there is more risk of under-estimating the cold emissions, as no measurement data is available from as cold a temperature as -29 °C. Therefore, warm engine emissions for driving vehicles are picked up from the World Road Association PIARC data (Figure 11) and cold engine emissions for driving vehicles are computed by multiplying the hot engine emissions by a factor of 5. For emissions from starting engines, the extrapolated graph from Figure 12 is applied.

### 5.1.2 Results

Figure 16 lists resulting $C_{1hmax,i}$ values found during the simulated 24-hour period at uniform air flow rates 3.6 $\frac{l}{s,m^2}$ and 7.2 $\frac{l}{s,m^2}$. It is evident that in the cold conditions of Simulation 1 the minimum airflow rate defined by Building Code D2, 3.6 $\frac{l}{s,m^2}$ is far from adequate with average concentrations exceeding the current criteria 30 ppm in all but one deck and one-hour averages reaching as high as 134 ppm in the most populated deck P2.

*Table 16. Deck specific maximum one-hour average CO concentrations, uniform 3.6 l/s,m² and 7.2 l/s,m²*

**Simulation 1 Zone II Dimensioning Temperature -29 °C**
**Results**

$C_{1hmax,i}$

| Deck | 3.6 l/s,m² | 7.2 l/s,m² | |
|---|---|---|---|
| P4 | 59 | 14 | ppm |
| P3 | 59 | 14 | ppm |
| P2 | 134 | 67 | ppm |
| P1 | 74 | 53 | ppm |
| P01 | 55 | 25 | ppm |
| P02 | 56 | 26 | ppm |
| P03 | 33 | 15 | ppm |
| P04 | 28 | 11 | ppm |

At a uniform 7.2 $\frac{l}{s,m^2}$ the situation is significantly better, with the 30 ppm criteria being met in most of the decks, in some with significant margin to spare. Before finding the deck specific air flow rates deemed optimal and resulting $C_{1hmax,i}$ values presented in Table 17, the guessing procedure Eq. 44 was repeated and re-simulated several times.

*Table 17. Deck specific optimal air flow rates and resulting max. 1-h-averages in -29 °C*

**Simulation 1 Zone II Dimensioning Temperature -29 °C Results**

**Deck specific optimal air flow rates in -29 °C**

| Deck | $C_{1hmax,i}$ | | $q'_{DSO,i}$ | |
|---|---|---|---|---|
| P4 | **35** | ppm | **6.1** | l/s,m² |
| P3 | **35** | ppm | **3.0** | l/s,m² |
| P2 | **31** | ppm | **21.5** | l/s,m² |
| P1 | **28** | ppm | **5.5** | l/s,m² |
| P01 | **32** | ppm | **6.4** | l/s,m² |
| P02 | **31** | ppm | **4.0** | l/s,m² |
| P03 | **27** | ppm | **2.2** | l/s,m² |
| P04 | **32** | ppm | **2.0** | l/s,m² |

### 5.1.3 Convergence

Convergence of the pressure correction method is monitored by plotting the maximum error made in the continuity equation for each node and the maximum residual from the momentum equation Eq. 7. For a 24-hour simulation where nothing changes in the flow variables, the plot looks flat for most of the duration since the flow field needs to be iterated only in the first few timesteps.

Figure 33 shows convergence plotting for the 24-hour simulation. For comparison, Figure 34 shows convergence plotting for the first few time steps of the simulation run to better display the progress of the iterations. The jump in residuals marks the stepping into a new timestep. The pressures and mass flows of the previous time step work as an initial guess for the iteration in the next timestep, hence the jump in residuals diminishes (diminishing vertical volatility in Figure 34) and the convergence of the iteration gets faster (diminishing horizontal intervals in Figure 34) with successive time steps.

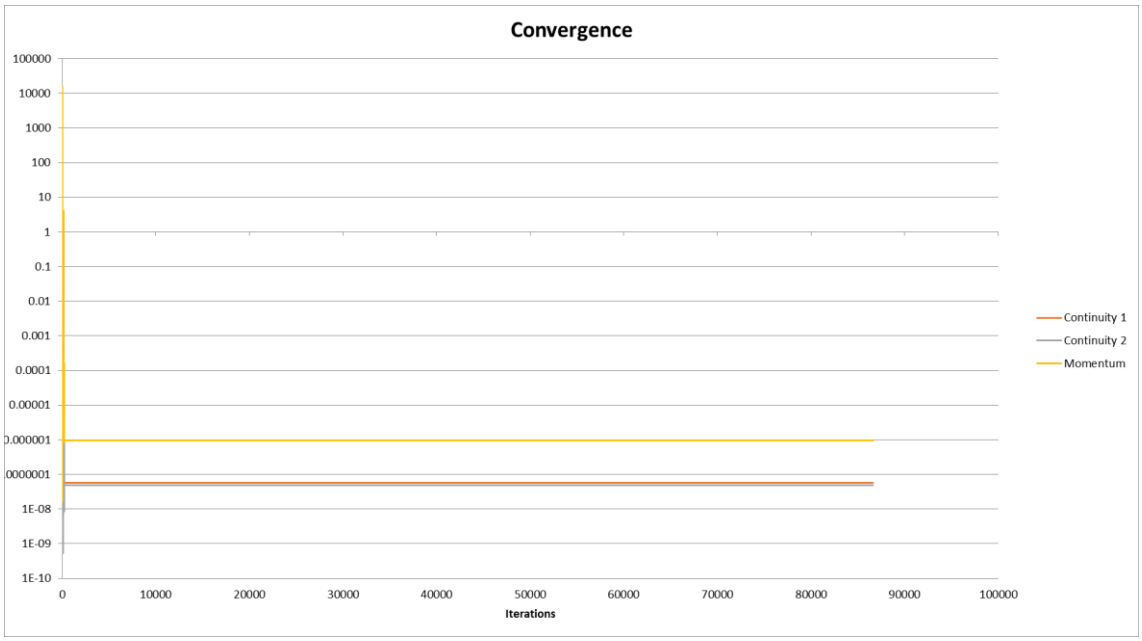


*Figure 33. Convergence plot for a 24 h simulation with no changes in flow variables*

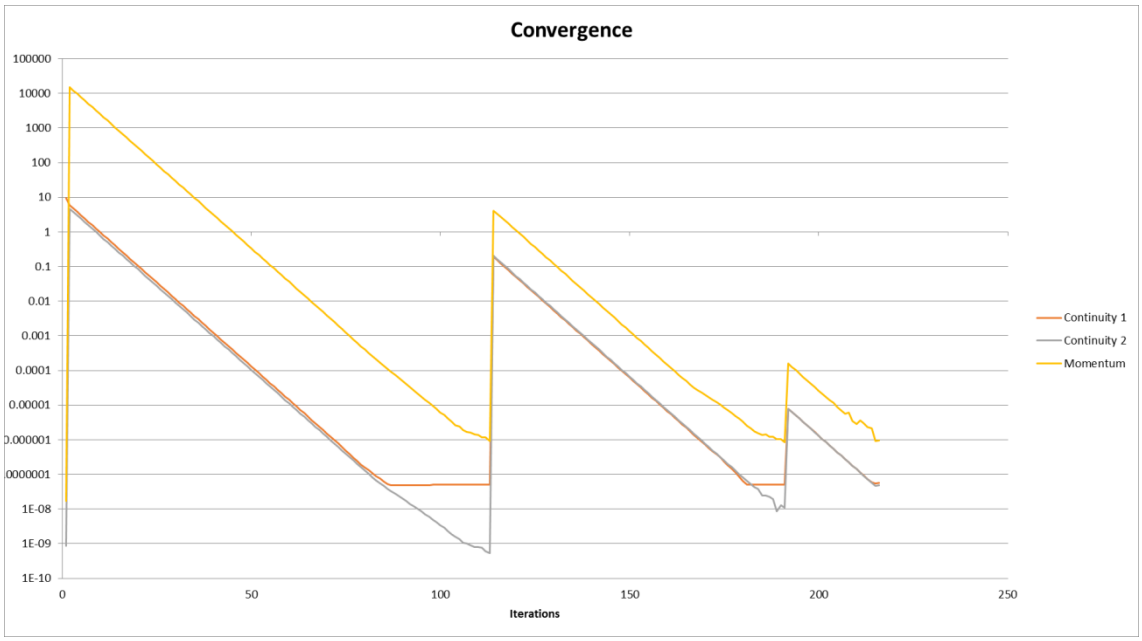


*Figure 34. Convergence plot detail, first few timesteps*

## *5.2 Simulation 2: Summer conditions, +23 °C*

### 5.2.1 Input data

Ambient temperature and CSEE's have a significant impact on the resulting CO concentrations. Next, in stark contrast of the worst-case scenario simulated in Simulation 1, a 24-hour

period resembling summer conditions is simulated with a range of air flow rates. First the D2 mandated minimum of uniform 3.6 $\frac{l}{s,m^2}$ is tested. As mentioned in Chapter 2.4, the current official dimensioning criteria allows for air flow rates smaller than the D2 minimum if contaminant load is known and the adequacy of the chosen air flow rate can be shown. With this in mind, uniform 2.0 $\frac{l}{s,m^2}$ and uniform 1.0 $\frac{l}{s,m^2}$ are simulated. Table 18 shows input data used for simulating summer conditions. Lastly, $q'_{DSO,i}$ values are forked out by adjusting air flow rates according to Eq. 44.

*Table 18. Specific input data for Simulation 2*

| Simulation 2 Summer conditions +23 °C<br>Input data | | |
|---|---|---|
| Temperature | +23 °C | °C |
| Air density | 1.19 | kg/m³ |
| Carbon monoxide density | 1.15 | kg/m³ |
| Ambient CO Concentration | 0.5 | ppm |
| Average driving speed | 10 | km/h |
| CO emiss., gasoline, arriving | 5.78E-06 | kg/s |
| CO emiss., gasoline, leaving | 5.78E-06 | kg/s |
| CO emiss., diesel, arriving | 1.86E-06 | kg/s |
| CO emiss., diesel, leaving | 1.86E-06 | kg/s |
| CO emiss., start, gasoline | 6.66E-03 | kg |
| CO emiss., start, diesel | 1.14E-03 | kg |

| Deck | Airflow rate | |
|---|---|---|
| P4 | 3.6 ; 2.0 ; 1.0 ; 0.13 | l/s,m² |
| P3 | 3.6 ; 2.0 ; 1.0 ; 0.14 | l/s,m² |
| P2 | 3.6 ; 2.0 ; 1.0 ; 1.34 | l/s,m² |
| P1 | 3.6 ; 2.0 ; 1.0 ; 0.36 | l/s,m² |
| P01 | 3.6 ; 2.0 ; 1.0 ; 0.45 | l/s,m² |
| P02 | 3.6 ; 2.0 ; 1.0 ; 0.26 | l/s,m² |
| P03 | 3.6 ; 2.0 ; 1.0 ; 0.09 | l/s,m² |
| P04 | 3.6 ; 2.0 ; 1.0 ; 0.11 | l/s,m² |

The vehicle emissions are taken to be directly those found in the PIARC data (Figure 11), both for arriving and leaving vehicles. For engine starts the graph in Figure 12 is utilized, that is to say the measurement results by Weilenmann et al measured in +23 °C. Ambient CO concentration is chosen to be 0.5 ppm.

### 5.2.2 Results

Table 19 lists resulting $C_{1h,max,i}$ values from the three runs at uniform air flow rates in Simulation 2.

*Table 19. Deck specific maximum one-hour average CO concentrations, Simulation 2*

**Simulation 2 Summer conditions +23 °C**
**Results**

**$C_{1hmax,i}$ , ppm**

| Deck | 3.6 l/s,m² | 2.0 l/s,m² | 1.0 l/s,m² |
|---|---|---|---|
| P4 | 2 | 4 | 10 |
| P3 | 4 | 6 | 13 |
| P2 | 9 | 12 | 28 |
| P1 | 6 | 13 | 20 |
| P01 | 5 | 6 | 11 |
| P02 | 4 | 6 | 9 |
| P03 | 3 | 5 | 4 |
| P04 | 1 | 3 | 10 |

Notably, $C_{1hmax,i}$ is significantly below $C_{target}$ for most of the decks even at the smallest simulated uniform air flow rate of 1.0 $\frac{l}{s,m^2}$. Table 20 shows the found deck specific optimal airflow rates and corresponding $C_{1hmax,i}$ values that satisfy Eq. 43.

*Table 20. Deck specific optimal air flow rates and resulting max. 1-h-averages in +23 °C*

**Simulation 2 Summer conditions +23 °C**
**Results**

**Deck specific optimal air flow rates in +23 °C**

| Deck | $C_{1hmax,i}$ | | $q'_{DSO,i}$ | |
|---|---|---|---|---|
| P4 | 34 | ppm | **0.13** | l/s,m² |
| P3 | 29 | ppm | **0.14** | l/s,m² |
| P2 | 26 | ppm | **1.34** | l/s,m² |
| P1 | 26 | ppm | **0.36** | l/s,m² |
| P01 | 35 | ppm | **0.45** | l/s,m² |
| P02 | 27 | ppm | **0.26** | l/s,m² |
| P03 | 34 | ppm | **0.09** | l/s,m² |
| P04 | 26 | ppm | **0.11** | l/s,m² |

## 5.3 Simulation 3: Comparison with Ansys Fluent CFD analysis, -10 °C

### 5.3.1 Input data

A set of simulation runs is built to compare results produced by the Excel based model with results obtained by Ansys Fluent simulation. The geometries in the two models are not identical. For this reason, even when using the same traffic and emissions data, the resulting CO concentrations are as such not meaningful to compare between the two models. Instead, comparison is made between the optimal air flow rates per square meter that the two models suggest.

The input data used for this set of simulations is as close as possible to identical to the values that have been used in Fluent simulation. The traffic data used is the same as in Simulations 1 and 2. Vehicle emissions for warmed up engines are those found in the PIARC data (Figure 11), whereas cold engine emissions are PIARC data values doubled. Emissions from engine starts are read from the graph in Figure 12 at -10 °C. The simulated airflow rates are, as in Simulation 1, chosen as uniform 3.6 $\frac{l}{s,m^2}$, 7.2 $\frac{l}{s,m^2}$ and then deck specific air flow rates computed based on the results from the first two simulation runs, using eq. 44. The input data used for this set of simulations is gathered in Table 21.

*Table 21. Specific input data for Simulation 3*

| Simulation 3 Comparison to Ansys Fluent CFD analysis -10 °C Input data | | |
|---|---|---|
| Temperature | -10 °C | °C |
| Air density | 1.34 | kg/m³ |
| Carbon monoxide density | 1.30 | kg/m³ |
| Ambient CO Concentration | 0.6 | ppm |
| | | |
| Average driving speed | 10 | km/h |
| CO emiss., gasoline, arriving | 5.78E-06 | kg/s |
| CO emiss., gasoline, leaving | 1.16E-05 | kg/s |
| CO emiss., diesel, arriving | 1.86E-06 | kg/s |
| CO emiss., diesel, leaving | 3.72E-06 | kg/s |
| | | |
| CO emiss., start, gasoline | 4.10E-02 | kg |
| CO emiss., start, diesel | 6.00E-03 | kg |

| Deck | Airflow rate | |
|---|---|---|
| P4 | 3.6 ; 7.2 ; 1.0 | l/s,m² |
| P3 | 3.6 ; 7.2 ; 1.4 | l/s,m² |
| P2 | 3.6 ; 7.2 ; 7.0 | l/s,m² |
| P1 | 3.6 ; 7.2 ; 2.6 | l/s,m² |
| P01 | 3.6 ; 7.2 ; 2.1 | l/s,m² |
| P02 | 3.6 ; 7.2 ; 1.7 | l/s,m² |
| P03 | 3.6 ; 7.2 ; 1.0 | l/s,m² |
| P04 | 3.6 ; 7.2 ; 0.9 | l/s,m² |

### 5.3.2 Results

For Simulation 3, the results extracted are $C_{1hmax,i}$ values for ease of comparison with results from Simulations 1 and 2 and one-hour averages from the peak traffic hour, for ease of comparison with results from Ansys simulation runs. Predictably, the resulting maximum averages are often found at the peak traffic hour, but not always, and so a distinction is made. Table 22 and Table 23 list resulting deck specific maximum one-hour averages and peak-hour averages simulated in Simulation 2. The concentration values are not directly comparable between the models. For both models, applying Eq. 44 several times, deck specific optimal air flow rates have been found. In the case of the Fluent simulations, the simulations are very time consuming and the forking of $q'_{DSO,i}$ values had to be stopped prematurely. Equation 43 holds for all but two decks, however, and the results are held satisfactory.

*Table 22. Maximum one-hour averages and peak-hour averages, Excel simulation*

**Simulation 3 Comparison to Ansys Fluent CFD analysis -10 °C**
**Results**

| | CO maximum one-hour averages | | | CO peak-hour averages | | | |
|---|---|---|---|---|---|---|---|
| **Deck** | **3.6** | **7.2** | $q'_{DSO,i}$ | **3.6** | **7.2** | $q'_{DSO,i}$ | **l/s,m²** |
| P4 | 10 | 6 | **29** | 9 | 2 | **13** | ppm |
| P3 | 10 | 7 | **26** | 10 | 6 | **11** | ppm |
| P2 | 47 | 31 | **33** | 47 | 31 | **33** | ppm |
| P1 | 43 | 17 | **31** | 43 | 17 | **31** | ppm |
| P01 | 20 | 11 | **32** | 20 | 8 | **28** | ppm |
| P02 | 16 | 8 | **31** | 5 | 4 | **28** | ppm |
| P03 | 10 | 5 | **26** | 8 | 4 | **10** | ppm |
| P04 | 10 | 5 | **28** | 10 | 4 | **28** | ppm |

*Table 23. Deck specific CO concentrations in exhaust air during peak traffic hour, Ansys Fluent simulations*

**Simulation 3 Comparison to Ansys Fluent CFD analysis -10 °C**
**Results**

| Ansys simulated exhaust air CO concentration for peak traffic hour | | | | |
|---|---|---|---|---|
| **Deck** | **3.6** | **7.2** | $q'_{DSO,i}$ | **l/s,m²** |
| P4 | 3 | 3 | **4** | ppm |
| P3 | 23 | 8 | **11** | ppm |
| P2 | 67 | 43 | **32** | ppm |
| P1 | 37 | 24 | **28** | ppm |
| P01 | 30 | 16 | **28** | ppm |
| P02 | 23 | 12 | **33** | ppm |
| P03 | 16 | 8 | **29** | ppm |
| P04 | 8 | 4 | **32** | ppm |

## 5.4 Simulation 4: Ventilation system performance with VAV, -29 °C

A modification is made to the VBA program to simulate a realistic ventilation configuration with VAV controlled by CO-concentration. The structure of the VBA program (Appendix 3) remains essentially the same. The only difference is that instead of initializing mass flow values at the supply and exhaust nodes with user-defined air flow rates *before the time-loop*, mass flow values at supply and exhaust nodes are defined *within the time loop* i.e. within each timestep as a share of maximum air flow rate (share of $q'_{DSO.i}$ values from Simulation 1), determined by the CO concentrations from the previous time step.

The set of rules governing the VAV control are exactly those by Talotekniikkainfo described in Chapter 2.4. The VAV control is assumed to have virtually no response time, the air flow rate corresponding to the concentration of the previous time step is effective right at the next time step. The input data is identical to that of Simulation 1 and can be reviewed from Table 15. Again, the supply and exhaust air flow rates are always in balance for every deck.

The rules governing VAV control in this simulation, based on those discussed in Chapter 4.2, are presented in Table 24. The on-demand controlling between 30% and 100% is done in six steps of 10%, with the corresponding concentration range 9-50 ppm also devided into six steps. In the on-demand control, the smallest allowable air flow rate is naturally selected.

*Table 24. Rules governing VAV control in Simulation 4*

**VAV Contol Rules**

| | | | | | |
|---|---|---|---|---|---|
| Operating hours | 06:00 | 22:00 | | | |
| **Rule** | **Condition** | | | | **Percentage of maximum air flow rate** |
| Ventilation switched off outside of parking space operating hours if | $C_{CO}$ | < | 6 | ppm | **0 %** |
| Ventilation reduced to a minimum of during operating hours if | $C_{CO}$ | < | 9 | ppm | **30 %** |
| Ventilation controlled on an on-demand basis if | $C_{CO}$ | = | 9 - 50 | ppm | **30% - 100%** |
| Ventilation at maximum air flow rate if | $C_{CO}$ | > | 50 | ppm | **100 %** |
| **Control steps between 30% - 100%** | | | | | |
| | $C_{CO}$ | < | 9 | ppm | 30% |
| | $C_{CO}$ | > | 9 | ppm | 40% |
| | $C_{CO}$ | > | 16 | ppm | 50% |
| | $C_{CO}$ | > | 23 | ppm | 60% |
| | $C_{CO}$ | > | 30 | ppm | 70% |
| | $C_{CO}$ | > | 36 | ppm | 80% |
| | $C_{CO}$ | > | 43 | ppm | 90% |
| | $C_{CO}$ | > | 50 | ppm | 100% |

The monitoring of CO-concentration is simulated as if there was a CO sensor in each of the five (real) control volumes on each deck. The deck specific air flow rate is adjusted higher if CO concentration inside any control volume rises enough to varrant an adjustment according to Table 24. The example VAV rules also mention that an alarm should go off whenever CO concentrations exeed 70 ppm. Such instances are recorded during the simulation.

### 5.4.1 Results

The percentage of maximum air flow rate used at each deck is recorded for the simulated time. From this data, the share of the day during which a specific percentage was used, is calculated. The calculation is a simple percentage calculation. To illustrate the principle, let $N_{x\%,i}$ be the number of seconds that the the air flow rate at deck $i$ was x % of maximum air flow rate during the simulated time period and let $t_{simulated}$ be the total simulated time in seconds. The percentages reported in Figure 35 are counted by equation 45

$$\frac{N_{x\%,i}}{t_{simulated}} * 100\ \% = fraction\ of\ day\ \ x\ \%\ of\ q_{DSO,i}\ was\ used \qquad (45)$$

$C_{1hmax,i}$ values are reported in Table 25.

*Table 25. Maximum one-hour average CO concentrations found during Simulation 4*

| Deck | 4 | 3 | 2 | 1 | 01 | 02 | 03 | 04 |
|---|---|---|---|---|---|---|---|---|
| $C_{1hmax,i}$ | 49 | 49 | 34 | 38 | 36 | 47 | 37 | 41 |

The instructions for VAV control by Talotekniikkainfo mention that an alarm should go off when CO concentration exceeds 70 ppm. The seconds where transient CO concentration exeeds 70 ppm have been counted for each deck and from this data Table 26 is produced.

*Table 26 Recorded instances of alarms during the simulated 24-hour period*

| Deck | Alarm on [hh:mm:ss] | Percentage of simulated time | Longest continuous alarm [min, s] |
|---|---|---|---|
| **P4** | 00:23:51 | 1.7 % | 2 min 19 s |
| **P3** | 01:07:41 | 4.7 % | 5 min 12 s |
| **P2** | 01:10:16 | 4.9 % | 1 min 56 s |
| **P1** | 01:16:17 | 5.3 % | 4 min 46 s |
| **P01** | 00:57:37 | 4.0 % | 2 min 11 s |
| **P02** | 01:05:24 | 4.5 % | 5 min 35 s |
| **P03** | 00:25:49 | 1.8 % | 3 min 38 s |
| **P04** | 00:41:22 | 2.9 % | 6 min 10 s |
| **Total** | 07:28:17 | 29.7 % | |

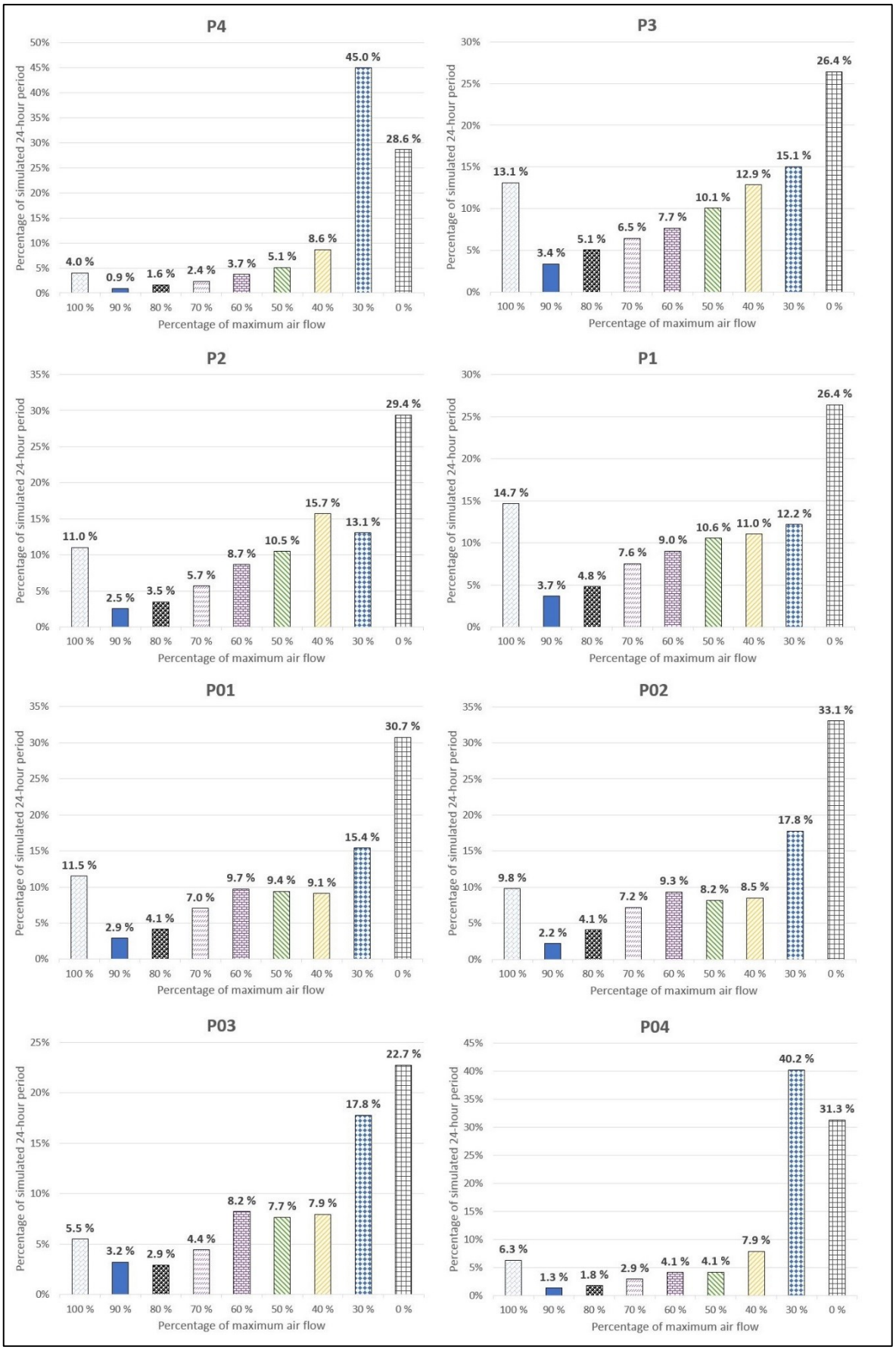


*Figure 35 Percentages of maximum air flow rate used during the simulated 24-hour period, Simulation 4*

### 5.4.2 Convergence

Figure 36 shows convergence plotting for Simulation 4. The residual curves are notably different from those of Figure 33 since with the VAV control, the flow field changes whenever air flow rates are adjusted with the transient CO-concentration. Where iteration only happened during the first few time steps in Simulation 1, the flow field is iterated thousands of times during Simulation 4. The convergence plot is shown on a log-log scale to see the progress of the iterations in detail for the first 1000 iterations.

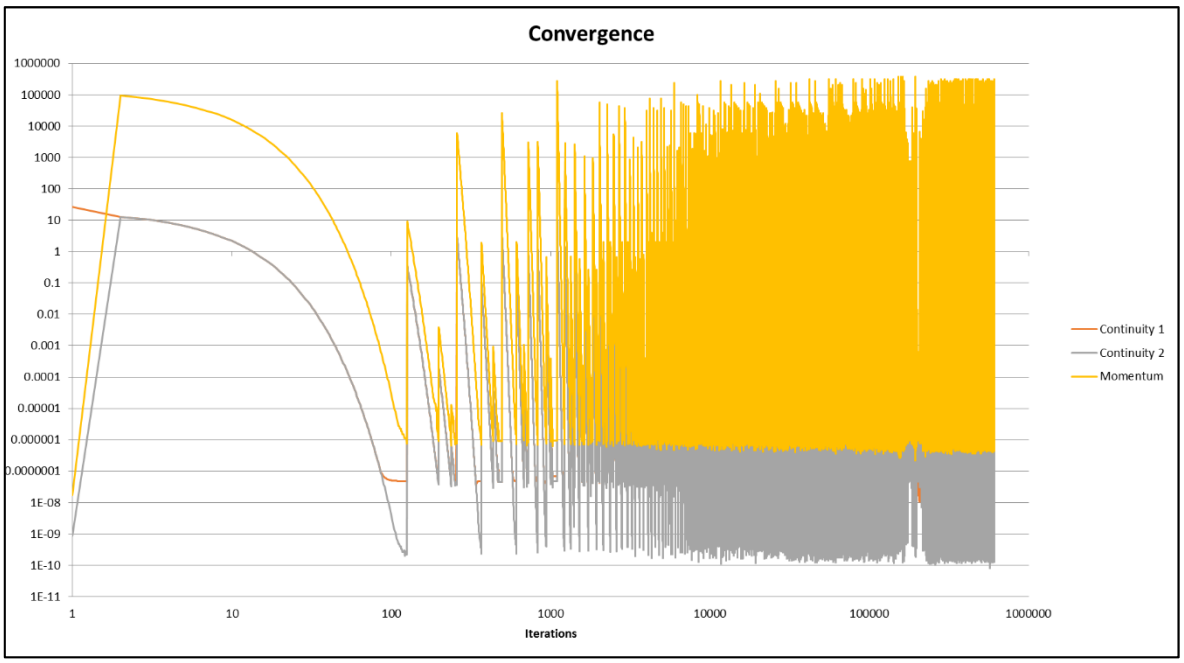


*Figure 36 Convergence plotting for VAV Simulation 4*

# 6 Analysis of simulation results

## 6.1 Simulation 1: Dimensioning of air flow rates for the ventilation system of Tampereen Kansi parking space

Simulating the worst-case scenario in terms of both temperature and ambient CO concentration resulted in somewhat large CO concentrations, certainly enough to be dangerous for the health of visitors in the parking space. Based on the simulations, for adequate contaminant removal in these conditions, higher airflow rates are needed than the hitherto applied minimum 3.6 $\frac{l}{s,m^2}$, due to CSEE's elevating the vehicle emission rates significantly. Emissions from cold engine starts especially play a critical role.

Recall the two allowed ways of dimensioning mentioned in Chapter 2.4: dimensioning by known contaminant load and dimensioning by minimum airflow rates per unit of floor area. A dimensioning according to the optimum deck specific air flow rates in the worst-case conditions of Simulation 1 is presented in Table 27. The sum of airflow rates in $[m^3/s]$ represents the capacity required by fans that serve the parking space. Note that the deck floor areas used are the actual floor areas measured from architect drawings. For comparison, a dimensioning calculation using the D2 minimum air flow rate is shown and the difference of the total air flow rates arrived at via the two ways of dimensioning, is computed.

*Table 27. Sizing of ventilation system based on known CO load and based on D2 minimum air flow rate*

| **Deck** | P4 | P3 | P2 | P1 | P01 | P02 | P03 | P04 |
|---|---|---|---|---|---|---|---|---|
| **Airflow rate [l/s,m²]** | 6.1 | 3.0 | 21.5 | 5.5 | 6.4 | 4.0 | 2.2 | 2.0 |
| **Deck floor area** | 1250 | 1800 | 1250 | 1800 | 1250 | 1650 | 1250 | 1650 |
| **Airflow rate [m³/s]** | 7.6 | 5.4 | 26.9 | 9.9 | 8.0 | 6.6 | 2.8 | 3.3 |
| **SUM** | **70.5 m³/s** | | | | | | | |

| **Deck** | **P4** | **P3** | **P2** | **P1** | **P01** | **P02** | **P03** | **P04** |
|---|---|---|---|---|---|---|---|---|
| **Airflow rate [l/s,m²]** | 3.6 | 3.6 | 3.6 | 3.6 | 3.6 | 3.6 | 3.6 | 3.6 |
| **Deck floor area** | 1250 | 1800 | 1250 | 1800 | 1250 | 1650 | 1250 | 1650 |
| **Airflow rate [m³/s]** | 4.5 | 6.5 | 4.5 | 6.5 | 4.5 | 5.9 | 4.5 | 5.9 |
| **SUM** | **42.8 m³/s** | | | | | | | |

| **Difference** | **64 %** |
|---|---|

The result is clear in that the dimensioning based on known contaminant load is significantly larger than the one based on the D2 minimum air flow rate. This is in stark contrast with the hypothesis that was started from in Chapter 1. A reduction in the sizing of the parking space ventilation system can not be justified by simulating known transient contaminant load in -29 °C as has been done in the present work. On the contrary, the result from dimensioning by known contaminant load calls for an approximately 64 % larger total air flow rate than the result when dimensioning by minimum airflow rate per unit of floor area.

This is however merely one dimensioning calculation with one set of assumptions behind it. Recall that a safety factor was used for the amount of traffic of the simulated 24-hour period. Due to nearby heat sources such as surrounding buildings and nearby piping of district heating, temperatures in the Tampereen Kansi parking space might not mimic outside temperatures exactly. Moreover, a search of temperatures and daily lowest temperatures from Tampere Tampella weather station for the time period 01.12.2016-31.03.2018 [39] (thereby including daily lowest temperatures from three previous winters) reveals that the lowest temperature during this period is -23.8 °C and temperature has been below -20 °C on only five days in total. With these numbers in mind, the worst-case scenario created for dimensioning in Simulation 1 represents a true extreme.

Since $q'_{DSO,i}$ values were simulated in three temperatures, this enables interpolation, extrapolation and graphing of $q'_{DSO,i}$ as a function of temperature. In Figure 37 this kind of graphing is done for $q'_{DSO,i}$ values. Since the engine starts are the most significant contributing factor of CO emissions and the emissions from engine starts where seen to behave very close to exponentially with temperature, an exponential trendline fitting is found to fit the $T, q'_{DSO,i}$ -points with good correlation as well. Table 28 reports the functions of the trendlines and the correlation factor ($R^2$ -value) for each trendline. The functions can in essence be used as air flow rate dimensioning formulas after deciding which temperature the dimensioning is to be based on. Note that for Figure 37, the $q'_{DSO,i}$ values found in Simulations 1-3 have been multiplied by their corresponding deck floor areas and the air flow rates are presented in $[m^3/s]$. Finally, Figure 38 shows similar graphing for the total air flow rate required by the parking space ventilation, as a function of temperature.

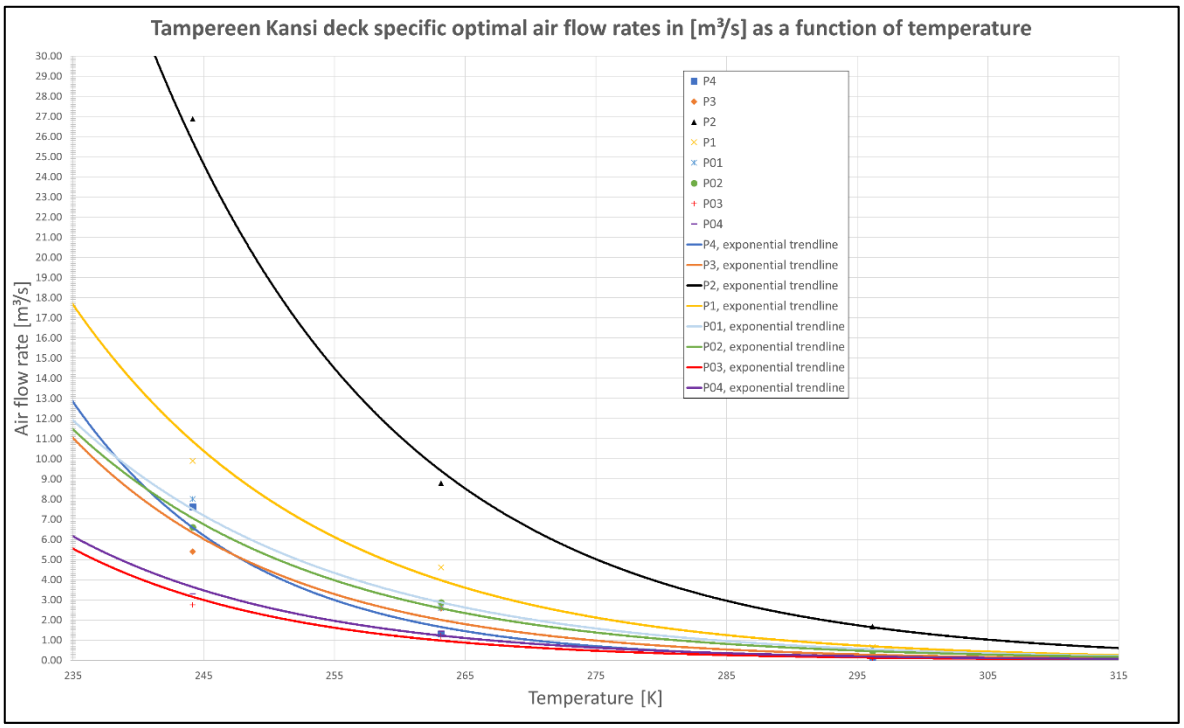


*Figure 37. Results for deck specific optimal air flow rates as function of temperature, with exponential trendline fittings*

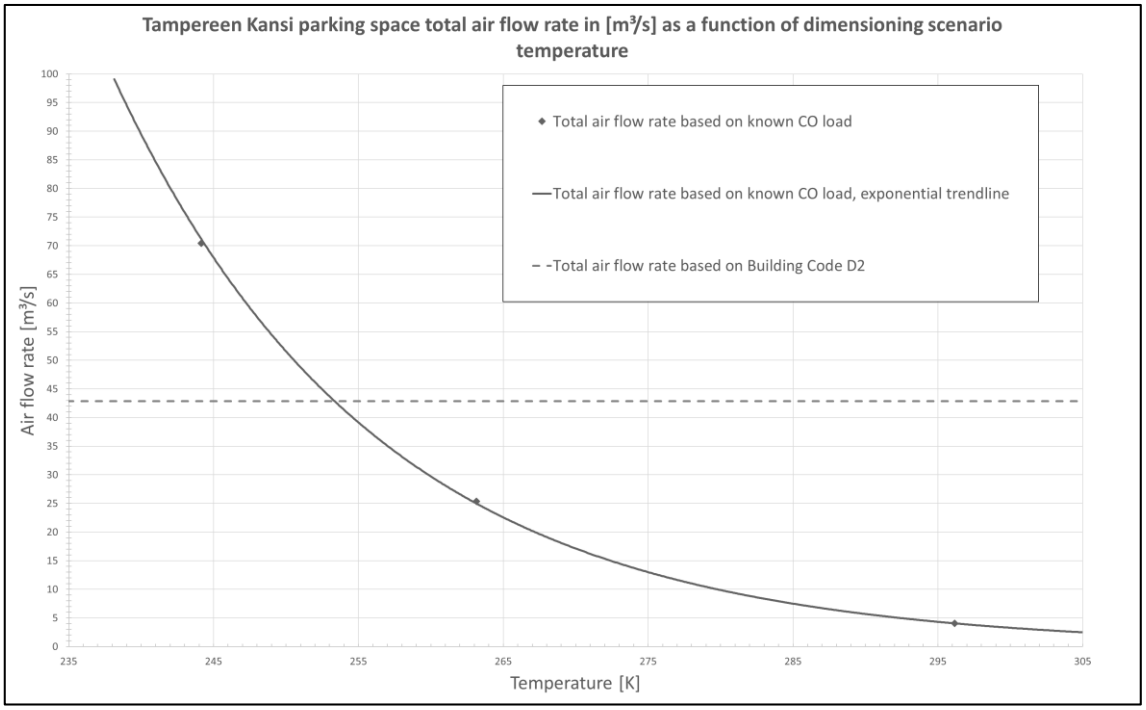


*Figure 38. Total air flow rate requirement as a function of temperature*

*Table 28. Air flow rate dimensioning formulas*

| Deck | Air flow rate dimensioning formula [m³/s] | $R^2 - value$ |
|---|---|---|
| 4 | $q_{P4} = 3 * 10^8 e^{-0.073x}$ | 0.9890 |
| 3 | $q_{P3} = 2 * 10^7 e^{-0.061x}$ | 0.9812 |
| 2 | $q_{P2} = 10^7 e^{-0.053x}$ | 0.9982 |
| 1 | $q_{P1} = 5 * 10^6 e^{-0.053x}$ | 0.9915 |
| 01 | $q_{P01} = 2 * 10^6 e^{-0.051x}$ | 0.9956 |
| 02 | $q_{P02} = 3 * 10^6 e^{-0.053x}$ | 0.9956 |
| 03 | $q_{P03} = 10^7 e^{-0.062x}$ | 0.9868 |
| 04 | $q_{P04} = 4 * 10^6 e^{-0.057x}$ | 0.9920 |
| Total | $q_{tot} = 5 * 10^7 e^{-0.055x}$ | 0.9999 |

$where\ x\ is\ temperature\ in\ [K]$

From Figure 38 it can be read that based on the simulated results, if the dimensioning of air flow rates is based on known CO load, the total air flow rate equals a dimensioning based on the D2 minimum if the dimensioning scenario temperature is chosen to be $253\,K \approx -20\,°C$. A colder dimensioning scenario temperature results in higher total air flow rate requirement. It follows that savings in total air flow rate and subsequently savings in required fan power can be made, compared to a dimensioning based on the D2 minimum, if a dimensioning scenario temperature is chosen that is higher than $-20\,°C$.

An important observation that is made with the transient CO concentration data produced by Simulation 1 is that the istantaneous CO concentrations reach significantly higher than the one-hour averages. Figure 39 and Figure 40 show instantaneous and averaged concentrations respectively from the simulation run at optimal $q'_{DSO,i}$ values, plotted for the most polluted cell, which is predictably found at the most frequently visited deck P2 at the innermost end of the deck. The instantaneous graphing shows spikes at moments when a vehicle passes the zone or an engine start occurs inside the zone. Between these events the concentration tends to lower back towards the ambient concentration, which the outside air is carrying into the parking space. Notably, instantaneous concentrations reach as high as close to 200 ppm, the instantaneous maximum being 194 ppm, although $C_{1hmax,P2} = 31\ ppm$. Looking more closely at the transient concentration data where the instantaneous 194 ppm concentration occurs reveals that for the concentration to descend down below the alert level of 70 ppm mentioned in Chapter 2.3, takes 38 seconds, below the full-capacity-ventilation level 50 ppm in 52 seconds and below 30 ppm in 120 seconds.

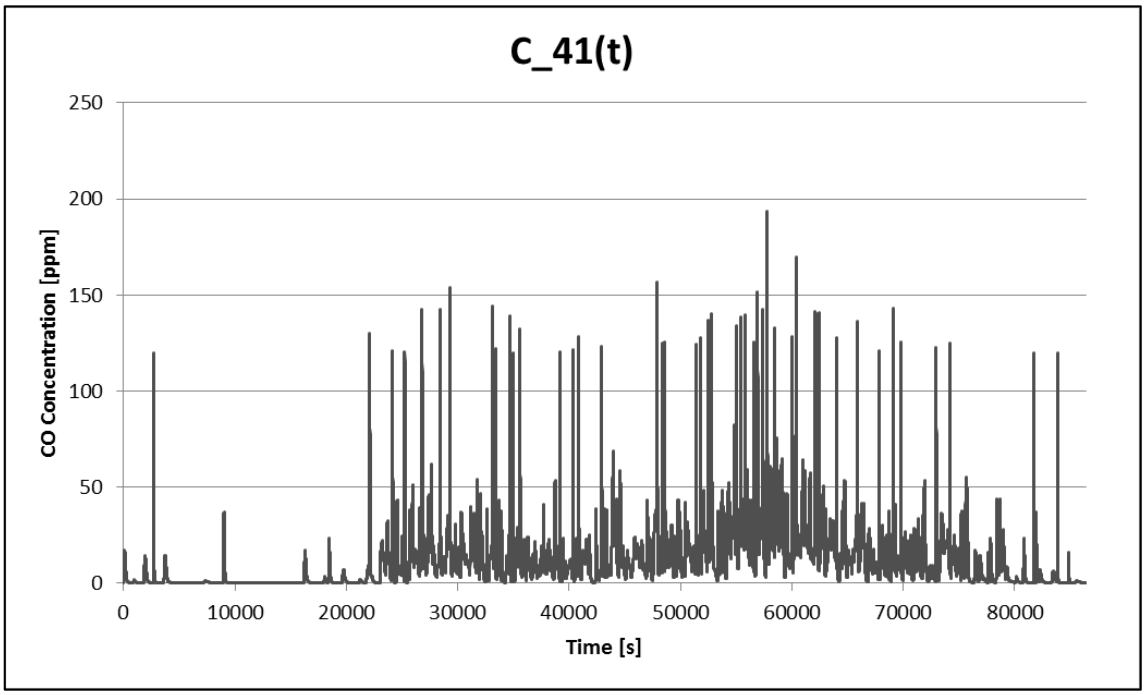


*Figure 39. Instantaneous CO concentration in most polluted cell, Simulation 1 at optimal l/s,m²*

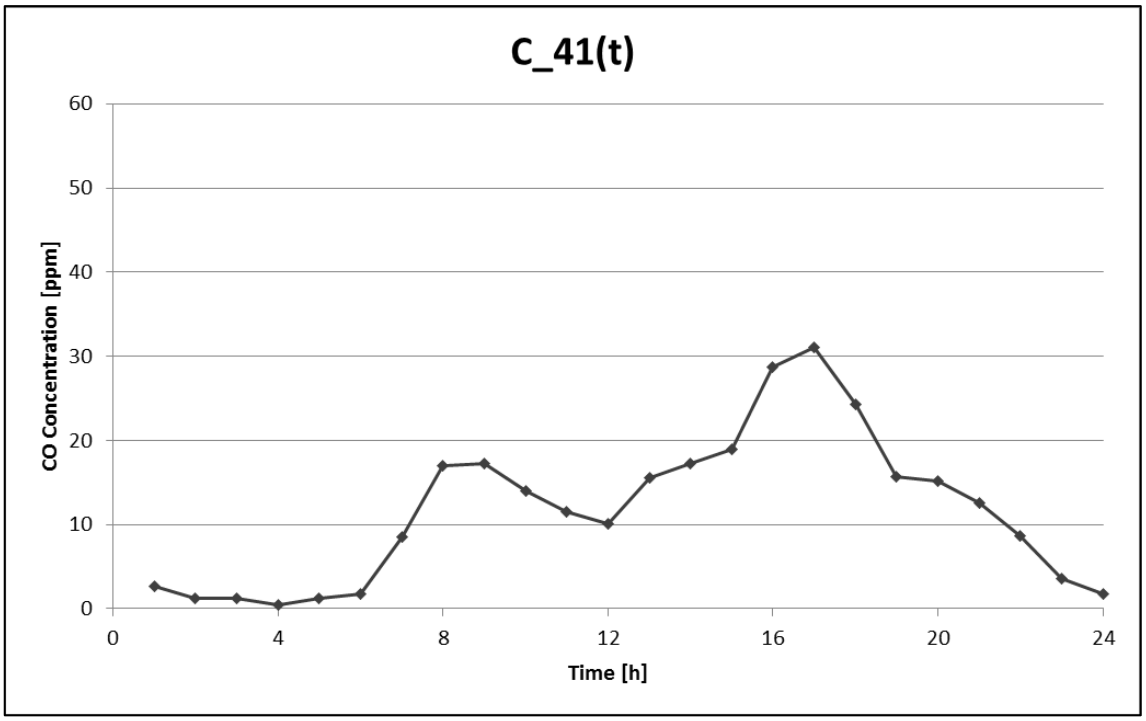


*Figure 40. One-hour average CO concentration in most polluted cell, Simulation 1 at optimal l/s,m²*

## 6.2 Simulation 2: Summer conditions

The simulations for summer conditions showed adequate contaminant removal at all simulated uniform airflow rates 3.6 $\frac{l}{s,m^2}$ , 2.0 $\frac{l}{s,m^2}$ and as low as 1.0 $\frac{l}{s,m^2}$. The 30 ppm criteria was met in all of the decks at the smallest simulated uniform airflow rate 1.0 $\frac{l}{s,m^2}$ during the simulated 24-hour period. The results suggest that from the viewpoint of CO concentration and energy efficiency, optimal airflow rates in summer conditions are found even lower than 1.0 $\frac{l}{s,m^2}$, with $q'_{DSO,i}$ values ranging from 0.09 $\frac{l}{s,m^2}$ to 1.34 $\frac{l}{s,m^2}$ . At air flow rates that low, other aspects of indoor climate such as the removal of humidity and odours; concentrations of other contaminants such as CO2 or particles; might come into play as more important factors than CO concentration. A regulation published by the Finnish Ministry of the Environment states 0.35 $\frac{l}{s,m^2}$ as a general minimum air flow rate for building ventilation. [9]

## 6.3 Simulation 3: Comparison between Excel and Ansys Fluent simulations

Figure 41 shows results for $q'_{DSO,i}$ computed by Ansys Fluent simulations and the Excel based model. Results from Fluent simulations are higher for most of the decks. Recall the stochastic weigths of received traffic for each deck from Table 14. Judging from the weights and the differences between Fluent and Excel results for each deck, it seems that the more

traffic the deck has had, the greater the difference between results from the two models. Decks 3 and 4 are outliers in this sence, but they can be left out of the comparison since the $q'_{DSO,i}$ optimization is incomplete for those decks when it comes to the Fluent simulation runs. For decks 2-04, the results from Fluent simulations are on average 72 % higher than those from the Excel model.

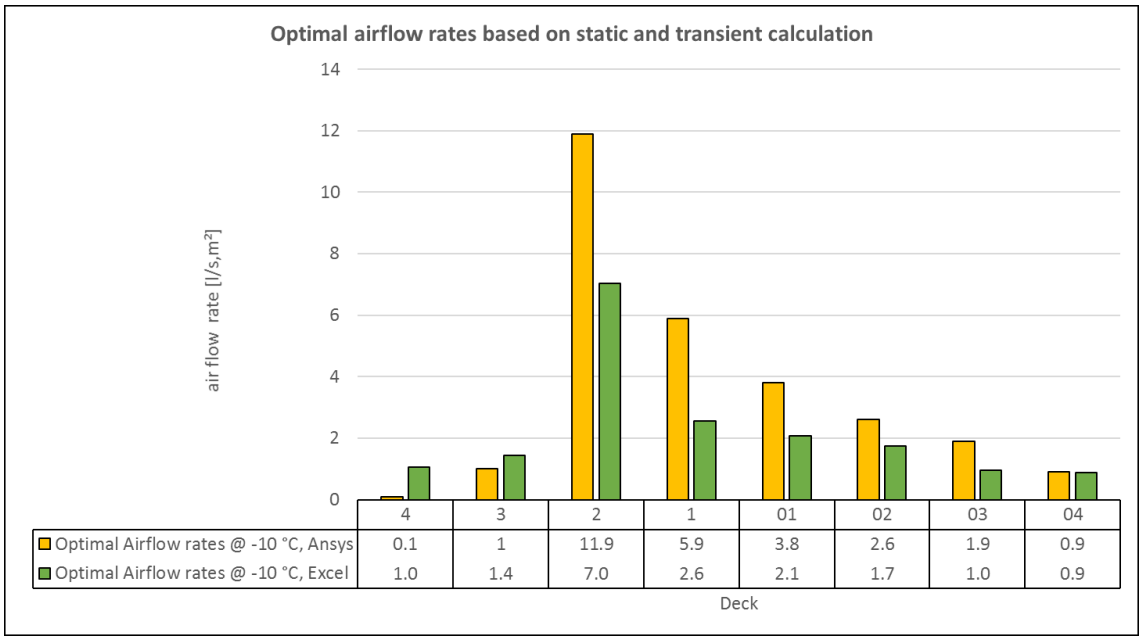


*Figure 41. $q'_{DSO,i}$ results from Ansys and Excel simulations*

There are at least a couple of factors that explain the difference between the results from the two models. The Fluent model has a cell resolution several orders of magnitude higher than that of the Excel model. The Fluent model captures local changes in CO concentration, such as the packing of the CO concentration in the exhaust end of the decks, far more accurately than the Excel model, which in part explains the higher concentrations in exhaust air computed in the Fluent model. With the Fluent model, the CO concentrations used for $q'_{DSO,i}$ calculation via Eq. 44 were measured from the exhaust air. In the Excel model, the packing of the CO concentration towards the exhaust end is also visible to some degree, but the CO load in a zone at any given moment is always fully mixed into the air volume of that zone. This results in lower measured CO concentration, particularly at the exhaust end of the deck.

The Ansys simulations have been carried out using calculation settings and mesh specifications laid out in Chapters 3.2.3 and 4.1. Figure 42 shows contour graphics of carbon monoxide concentration on two planes that span the length of the decks inside the parking space, clearly showing the packing of CO concentration in the exhaust end of the decks. The packing effect is stronger on decks with higher traffic count and subsequently higher CO load and air flow rate. This explains why the difference in results between Ansys and Excel models is more pronounced on decks with higher traffic count. Note that the units and scale are in mass fraction, but as the density of carbon monoxide is close to the density of air in -10 °C, the mass fraction is approximately equal to volume fraction.

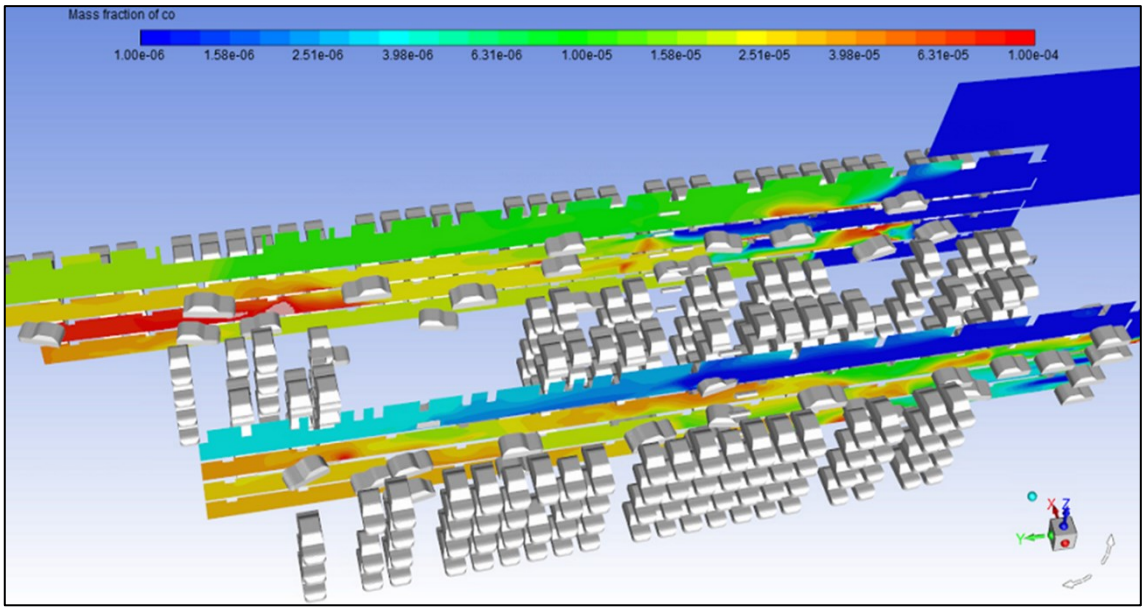


*Figure 42. Contour graphics of carbon monoxide concentration distribution inside the parking space*

The low resolution can be thought of as the main weakness of the Excel model. Another explaining factor for the differences in results between the two models, is the main weakness of the Fluent model in turn: the Fluent model is unable to capture the levelling of CO concentration between impulses of CO load from transient traffic. In the Excel model $q'_{DSO,i}$ values were computed from $C_{1hmax,i}$ concentrations, in which the intermediate falling of CO concentration towards the ambient concentration $\Phi_0$, is factored in. These two reasons – the significant difference in cell resolution and intermediate levelling of CO concentration in the Excel model – are held as the sources for the differences in $q'_{DSO,i}$ results produced by the two models.

## 6.4 Simulation 4: Performance with VAV

The percentages reported in Figure 35 reveal that for all of the decks, roughly a quarter to a third of the simulated 24-hour period is spent with the ventilation completely switched off (0% of maximum air flow rate). For decks P4 and P04 with low traffic count, over 40 % of the time period is spent using 30% of the maximum air flow rate. Ventilation at maximum air flow rate occurs even at most under 15 % of the simulated time period (deck P1) and for half of the decks ventilation is at maximum air flow for under 10 % of the simulated time period.

Notably the $C_{1hmax,i}$ values reported in Table 25 are well beyond $C_{target}$ for many of the decks, climbing into the 40-50 ppm range. This is explained by the control intervals in the VAV rules relating 100 % of maximum air flow rate with a concentration of 50 ppm instead of 30 ppm. This is an interesting finding in the sence that the instructional text written by Talotekniikkainfo, the VAV rule example included, is meant to guide HVAC designers in

the practical application of the current building code. Based on this finding, however, applying the presented example VAV rules leads to a situation that is in contradiction with the building code.

The instructional text by Talotekniikkainfo instructs that an alarm should go off if local CO concentration exceeds 70 ppm. As is also evident from the instantaneous CO concentration graph from Simulation 1, Figure 39, 70 ppm is momentarily exceeded many times within the simulated time period. In fact, at -29 °C a single ignition of a gasoline driven vehicle is enough to momentarily raise the CO concentration well over 70 ppm. The spikes in concentration are for the most part brief, however. Table 26 lists summed up simulated seconds during which transient CO concentration has been over 70 ppm for each of the decks. From the “Longest continuous alarm” column it can be read that the longest continuous periods with CO concentration exceeding 70 ppm have ranged from roughly 2 to 6 minutes. How long of a time period in such a CO concentration becomes dangerous to the health of the visitors of the parking space, is left uncommeneted. It can be argued, though, that brief spikes in CO concentration do not constitute a hazard and that the the alarm should not go off immediately upon the measurement of a heightened CO concentration lest the alarm be ringing for nearly a third of the time in some part of the parking space, as is the case on this simulated cold winters day. Rather, the alarm should go off if a heightened CO concentration is measured for an extended period of time.

# 7 Conclusion and remarks

## 7.1 Main results

For systematic covering of the main results found in the present work, the research questions listed in Chapter 1 are reviewed one by one.

1. What factors influence the dimensioning of air flow rates for parking spaces?

Due to CSEEs, emission rates from vehicles are significantly increased with a decline in temperature. Emissions from engine starts, particularly those of gasoline driven vehicles, were found to be the most significant contribution to the carbon monoxide load of the parking space. In cold temperature, even a single start of a gasoline driven engine is seen as a clear spike in the transient CO concentration graphing and momentarily results in a concentration that warrants an alarm. Emissions from engine starts were seen to grow close to exponentially with declining temperature.

Since gasoline driven engines produce significantly higher CO emissions at start up than their diesel driven counterparts, the share of diesel driven vehicles is of importance as a factor when calculating CO load.

Since cold temperature significantly hinders the performance of catalyzers, newer vehicles are not much cleaner in terms of CO emissions when driven cold, and the age of the vehicle stock can thereby be said to be of lesser importance when calculating CO load for a scenario in cold temperature.

The dimensioning, if done based on known CO load, is therefore greatly influenced by the chosen dimensioning scenario: the estimated traffic count and the temperature in which the estimated traffic happens.

2. What is the optimal dimensioning for air flow rates in the Tampereen Kansi parking space, based on a known diurnal carbon monoxide load?

The optimal deck specific air flow rates and resulting total air flow rate for the Tampereen Kansi parking space, were computed in a dimensioning scenario of 24 hours of traffic in temperature -29 °C, see Table 17. The total air flow rate requirement can be reviewed from Figure 38.

In light of weather data from recent years, the chosen dimensioning scenario is quite extreme. A safety factor of 1.72 was also used in the estimate for amount of traffic. The dimensioning that was done based on known CO load in -29 °C is 64 % larger in total air flow rate than a dimensioning based on the D2 minimum air flow rate per square meter of floor area. On the other hand, the simulation done in -29 °C with the minimum air flow rate $3.6\,\frac{l}{s,m^2}$ showed dangerous levels of CO concentration for extended periods of time. For the most populated

deck, the simulation done with a uniform $7.2 \frac{l}{s,m^2}$ also showed dangerous CO concentration for extended periods of time, particularly in the most populated deck.

In conclusion, the dimensioning carried out in the present work is by no means final and the dimensioning scenario can well be chosen to be a less extreme temperature and the safety factor in traffic amount can be adjusted. However, what is clearly shown is that the D2 minimum air flow rate is not adequate on cold winters days for a parking space with no heating.

After choosing a temperature for a dimensioning scenario, corresponding deck specific optimal air flow rates can be read from Figure 37 or reproduced by the dimensioning formulas in Table 28. Savings in total air flow rate and required fan power, when compared to a dimensioning done based on the D2 minimum, can be expected if the dimensioning scenario temperature is chosen to be higher than $-20\ °C$.

3. How do results computed via time-averaged static Ansys Fluent CFD analysis compare with those computed via transient time-accurate MS Excel based calculations?

The sizing results produced by Ansys Fluent simulations are significantly larger than those produced by the Excel model. The difference is more pronounced the higher the traffic count of the deck is. The main sources of the difference in results are held to be the more accurate capturing of local CO distribution in the Fluent model as well as the intermittent levelling of CO concentration in the Excel model.

4. How does the ventilation system of Tampereen Kansi perform with an example VAV configuration controlled by CO-concentration?

When the -29 °C dimensioning scenario is simulated with an example VAV configuration offered by Talotekniikkainfo (see Chapter 2.4), air flow rates behave according to Figure 35 throughout the simulated 24-hour period. For most of the decks, the ventilation is used at a minimum of 30% of maximum air flow rate or completely switched off for a considerable fraction of the simulated 24-hour period.

$C_{1hmax,i}$ concentrations from the VAV simulation, reported in Table 25, show that the currently applied building code criteria of one-hour average CO concentration staying under 30 ppm *is not* met using the example VAV configuration. The finding suggests that the application of the instructional text written by Talotekniikkainfo leads to a situation that is in contradiction with the building code.

## 7.2 Error sources and future development needs

The Excel model used for Simulations 1-4 is quite crude in terms of resolution. The cruder the resolution, the more the model relies on the *fully mixed* assumption and the more information is lost on the local changes in contaminant concentration. As is, the parking space

decks are divided into five real cells plus two ghost cells. Increasing the resolution i.e. dividing the decks into smaller control volumes, would increase the information obtained on the spatial distribution of the examined contaminant. Increasing the resolution in the Excel model is certainly possible, but it is currently not a trivial user-friendly task and requires manual alterations to the equations that are part of the code. Ideally, resolution should be one of the calculation settings chosen by the user, and the code would conform to the chosen resolution. The programming of the VBA program behind the Excel model was done with versatility in mind – the tool is to be used in future projects other than Tampereen Kansi as well – and many customization options were implemented. Alas, adjustable resolution as a user-defined option proved to be an insurmountable programming challenge: it would indirectly necessitate the automatization of code generation for the equations of the pressure correction method for an arbitrary amount of cells. More complexity would also be introduced to the building of the vehicle routes, which was one the most challenging features to implement in the programming even for a fixed and moderate amount of cells. None the less, in established CFD programs, one can essentially set the mesh resolution ad arbitrium, and this should be strived for in future upgrades to the Excel model as well.

The chosen input data plays a critical role in any simulation. In the present work, the role of the vehicle emissions data becomes crucial. In Chapter 2.3.2 many sets of emissions data from different sources were shown to illustrate the point that different measurement results, from measurements made in similar temperatures, do not necessarily agree with each other and that choosing the correct exact emission rates for multiple temperatures is not a simple task. Further challenge was posed by the fact that measurement data from the rather extreme conditions of -29 °C was not found. Sensitivity analysis using a range of emission rates becomes a meaningful subject for future research.

Another crucial item in the input data is the used traffic schedule, in conjunction with the spread of traffic onto the parking decks. Ideally, it would be appropriate to base the traffic schedule on realized historical traffic data from existing parking spaces that serve similar buildings as the parking space that is to be simulated. The spread of traffic within the parking space should also ideally be based on realized routes and driving behavior of live users of existing parking spaces. For the purposes of the present work, the experience and expertise of Ramboll Traffic & Infrastructure department was trusted in these matters.

The utilized hour-based diurnal traffic schedule was converted into a second-based schedule by dividing each hours' arriving and leaving vehicles *evenly* onto the seconds within the respective hour. This even spreading in time results in a situation where several engine starts, that are the most prominent single impulse of emissions, never occur right at the same time in the simulations. In practice, several vehicles starting their engines at the same time is an utterly possible and by no means rare event but as it is, this event never gets simulated. The starting location of a leaving vehicle is randomized. Further randomization for the exact starting time within the hour would make the event of simultaneous engine-starts possible. This is an item for future development of the Excel calculation tool.

In addition to the desirable features already mentioned, many improvements can be made to the VBA program on the programming level. The code as it is features many instances of repetitive code, the goal of which could likely be achieved with more compact programming, resulting in reduced simulation run-times.

# References

1. Sisäasiainministeriö. *Suomen Rakentamismääräyskokoelma D2, Rakennusten Ilmanvaihto, Määräykset Ja Ohjeet, 1978*. Helsinki: 1978. [cited 23.02.2018] Available: http://www.ym.fi/download/noname/%7B09B36046-1078-484E-B9F0-9BA3BC5F0701%7D/100780

2. Ympäristöministeriö. *Suomen Rakentamismääräyskokoelma D2 Rakennuksen Sisäilmasto Ja Ilmanvaihto, Määräykset Ja Ohjeet, 1987.* Helsinki: Painatuskeskus Oy, 1987. [cited 23.02.2018]. ISBN 951-37-0801-2 Available: www.ym.fi/download/noname/%7B3C555C28-04E8-4DDC-B6F5.../100782

3. Ympäristöministeriö. *Suomen Rakentamismääräyskokoelma D2 Rakennusten Sisäilmasto Ja Ilmanvaihto, Määräykset ja Ohjeet, 2003.* Helsinki: 2003 [cited 23.02.2018]. Available: http://www.ym.fi/download/noname/%7BCE4601D6-732C-4C9A-BC82-AA16C7EF4D29%7D/101112

4. Ympäristöministeriö. *Suomen Rakentamismääräyskokoelma D2 Rakennuksen Sisäilmasto ja Ilmanvaihto, Määräykset ja Ohjeet, 2010.* Helsinki: 2010. [cited 23.02.2018]. Available: http://www.ym.fi/download/noname/%7BD7685B7F-AE4B-4DD3-B689-BC8418933265%7D/102967

5. Ympäristöministeriö. *Suomen Rakentamismääräyskokoelma D2, Rakennuksen Sisäilmasto Ja Ilmanvaihto, Määräykset ja Ohjeet, 2012*. Helsinki: 2012. [cited 23.02.2018]. Available: http://www.ym.fi/download/noname/%7B5EB5B5EC-4DF9-44B9-A315-94D1E6B84AFE%7D/134437

6. Suomen Virallinen Tilasto, (SVT). *Moottoriajoneuvokanta, Rekisterissä Olleiden Ajoneuvojen Lukumäärä 1980-2016.* Helsinki: Tilastokeskus, 2017. [cited 23.02.2018]. ISSN 1798-856X Available: http://pxnet2.stat.fi/PXWebPXWeb/pxweb/fi/StatFin/StatFin__lii__mkan/statfin_mkan_pxt_001.px/

7. Eckhardt, Jenni. *Tieliikenteen Hiilimonoksidipäästöt CO [T/a] LIISA 2016 Laskentajärjestelmä, VTT.* [Online material] [cited 09.02.2017]. Available: http://lipasto.vtt.fi/liisa/aikasarja.htm

8. ASHRAE. *ASHRAE Handbook - HVAC Applications Chapter 15 - ENCLOSED VEHICULAR FACILITIES*. Atlanta: ASHRAE, 2015. ISBN 978-1-936504-93-0. Availability: Requires registration

9. Ympäristöministeriö. *Ympäristöministeriön Asetus Uuden Rakennuksen Sisäilmastosta Ja Ilmanvaihdosta.* Helsinki: Ympäristöministeriö, 2017. [cited 18.07.2018]. Available: http://www.ym.fi/download/noname/%7BAAD7DB92-F571-4766-A3F1-BFF63383191B%7D/133875.

10. SRV. *Kansi Ja Areena. [Online material]* [cited 25.02.2018]. Available: https://www.srv.fi/kansi-ja-areena

11. SRV. *Kansi Ja Areena - Taustatietoa.* [Online material] [cited 25.02.2018]. Available: https://www.srv.fi/kansi-ja-areena/taustatietoa

12. Tampereen kaupunki. *Tampereen Kansi Ja Areena* [Online material] [cited 27.02. 2018]. Available: https://www.tampere.fi/tampereen-kaupunki/ohjelmat/keskusta-hanke/tampereen-kansi-ja-areena.html

13. Tampereen kaupunki, Maunu, A. *Tampereelle Suunnitellun Monitoimiareenan Osakassopimus Allekirjoitettiin.* [Online material] [cited 27.02.2018]. Available: https://www.tampere.fi/tampereen-kaupunki/ajankohtaista/tiedotteet/2017/10/03102017_1.html

14. Koho, Tero. *Tampereen Kansi Pysäköintitilat – Rakennustapaseloste, LVIA-Järjestelmäkuvaus*. Espoo: Ramboll, 2018. [cited 27.02.2018]. Availability: Internal document

15. Suarez-Bertoa, Ricardo & Astorga, Covadonga. *Impact of Cold Temperature on Euro 6 Passenger Car Emissions.* Environmental Pollution. Vol. 234. 2017 p. 318-329. ISSN 0269-7491 [Electronic].

16. Jaikumar R & Nagendra Shiva, S. M. & Sivanandan, R. *Modeling of Real Time Exhaust Emissions of Passenger Cars Under Heterogenous Traffic Conditions.* Atmospheric Pollution Research no. 8. 2016 p. 80-88. ISSN 1309-1042 [Electronic].

17. Papakonstantinou, K. et al. *Air Quality in an Underground Garage: Computational and Experimental Investigation of Ventilation Effectiveness.* Energy & Buildings. vol. 35 no. 9 2003 p. 933-940. ISSN 0378-7788 [Electronic].

18. Al-Waked, Rafat, et al. *Indoor Air Environment of a Shopping Centre Carpark: CFD Ventilation Study.* Universal Journal of Mechanical Engineering. Vol 5. 2017 p. 113-123. DOI: 10.13189/ujme.2017.050402

19. Trafi & Verohallinto. *Dieselautojen Autojen Osuus Henkiloautojen Ensirekisteröinneistä Ja Henkilöautokannasta – Autoalan tiedotuskeskus.* [Online material] [cited 24.02.2018]. Available: http://www.autoalantiedotuskeskus.fi/tilastot/autokannan_kehitys/dieselautojen_osuus_henkiloautojen_ensirekisteroinneista_ja_henkiloautokannasta

20. Trafi - Liikenteen truvallisuusvirasto. *Trafi.fi - Lk-Ajoneuvojen Ikätilastot.* [Online Material] [cited 24.02.2018]. Available: https://www.trafi.fi/tietopalvelut/tilastot/tieliikenne/ajoneuvokanta/lk-ajoneuvojen_ikatilastot

21. Motiva. *Henkilö- Ja Pakettiautot.* [Online material] [cited 08.03.2018]. Available: http://www.motivanhankintapalvelu.fi/tietopankki/henkilo-_ja_pakettiautot

22. EU. *EUROOPAN PARLAMENTIN JA NEUVOSTON ASETUS (EY) N:O 715/2007.* Euroopan unionin virallinen lehti. EU 2007. [cited 18.07.2018]. Available: https://eur-lex.europa.eu/legal-content/FI/TXT/HTML/?uri=CELEX:32007R0715&from=EN

23. EQUA Ltd. *IDA RTV Simulation Software - PIARC Euro 4 Emission Tables*

24. Weilenmann, Martin & Favez, Jean-Yvesand & Alvarez, Robert. *Cold-Start Emissions of Modern Passenger Cars at Different Low Ambient Temperatures and their Evolution Over Vehicle Legislation Categories*. Atmospheric Environment vol. 43, no. 15 2009 p. 2419-2429. DOI: https://doi.org/10.1016/j.atmosenv.2009.02.005

25. Mäkelä, Kari & Auvinen, Heidi. *Suomen Tieliikenteen Pakokaasupäästöt, LIISA 2012 Laskentajärjestelmä – Tutkimusraportti.* Espoo: VTT, 2013 [cited 12.02.2018] Available: http://lipasto.vtt.fi/lipasto/liisa/liisa2012raportti.pdf

26. TM, VTT. *Talviauto 2018.* Tekniikan Maailma 04/2018. Helsinki: OtavaMedia, 2018.

27. Fantech. *Introduction to Car Park Impulse Ventilation.* [Online material] [cited 05.03.2018]. Available: http://www.fantech.com.au/FanRange.aspx?AppID=P2&RangeID=2018

28. Talotekniikkainfo. *Sisäilmasto Ja Ilmanvaihto –Opas.* [Online material] [cited 18.07.2018]. Available: https://www.talotekniikkainfo.fi/sisailmasto-ja-ilmanvaihto-opas

29. Tampereen Kaupunki. *Tampereen Ilmanlaatu 2016.* Ympäristönsuojelun julkaisuja 1/2017. ISSN 1798-0127 [Electronic].

30. Helsingin seudun ympäristöpalvelut –kuntayhtymä. *Ilmanlaatudata 2014.* Ilmanlaatu pääkaupunkiseudulla vuonna 2014 –raportti, HSY. Helsinki: 2014. [Online material] [cited 15.06.2018] Available: www.hsy.fi/ilmanlaatudata2014

31. Patankar, Suhas. *Numerical Heat Transfer and Fluid Flow.* Hemisphere Publishing Corporation, 1980 [cited 3.5.2018]. ISBN 0-89116-522-3.

32. Siikonen, Timo. *Laskennallisen Virtausmekaniikan Ja Lämmönsiirron jatkokurssi.* Espoo: Department of Applied Mechanics, Aalto University School Of Engineering, 2014 [cited 3.5.2018]. Available: http://docplayer.fi/6023297-Laskennallisen-virtausmekaniikan-ja-lammonsiirron-jatkokurssi-timo-siikonen.html

33. Mikkola, Tommi. *Simulation of Unsteady Free Surface Flows – Code Verification and Discretisation Error.* Espoo: Helsinki University Of Technology, 2009. ISBN 978-952-248-137-5. Available: https://aaltodoc.aalto.fi/handle/123456789/4667

34. Kreyszig, Erwin. *Advanced Engineering Mathematics 8th ed*. Singapore: Wiley Custom, 2003. ISBN 0-471-15496-2.

35. Tu, Jiyuan & Yeoh, Guan H & Liu, Chaoqun. *Computational Fluid Dynamics - A Practical Approach 2. ed.* Amsterdam: Elsevier, 2013. ISBN 9780080982434.

36. SAS IP Inc. *Ansys Fluent 17 Documentation.* [Online material] [cited 20.06.2018]. Available: https://www.sharcnet.ca/Software/Ansys/17.0/en-us/help/ai_sinfo/flu_intro.html

37. Nielsen, Peter V. *Computational Fluid Dynamics in Ventilation Design 1.th ed.* Brussels: Rehva, Federation of European Heating and Air-conditioning Associations, 2007. ISBN 2-9600468-9-7.

38. *LVI Kalenteri 2018.* Helsinki: Suomen Kalenterit Oy, 2017.

39. Ilmatieteenlaitos. *Temperature; Daily Lowest Temperature, Tampere Tampella 01.12.2016-31.03.2018* [Online material] [cited 18.07.2018]. Available: http://ilmatieteen-laitos.fi/havaintojen-lataus#!/

# List of appendages

# Appendix 1. Page 49 from HSY Ilmanlaatu 2015 -report

## Hiilimonoksidi CO

*Hiilimonoksidipitoisuuksien vuosikeskiarvot, mg/m³*

| | 94 | 95 | 96 | 97 | 98 | 99 | 00 | 01 | 02 | 03 | 04 | 05 | 06 | 07 | 08 | 09 | 10 | 11 | 12 | 13 | 14 |
|---|---|---|---|---|---|---|---|---|---|---|---|---|---|---|---|---|---|---|---|---|---|
| Töö | 1,0 | 0,9 | 0,9 | 0,8 | 0,7 | 0,6 | 0,6 | 0,5 | 0,5 | 0,6 | 0,5 | | | | | | | | | | |
| Man | | | | | | | | | | | | 0,4 | 0,3 | 0,3 | 0,3 | 0,3 | 0,3 | 0,3 | 0,3 | 0,2 | |
| Val | 0,4 | 0,5 | 0,5 | 0,4 | 0,5 | 0,4 | 0,4 | 0,3 | 0,3 | 0.3* | 0,3 | | | | | | | | | | |
| Var | | | | | | | | | | | | | | | | 0,2 | | 0,2 | 0,2 | 0,2 | |
| Lep2 | | | 0,6 | 0,4 | 0,5 | 0,5 | 0,4 | 0,4 | 0,4 | 0,4 | 0,4 | | | | | | | | | | |
| Lep3 | | | | | | | | | | | | 0,3 | 0,3 | 0,3 | 0,2 | | | | | | |
| Tik | | | 0.6* | 0,6 | 0,6 | 0,5 | 0,5 | 0,5 | 0,5 | 0,6 | 0,5 | 0,6 | 0,3 | 0,3 | 0,3 | 0,3 | 0,3 | 0,3 | 0,3 | 0,3 | 0,3 |

**tuloksia alle 90 %*

*Hiilimonoksidipitoisuuksien kuukausikeskiarvot, mg/m³*

| Kk | Tik | Rus |
|---|---|---|
| 1 | 0,3 | |
| 2 | 0,3 | |
| 3 | 0,3 | |
| 4 | 0,3 | |
| 5 | 0,2 | |
| 6 | 0,2 | |
| 7 | 0,2 | |
| 8 | 0,2 | |
| 9 | 0,3 | 0.3* |
| 10 | 0,3 | 0,2 |
| 11 | 0,3 | 0,2 |
| 12 | 0,3 | 0,2 |

**tuloksia alle 75 %*

*Hiilimonoksidimittausten ajallinen edustavuus, %*

| Kk | Tik | Rus |
|---|---|---|
| 1 | 95 | 0 |
| 2 | 100 | 0 |
| 3 | 100 | 0 |
| 4 | 100 | 0 |
| 5 | 100 | 0 |
| 6 | 100 | 0 |
| 7 | 100 | 0 |
| 8 | 100 | 0 |
| 9 | 100 | 51 |
| 10 | 100 | 100 |
| 11 | 100 | 98 |
| 12 | 100 | 91 |

*Yhteenveto hiilimonoksidin mittauksista, mg/m³*

| | Tik | Rus |
|---|---|---|
| Vuosikeskiarvo | 0,3 | |
| Suurin vuorokausiarvo | 1,1 | 0,5 |
| Suurin tuntiarvo | 4,0 | 1,9 |
| suurin 8 h liukuva keskiarvo | 2,2 | 1,1 |

*CO 8 h liukuva raja-arvo on 10 mg/m³.*
*CO 8 h liukuva ohjearvo on 8 mg/m³.*
*CO tuntiohjearvo on 20 mg/m³.*

# Appendix 2. Technical specifications for Fläkt Woods Low Profile jet fan

Jet Thrust Systems

## Dimensions and Drawings - '*LOW-PROFILE*' and '*LOW-PROFILE MAX*' Car Park Fan

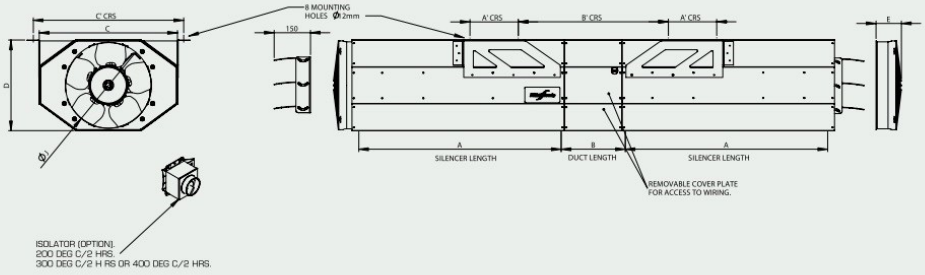


| Fan Dia (J) | Configuration | A | A' | B | B' | C | C' | D | E | Total Length | Temp Rating | Inlet | Outlet | Weight Kg |
|---|---|---|---|---|---|---|---|---|---|---|---|---|---|---|
| 315 | UNI-DIRECTIONAL | 835 | 200 | 265 | 620 | 530 | 580 | 335 | 90 | 2175 | 200°C/2HRS 300°C/2HRS OR 400°C/2HRS | BM & GUARD | DEFLECTOR | 90 |
| | TRULY REVERSIBLE | | | | | | | | | 2235 | | DEFLECTOR | DEFLECTOR | 90 |
| | UNI-DIRECTIONAL | | | | | | | | | 2055 | | BM & GUARD | GUARD | 90 |
| | TRULY REVERSIBLE | | | | | | | | | 2115 | | BM & GUARD | BM & GUARD | 90 |
| 355 | UNI-DIRECTIONAL | 835 | 200 | 265 | 620 | 570 | 620 | 375 | 105 | 2190 | | BM & GUARD | DEFLECTOR | 95 |
| | TRULY REVERSIBLE | | | | | | | | | 2235 | | DEFLECTOR | DEFLECTOR | 95 |
| | UNI-DIRECTIONAL | | | | | | | | | 2070 | | BM & GUARD | GUARD | 95 |
| | TRULY REVERSIBLE | | | | | | | | | 2145 | | BM & GUARD | BM & GUARD | 95 |
| 400 | UNI-DIRECTIONAL | 835 | 200 | 265 | 620 | 620 | 670 | 420 | 113 | 2198 | | BM & GUARD | DEFLECTOR | 106 |
| | TRULY REVERSIBLE | | | | | | | | | 2235 | | DEFLECTOR | DEFLECTOR | 106 |
| | UNI-DIRECTIONAL | | | | | | | | | 2078 | | BM & GUARD | GUARD | 106 |
| | TRULY REVERSIBLE | | | | | | | | | 2161 | | BM & GUARD | BM & GUARD | 106 |

All dimensions in mm

| Dia | Product Type | Thrust N | Volume $m^3/s$ | Sound Power $Lw_A$ | Sound Pressure $Lp_A$ @ 3m | Rpm | Nominal Power kW | Full Load Current (A) | Starting Current (A) |
|---|---|---|---|---|---|---|---|---|---|
| 315 | Low-Profile | 22/5.7 | 1.2/0.61 | 80/62 | 62/44 | 2900/1470 | 0.7/0.09 | 1.85/0.58 | 13/2.94 |
| 355 | Low-Profile | 38/9.8 | 1.9/0.97 | 84/66 | 66/48 | 2850/1450 | 1.05/0.14 | 2.4/0.8 | 13/2.94 |
| 400 | Low-Profile | 57/14.4 | 2.43/1.22 | 87/68 | 69/50 | 2920/1470 | 1.35/0.17 | 3.5/1.12 | 19.2/4.59 |
| 315 | Low-Profile MAX | 25.5/6.4 | 1.29/0.64 | 83/71 | 65/53 | 2775/1370 | 0.75/0.13 | 2.74/0.82 | 14.5/2.86 |
| 355 | Low-Profile MAX | 45.4/10.8 | 1.94/0.99 | 85/72 | 67/54 | 2775/1370 | 1.27/0.17 | 2.74/0.82 | 14.5/2.86 |
| 400 | Low-Profile MAX | 85.7/20.8 | 3/1.47 | 89/75 | 71/57 | 2875/1415 | 2.49/0.3 | 5.24/1.69 | 27.77/5.41 |

Sound Power Level, LW = dB re $10^{-12}$W
Sound pressure level, LpA = dB re 2 x $10^{-5}$PA, provided for comparative purposes at a distance of 3m, based on hemispherical propagation in free field conditions.
Please note data for 200°C without accessories

# Appendix 3. VBA Program structure as a block diagram